

5-1-2010

Development of presynaptic calcium dynamics and short-term plasticity in the SC-Ca1 synapse

Chessa Scullin

Follow this and additional works at: https://digitalrepository.unm.edu/biom_etds

Recommended Citation

Scullin, Chessa. "Development of presynaptic calcium dynamics and short-term plasticity in the SC-Ca1 synapse." (2010).
https://digitalrepository.unm.edu/biom_etds/18

This Dissertation is brought to you for free and open access by the Electronic Theses and Dissertations at UNM Digital Repository. It has been accepted for inclusion in Biomedical Sciences ETDs by an authorized administrator of UNM Digital Repository. For more information, please contact disc@unm.edu.

Chessa Scullin
Candidate

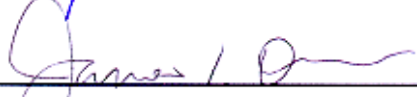
Biomedical Science
Department

This thesis is approved, and it is acceptable in quality
and form for publication:

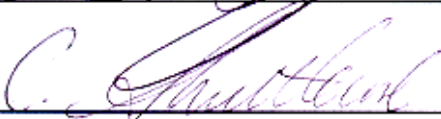
Approved by the Thesis Committee:


_____, Chairperson









**DEVELOPMENT OF PRESYNAPTIC CALCIUM DYNAMICS
AND SHORT-TERM PLASTICITY IN THE SC-CA1 SYNAPSE**

BY

CHESSA SCULLIN

B.S. CHEMICAL ENGINEERING

Submitted in Partial Fulfillment of the
Requirements for the Degree of

**Doctor of Philosophy
Biomedical Science**

The University of New Mexico
Albuquerque, New Mexico

May, 2010

DEDICATION

I would like to dedicate this to my family and William and his family for their support.

ACKNOWLEDGEMENTS

I would like to first thank all of the people who encouraged me to preserve and reminded me constantly of my love of science, more specifically Dr. L.D. Partridge and Dr. M.C. Wilson who were willing to expand their own horizons and mine allowing me to join their labs. They were both willing to participate in exciting critical discussions of my work creating an audacious work environment.

Dr. Partridge taught me the fundamentals of electrophysiology and patience. He also encouraged extracurricular activities such as bringing brains to primary and secondary school classrooms and grueling outdoor adventures. He also would not shy away from my attempts to use mathematical methods. M.C. Wilson taught me effective critique of data and techniques of molecular biology and genetics. He encouraged me to integrate my engineering background with fundamental research of neuroscience.

I would also like to thank my committee Dr. C.W. Shuttleworth, Dr. R. Hartley, and Dr. J. Thomas for their advice, guidance and not making it hard to schedule meetings. I would like to thank Dr. T. Buranda for giving his time, advice and guidance. I would like to thank J.W. Matthews for general mental support, being an adventurous soul and providing the use of his computers during numerous hours of modeling. I would like to thank all of the lab members past and present, who helped run copious numbers of PCR and helped maintain the mouse colonies, J. Sanderson and P. Zamudio for being good friends and always being willing to listen and give advice. I would like to thank the Neuroscience department faculty, students and staff for providing support; the BSGP office and IGERT program who keep their respective programs running and have been

freely available to solve problems; my brothers for keeping me grounded; and my parents for making me feel loved and reminding me I would eventually graduate.

I would also like to acknowledge funding sources provided by UNM IGERT Program on Integrating Nanotechnology with Cell Biology and Neuroscience (NSF-DGE-0549500) and NIH-RO1-MH48989 (M.C.W.) and NIH-R01-MH07386 (L.D.P.).

**DEVELOPMENT OF PRESYNAPTIC CALCIUM DYNAMICS
AND SHORT-TERM PLASTICITY IN THE SC-CA1 SYNAPSE**

BY

CHESSA SCULLIN

ABSTRACT OF DISSERTATION

Submitted in Partial Fulfillment of the
Requirements for the Degree of

**Doctor of Philosophy
Biomedical Science**

The University of New Mexico
Albuquerque, New Mexico

May, 2010

Development of presynaptic Ca^{2+} dynamics and short-term plasticity in the SC-CA1 synapse

by

Chessa Scullin

B.S., Chemical Engineering, University of New Mexico, 2004

ABSTRACT

Following a presynaptic action potential, there is a rapid rise of $[\text{Ca}^{2+}]_i$ in the immediate vicinity of Ca^{2+} channels that triggers membrane fusion and release of transmitter from vesicles within this microdomain. This presynaptic Ca^{2+} signal ($[\text{Ca}^{2+}]_{\text{pre}}$) then disperses to produce a residual Ca^{2+} ($[\text{Ca}^{2+}]_{\text{res}}$) that decays over the course of tens to hundreds of milliseconds. The $[\text{Ca}^{2+}]_{\text{res}}$ has important implications in synaptic plasticity and is the basis for working memory storage. Ultimately $[\text{Ca}^{2+}]_{\text{res}}$ is removed from the cytoplasm either into intracellular organelles or across the plasma membrane into the extracellular environment.

Calcium influx pathways, cytoplasmic Ca^{2+} buffering proteins, and Ca^{2+} extrusion processes in rodent neurons undergo considerable change during the first postnatal month. These changes have important functional significance in short-term plasticity – in particular paired-pulse facilitation (PPF) – at presynaptic terminals where neurotransmitter release is directly dependent on the dynamics of free cytoplasmic Ca^{2+} . To examine developmental changes in $[\text{Ca}^{2+}]_{\text{res}}$ dynamics in the Schaffer collateral synapses onto CA1 pyramidal neurons in *in vitro* hippocampal slices, we measured the timecourse of decay of $[\text{Ca}^{2+}]_{\text{res}}$ in presynaptic terminals following single and paired

orthodromic stimuli in the *stratum radiatum*. The contribution of the slow component compared to the total decay of $[Ca^{2+}]_{res}$ was reduced from >80% in newborn mice to ~50% in the more mature animals (>P24) and $[Ca^{2+}]_{res}$ had a distinct slow rising component in newborn mice (<P4), which was not apparent in older mice. This transition from a slow decay in early neonatal periods to the rapid decay in adults occurred gradually over the first 4 weeks of postnatal life, and appeared to be coincident with the major period of maturation of these synapses. The first goal of this study was to investigate the role of internal stores in regulating presynaptic $[Ca^{2+}]$ and in synaptic plasticity during this important period of synaptic development.

During this same developmental period, SNAP-25, a presynaptic vesicular release protein, undergoes changes in isoform expression. Alterations in SNAP-25 isoform expression have been linked to diseases with developmental onset such as schizophrenia, attention deficit hyperactivity disorder, and epilepsy (Corradini *et al.*, 2009).

Snap25^{tm2M^{cw}} mice (Tkneo), in which this developmental change of isoform expression is modified (Bark *et al.*, 2004), appear to retain an immature state of paired-pulse facilitation. The second goal of this study was to use these Tkneo mice as a tool to better understand the mechanisms of synaptic plasticity and to better understand how SNAP-25 regulation could underlie neurological disorders. We applied a model for paired-pulse facilitation (Schiess *et al.*, 2006), which describes facilitation as a function of two $[Ca^{2+}]_{res}$ -dependent pools of vesicles with different release probabilities. This model predicted the observed external $[Ca^{2+}]$ -dependent changes in paired-pulse ratio based on changes in the effectiveness of $[Ca^{2+}]_{res}$ and the resultant increased probability of release during the second pulse. We compared the presynaptic Ca^{2+} regulation in Tkneo mice to

that found at different developmental stages and observed a striking difference between both Tkneo and *Snap25*^{tm1M^{cw}} (SNAP-25 heterozygote null, HET) mice and similar-aged wild type (WT) mice in the degree of buffer saturation.

The first portion of this study suggests that maturation of cytoplasmic Ca²⁺ stores plays an important role in the [Ca²⁺]_{pre} regulation and the consequent synaptic plasticity that occurs during development. Interestingly, the second portion of the study indicates that [Ca²⁺]_{res} regulation and synaptic plasticity in SNAP-25 Tkneo mice are not dependent on contributions from cytoplasmic Ca²⁺ stores, but rather depend on contributions of cytoplasmic [Ca²⁺]_{res} saturation sensitivity and resultant effects on plasticity. Unfortunately, the contributions of SNAP-25 isoform to these mechanisms are still unknown.

TABLE OF CONTENTS

ABSTRACT	vi
LIST OF FIGURES	xii
LIST OF TABLES	xiii
CHAPTER 1 - INTRODUCTION	1
Learning and Memory.....	1
Hippocampus	4
Current Density Analysis.....	9
Short-term plasticity.....	11
Calcium domains and release.....	13
Organization of Neurotransmitter Release.....	14
Calcium hypothesis.....	16
Calcium Regulation and PPF	19
Development.....	22
SNAP-25.....	24
CHAPTER 2 - SPECIFIC AIMS	28
Hypothesis.....	28
Specific Aims.....	28
CHAPTER 3 - MODELING OF PRESYNAPTIC MECHANISMS	30
Presynaptic and Postsynaptic recordings	30
Release Probability and Vesicle Release	30
Model 1-Mechanism of $[Ca^{2+}]_{res}$ Clearance Model	32
Details of Modeling of $[Ca^{2+}]_{res}$ Clearance.....	34

Model 2-Presynaptic Depletion and Probability of Release Model.....	40
Details of Presynaptic Depletion and Probability of Release Model.....	40
Discussion.....	43
CHAPTER 4 - DEVELOPMENTAL CHANGES IN PRESYNAPTIC CA²⁺ CLEARANCE KINETICS AND SYNAPTIC PLASTICITY IN MOUSE SCHAFFER COLLATERAL TERMINALS.....	45
Abstract.....	45
Introduction.....	46
Materials and Methods.....	48
Results.....	53
Discussion.....	68
CHAPTER 5 - ALTERED REGULATION OF PRESYNAPTIC RESIDUAL CA²⁺ IS DEPENDENT ON SNAP-25 IN HIPPOCAMPAL SYNAPSES IN MICE.....	75
Abstract.....	75
Introduction.....	76
Materials and Methods.....	78
Results.....	84
Discussion.....	100
CHAPTER 6 - DISCUSSION	107
Major Findings.....	108
Limitations/Future Directions.....	113
Impact	119
APPENDIX A	122
<i>Snap25^{tm2Mcw}</i> mice.....	122
<i>Snap25^{tm1Mcw}</i> mice.....	123

APPENDIX B -PROGRAMS FOR $[Ca^{2+}]_I$ ANALYSIS.....	125
Import_abf10a.....	125
Reada/summarize.....	127
Testplot.....	129
Double Exponential Fit.....	130
APPENDIX C – POTENTIAL BIOMEDICAL APPLICATIONS OF COATED COLLOIDAL NANOCRYSTALS.....	131
A. Quantum Dots as sensors of membrane potential.....	132
B. Quantum Dots as sensors of pH.....	136

List of Figures

Figure 1.1 Hippocampal Pathways.	5
Figure 1.2 Paired pulse facilitation example.....	7
Figure 1.3 Layers of the hippocampus.....	9
Figure 1.4 Principles of current source density.	10
Figure 1.5 Vesicular recycling in the presynaptic terminal.	16
Figure 1.6 Vesicular Ca^{2+} Domains.....	17
Figure 1.7 Presynaptic Ca^{2+} regulation mechanisms.	21
Figure 1.8 Developmental timeline.....	23
Figure 3.1 Ca^{2+} clearance kinetics.	37
Figure 3.2 Flowchart showing model adapted from (Bark <i>et al.</i> , 2004).....	41
Figure 3.3 Relationship of R1 to R2.	42
Figure 4.1 Developmental increase in short-term synaptic plasticity.....	54
Figure 4.2 Developmental changes in presynaptic $\int v\Delta F/F_0$	56
Figure 4.3 Developmental changes in presynaptic $[\text{Ca}^{2+}]_{\text{res}}$ kinetics.....	58
Figure 4.4 Kinetic components of $[\text{Ca}^{2+}]_{\text{res}}$ evaluated from fits to $\Delta F/F_0$	60
Figure 4.5 Developmental changes in the effect of thapsigargin on $[\text{Ca}^{2+}]_{\text{pre}}$ clearance. .	63
Figure 4.6 Age-dependent differences in basal loading state of Ca^{2+} stores.	64
Figure 4.7 Developmental increase in $[\text{Ca}^{2+}]_{\text{res}}$ during paired-pulses.....	67
Figure 5.1 Effect of genotype on short-term facilitation.	85
Figure 5.2 Fits of model to paired-pulse fEPSP.	87
Figure 5.3 Facilitation during paired-pulses.	90
Figure 5.4 Presynaptic $[\text{Ca}^{2+}]_{\text{res}}$ kinetics during paired-pulses at 50 ms interpulse intervals.....	92
Figure 5.5 Determination of Ca^{2+} buffering.	96
Figure 5.6 Accumulation of background Ca^{2+} during stimulus trains.....	99
Figure 6.1 Schematic of developmental changes of the presynaptic terminal.....	109
Figure 6.2 Schematic of SNAP-25 effect at the presynaptic terminal.....	112
Figure A.1 Splicing Strategy.....	122
Figure A.2 Quantitative real time PCR.....	124
Figure C.1 QD exposed mouse hippocampal neurons.....	131
Figure C.2 Water-soluble Micelles.	133
Figure C.3 Potential sensing QD in cultured hippocampal neurons.....	134
Figure C.4 Potential sensing QD in rat hippocampal slices.....	135
Figure C.5 Overlap of emission spectra of SNARF and QD.....	141
Figure C.6 Absorption spectra of QD and SNARF-1, conjugation.	142
Figure C.7 FRET-based quenching of quantum dot/SNARF dye conjugates.	143
Figure C.8 SNARF-QD pH dependence.....	144
Figure C.9 Concentration-dependent quenching by SNARF-1.	145
Figure C.10 SNARF quenching of quantum dot emission is stable after storage.	146
Figure C.11 Fluorescent lifetime measurements.	147
Figure C.12 Lifetime recovery after photobleaching.....	148

List of Tables

Table 3-1 Fit Parameters for presynaptic Ca^{2+} Model 1	39
Table 3-2 Fixed Parameters for presynaptic Ca^{2+} Model 1	39
Table 3-3 Model 2 Fit Parameters for Figure 3.3	43
Table 5-1 Data from fits to following equation	88
Table C-1 Quantum Yield of commercial quantum dots.....	152
Table C-2 Quenching of quantum dots dependant on pH.....	153

Abbreviations

$\Delta F/F_0$ - Change in Mg Green fluorescence divided by the pre-stimulus fluorescence

$\int \Delta F/F_0$ - Integral of $\Delta F/F_0$

$\int \nu \Delta F/F_0$ - Integral of $\Delta F/F_0$ normalized to peak $\Delta F/F_0$

$\Delta R/R_0$ - Change in Fura2 fluorescence ratio divided by the pre-stimulus fluorescence ratio

$[Ca^{2+}]_{res}$ - Residual presynaptic Ca^{2+} concentration.

$[Ca^{2+}]_o$ - Extracellular Ca^{2+} concentration.

$[Ca^{2+}]_i$ - Intercellular Ca^{2+} concentration.

C. O. D. - Coefficient of Determination.

ER - Endoplasmic reticulum

F1 - $\Delta F/F_0$ of the first of paired pulses

F2 - $\Delta F/F_0$ of the second of paired pulses

fEPSP - Field excitatory postsynaptic potential.

FRET - Förster Resonance Energy Transfer

HET-*Snap25*^{+/-} or heterozygous *Snap25*^{tm1M^{cw}} mice

PMT - Photomultiplier tube.

PPF - Paired pulse facilitation

PPR - Paired pulse ratio

P_R - Probability of release

QD-Quantum Dot, fluorescent colloidal nanocrystal

R_o - Förster distance

R1 - fEPSP of first pulse of a pair of pulses

R2 - fEPSP of second pulse of a pair of pulses

SC-CA1 - Schaffer collateral to CA1 pyramidal neuron

SERCA - Sarco- endoplasmic reticulum Ca^{2+} ATPase

SNAP-25 - Synaptosomal-associated protein 25 kDa

SNARE - Soluble N-ethylmaleimide-sensitive factor

Tkneo - *Snap25*^{Tkneo/Tkneo} or homozygous *Snap25*^{tm2M^{cw}} mice

VGCC - Voltage gated Ca^{2+} channel

WT - wild-type mice

Chapter 1 - Introduction

The first few postnatal weeks are important for the development of brain function in the mouse and, in particular, this is the time period during which the hippocampus develops into its mature form. Importantly, the equivalent period of hippocampal development in humans is a time period during which many mental health diseases have their onset. We have focused on the Shaffer collateral to CA1 pyramidal neuron (SC-CA1) synapse of the hippocampus because of its well-characterized properties of synaptic plasticity and role in long-term memory formation. This plasticity has been shown to be developmentally regulated and dependent on presynaptic residual Ca^{2+} ($[\text{Ca}^{2+}]_{\text{res}}$), but the mechanisms underlying these developmental changes are not well known. The first part of this study investigates alterations in $[\text{Ca}^{2+}]_{\text{res}}$ in the developing mouse hippocampus and correlates these to changes in synaptic plasticity. This is a period during which there is considerable transformation in the expression of presynaptic proteins with important consequences in the development of mature plasticity. The second part of this study is an investigation of the effect of genetic alteration of expression of the important presynaptic protein SNAP-25 on synaptic plasticity and $[\text{Ca}^{2+}]_{\text{res}}$ kinetics.

Learning and Memory

Memory can be divided into two general categories: procedural and declarative. Procedural memory, also called non-declarative, or implicit memory, incorporates perceptual and motor learning and can be either short-term or long-term. Some examples of procedural memory are habituation, sensitization, priming, eye-blink conditioning, puzzle solving, bicycle riding, and the use of numbers. Declarative memory, also called

explicit memory, consists of memories of places, events, facts, and people and it tends to be learned quickly and forgotten as quickly. Declarative memory has two parts: episodic and semantic. Episodic memory is that of the what, where, and when of events in our lives. Semantic memory refers to facts and knowledge that are not linked to a specific event, but help us make categorizations and concepts (Anderson, 1976; Anderson *et al.*, 2004; Anderson *et al.*, 2008).

Episodic and semantic memory, conscious recollection, and flexible expression are primarily affected in patients with temporal lobe epilepsy. Epilepsy is defined as the periodic and unpredictable occurrence of seizures occurring as a sudden attack, spasm, or convulsion that are thought to occur when the balance of excitatory and inhibitory transmission in the brain is disrupted. For instance in the hippocampus, a granule cell of the dentate gyrus excites 10 inhibitory neurons for each CA3 neuron excited (Henze *et al.*, 2002) and disruption of this major inhibitory influence can recruit neuronal circuits into hyper-excitability that can initiate or propagate seizure activity. While seizures vary in onset, duration, strength, and location, they typically start in one brain region and spread to other contiguous regions. The most common type of epilepsy in adults is temporal lobe epilepsy, which most often results from hippocampal sclerosis, a hardening or induration of a tissue, and the study of this condition has provided great insight into the function of the hippocampus. For example, in the 1950s, Wilder Penfield stimulated the temporal lobe including the hippocampus, in the process of identifying epileptic foci in patients Penfield, (Penfield, 1952). These patients reported the triggering of mental experiences such as hearing voices or music and having flashbacks of past experiences at the time when the temporal lobe or hippocampus was stimulated.

H.M., Henry Gustav Molaison, is perhaps the most famous case study of the importance of the hippocampus for learning and memory. At the age of 9, he suffered brain trauma after a bicycle accident, which resulted in the onset of blackouts and seizures. At the age of 27, he suffered from sudden and severe seizures and he could not continue his job of repairing motors. In 1953 after an increasing severity of his seizures, he underwent a bilateral removal of his temporal lobes including the medial temporal cortex, amygdala, and two-thirds of the hippocampus. This resulted in both retrograde and anterograde amnesia such that he was not able to form new long-term memories or recall major personal or social events. For example, he could not identify himself in recent pictures nor could he identify the doctor who had treated him for over 40 years. However, he still had the ability to form short-term memories lasting a few minutes, and learn new motor tasks (Corkin, 2002). This inability to form long-term memories continued until his recent death on December 2, 2008 (Carey, 2008). His brain is now being studied to better characterize his lesion and determine the exact cause of the amnesia (Landau, 2009).

These observations are not limited to H.M.; rather they are an unfortunate and common sequella of temporal lobe excision. R.B., a patient who had a more specific lesion of the hippocampal CA1 region also showed a deficit in the ability to form new memories of people, places, and events and in his recall of the two years before the lesion occurred (Zola-Morgan *et al.*, 1986). This and other cases have further supported the concept that the hippocampus plays an important role in memory recall, in the formation of declarative memory, and especially in the consolidation of short-term memory (seconds to hours) into long-term memory (hours to years). Numerous animal models,

including those based on physical and chemical lesions and genetic alterations have been used to study the hippocampus and its role in memory formation. In general, these studies have also led to the understanding that the hippocampus plays a role in memory recall – especially of declarative memory (Anderson *et al.*, 2004).

Animal studies have also shown that the hippocampus plays an important role in spatial learning. This is especially apparent with the discovery of place cells in the hippocampus (O'Keefe & Dostrovsky, 1971), and more recently the discovery of grid cells in the entorhinal cortex (Hafting *et al.*, 2005; Fyhn *et al.*, 2008). An important concept is the idea that the network design of the hippocampus creates a gamma frequency filter (interspike interval 10-40 ms), which tunes grid cell firing and leads to crafting of place fields (de Almeida *et al.*, 2009). Further, the organization and recurrent circuitry of the hippocampus is understood to propagate, if not cause, theta waves (4 to 7 Hz), which are in turn believed to help synchronize multiple parts of the brain during memory tasks (Villarrreal *et al.*, 2007; Lubenov & Siapas, 2009).

Hippocampus

The hippocampal formation is an archicortical structure that is located in the temporal lobe in humans and beneath the parietal and temporal neocortex in rodents (see Figure 1.1). It has been extensively studied because of its aforementioned role in learning and memory. In 1587, Arantius named the hippocampus, Greek (ἵπποκαμπος) for sea horse, due to its shape in humans (Amaral & Lavenex, 2007). The interior cellular anatomy and pathways of the hippocampus were first described in the early 20th century by Santiago Ramon y Cajal.

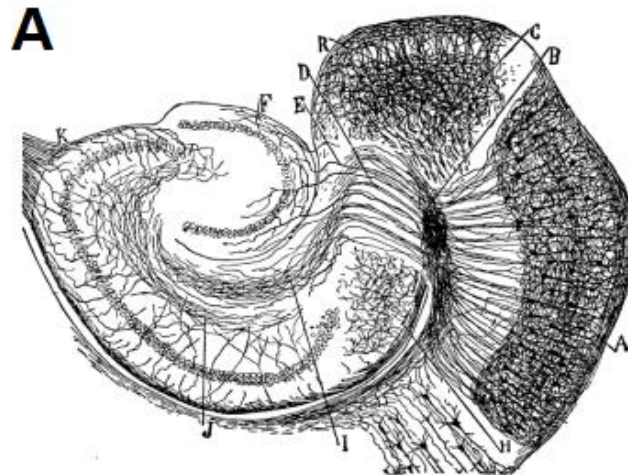


FIG. 493. — Coupe horizontale du ganglion temporal supérieur et de la corne d'Ammon immédiatement au-dessous du plan du cordon angulaire; souris âgée de quinze jours. Méthode de Golgi.

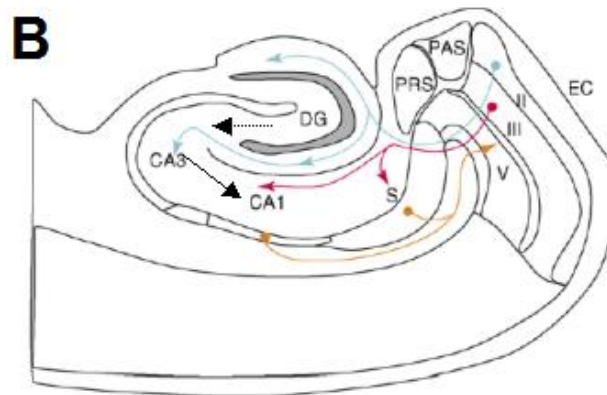


Figure 1.1 Hippocampal Pathways.

A. Drawing of the human hippocampus and its connections to the entorhinal cortex (Ramón y Cajal, 1911). **B.** Simplified drawing showing the pathways of the hippocampus, entorhinal cortex (EC), subiculum (S), dentate gyrus (DG), cornu ammonis regions 1 and 3 (CA1 and CA3), dentate gyrus (DG), parasubiculum (PAS), and presubiculum (PRS) (Witter & Moser, 2006). Arrows indicate direction of signal transduction.

The hippocampal CA (*cornu ammonis*, Latin - horn of Ammon) region was named by De Garengot in 1742 based of its similarity to the shape of the horns of the ram of the Egyptian deity of creation Amun Kneph. Nearly two centuries later in 1934, the CA region was divided into 4 subregions by Lorente de Nó, an apprentice of Ramon y Cajal (Amaral & Lavenex, 2007).

The synaptic connections of the hippocampus are commonly described as a trisynaptic circuit, although this is not entirely appropriate. As shown by the arrows in Figure 1.1B, axons from neurons in the entorhinal cortex enter the dentate gyrus as the perforant path, named due to its 'perforating' of the hippocampal fissure. These glutamatergic axons terminate on the granule cells of the dentate gyrus - the first synapse. The axons of these granule cells, called mossy fibers, form glutamatergic synapses in the adult with pyramidal cells of the CA3 region - the second synapse. Finally, the CA3 pyramidal cells send axons to the septum and also as Schaffer collaterals to the CA1 region - the third synapse. The CA1 pyramidal neurons send axons out of the hippocampus to the subiculum and to the septum and these connections constitute the output of the regional processing of the hippocampus. In addition to the trisynaptic circuit, other important functional circuits are found in the hippocampus and these are shown in Figure 1.1B. For example, perforant path fibers synapse in CA3 and CA1 in addition to their endings in dentate and the CA1 pyramidal cells receive input not only from CA3, but also from layer III of the entorhinal cortex. There are also important interneuronal, recurrent and collateral circuits within the hippocampus that are not shown in Figure 1.1 (Ramón y Cajal, 1911; Witter & Moser, 2006).

The hippocampal formation is admirably suited for electrophysiological studies of brain circuitry and function because of its organization. There are roughly 200,000-300,000 CA3 pyramidal cells, 300,000-400,000 CA1 pyramidal cells, and 700,000-1,000,000 granule cells in the adult rodent hippocampus. As is apparent in Figure 1.1, all of these are arranged in narrow bands with overlapping dendritic trees. This structure aligns the current flow around the dendrites creating summing flux fields from the large

number of cells, which generate measurable extracellular field potentials in response to simultaneous dendritic stimulation (Andersen *et al.*, 1969). For example, Figure 1.2 shows the field potentials (slower downward deflections) following two presynaptic stimuli, which are revealed by the stimulus artifacts (sharp downward deflections) spaced 50 ms apart. The manner by which the cellular alignment of the entire area of the hippocampus allows electrical fields to be measured will be further considered below in the discussion of current density analysis.

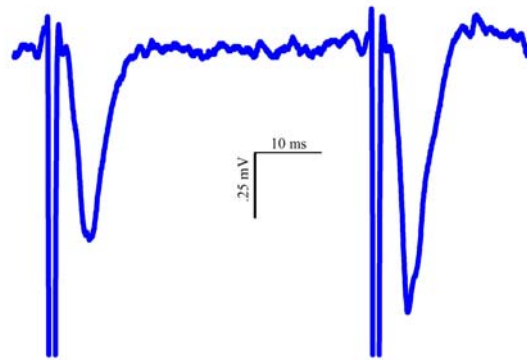


Figure 1.2 Paired pulse facilitation example.

Paired pulse facilitation shown by field potential recordings from stimulation of the SC, recording electrode placed in the stratum radiatum of CA1.

In addition to the gross arrangement of neurons in the hippocampus, there is finer structure within each region resulting in important differences in excitability. In the adult across all of the subfields, 88% of the synapses are excitatory whereas 12% are inhibitory. The CA1 region is separated into distinct strata as shown in Figure 1.3. The *alveus* is the most superficial layer and contains axons directed to the fornix. The *stratum oriens* contains the cell bodies of the basket cells, and basal dendrites of pyramidal neurons, and is the location of recurrent connections that constitute approximately 23% of the excitatory synapses and 29% of the inhibitory synapses of the CA1 region. The *stratum pyramidale* of the CA1 region contains the cell bodies of the pyramidal neurons

and is the site of about 1% of the excitatory synapses and 9% of the inhibitory synapses. The *stratum lucidum*, which is the thinnest layer and often left unlabeled, is found immediately below the *stratum pyramidale* of the CA1 region is named for its relative transparency compared to other layers of the hippocampus, and it contains approximately 18% of the excitatory and 10% of the inhibitory synapses. The *stratum radiatum* of the CA1 contains Schaffer collateral fibers and some interneurons including basket cells, bistratified cells, and radial trilaminar cells and it is estimated to have about 28% of the excitatory synapses and 19% of the inhibitory synapses. The *stratum lacunosum* of the CA1 is a thin stratum that contains both Schaffer collateral fibers and perforant path fibers from the entorhinal cortex. The *stratum moleculare* is the deepest stratum and here there are primarily perforant path fibers forming synapses on the distal dendrites of the pyramidal cells. The combined *stratum lacunosum-moleculare* of the CA1 contains about 30% of the excitatory synapses and 33% of the inhibitory synapses (Megias *et al.*, 2001; Matsuda *et al.*, 2004; Ventriglia & Maio, 2005). The differences in the excitatory-inhibitory balance of the layers, understandably produces different waveforms as measured in the field potentials.

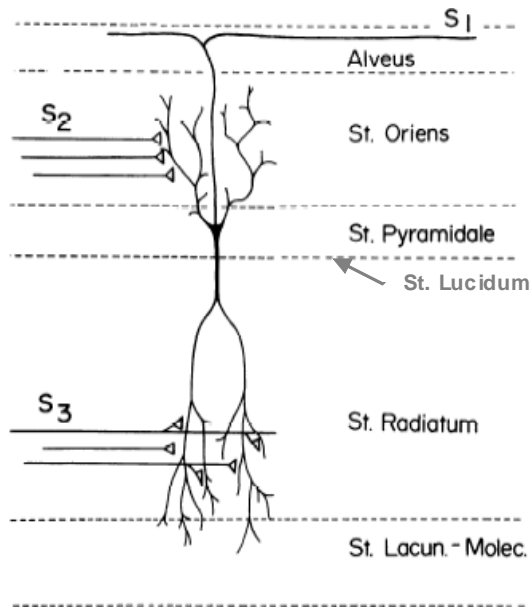


Figure 1.3 Layers of the hippocampus.

Drawing of a CA-1 pyramidal neuron and its orientation through the layers of the hippocampus, the indicated synaptic inputs do not represent an accurate ratio of actual synapses. Adapted from (Richardson *et al.*, 1987).

Current Density Analysis

The structure of the hippocampus with aligned cell bodies and parallel dendrites provides the basis for summation of extracellular fields. Stimulation of multiple presynaptic fibers causes the simultaneous activation of a group of postsynaptic dendrites, which then results in current influx into the dendrites, or a “sink” (Figure 1.4A). The soma of the cell provides the “source” for this current. The flow of the resultant extracellular current through the resistance of the *intercellular* space produces a field potential of a few mV, which is large enough to be detected with an extracellular electrode (Figure 1.4B). This can then be compared with a distant ground and amplified to obtain a measure of the dendritic potential change, which is known as the field excitatory postsynaptic potential or fEPSP.

An extracellular recording electrode measures the current change from a volume up to 50-300 μm from the tip, allowing it to record synaptic activity within this region.

Importantly, the location of the stimulus and recording electrodes affects the signal waveform. This is due to the resulting differences in the locations of the sources and sinks and hence the extracellular current density. For example, excitation of the *stratum radiatum* produces a downward deflection when recorded in the *stratum radiatum*, but a recording electrode in the *stratum lacunosum-moleculare* produces an upward deflection (Figure 1.4B) and recording in the *stratum pyramdale* produces an upward deflection with a superimposed downward deflection resulting from somatic action potentials. These fEPSPs can be analyzed by calculating either the initial slope or the amplitude of the signal and changes in either of these measurements accurately reflect the plasticity of the synapses in a specific region.

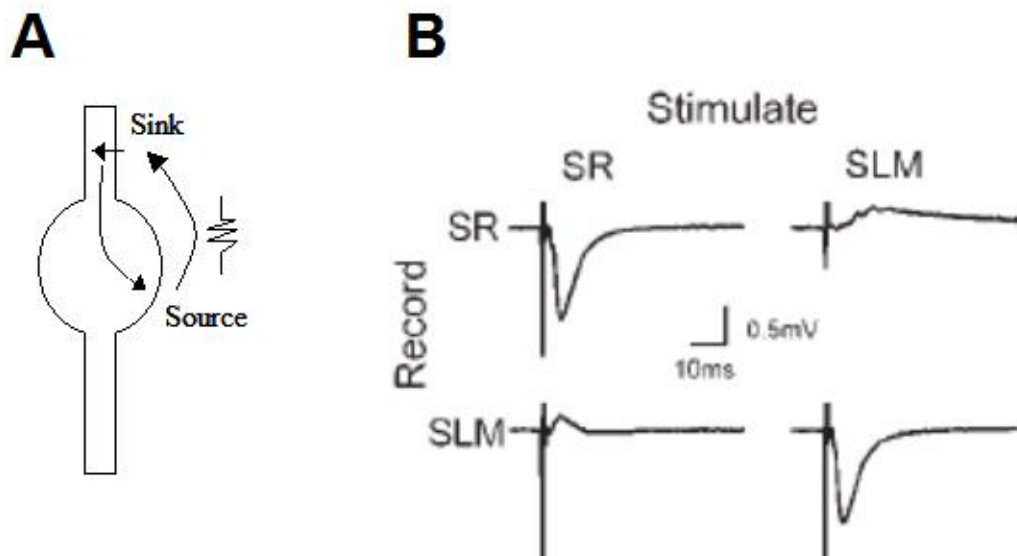


Figure 1.4 Principles of current source density.

A. Current sources and sinks, **B.** Example of recording and stimulus location resulting in differences in deflection of the peak field potential SR-stratum radiatum, SLM- *stratum lacunosum-moleculare* (Speed & Dobrunz, 2009)

Short-term plasticity

The brain displays many forms of plasticity - the mechanism of which are currently being researched - that are crucial to our abilities to learn, remember, and recall. It is thought that memories are first stored in a short-term liable state then consolidated into a longer-term storage form. Although Ramon y Cajal was the first to suggest that changes in synaptic efficacy are important in the storage of memory, it was the Canadian psychologist Donald O. Hebb who first formulated the following idea now known as 'Hebb's learning Rule':

“When an axon of cell A is near enough to excite a cell B and repeatedly or persistently takes part in firing it, some growth process or metabolic change takes place in one or both cells such that A's efficiency, as one of the cells firing on B is increased” (Hebb, 1949)

Synaptic plasticity encompasses long term potentiation (LTP), short-term facilitation, augmentation, depression, and other modifications of synaptic efficacy, which have time courses ranging from milliseconds to hours and longer. Timothy Bliss and Terji Lomo carried out important early experiments recording the phenomena of synaptic plasticity in working synapses in the 1970s. They observed that there is a persistent enhancement of the response to a single stimulus delivered before and after a high-frequency tetanus, which is known as long-term potentiation (LTP) (Bliss & Lomo, 1973). Although long-term plasticity, such as LTP, involves important postsynaptic translational or transcriptional modifications, short-term plasticity is believed to result from a transient increase in the activation of presynaptic proteins by the presynaptic $[Ca^{2+}]_{res}$ from a previous stimulus. This presynaptic protein activation promotes enhanced vesicle fusion in response to subsequent stimulation (Zucker & Regehr, 2002).

Specifically, paired-pulse facilitation (PPF) is the enhancement of presynaptic neurotransmitter release in response to a second pulse occurring between 50 and 300 ms after an initial pulse (e.g. see Figure 1.3). For example, a 50 ms interpulse-interval produces the maximal paired facilitation at the SC-CA1 synapse (Partridge & Valenzuela, 2002). Importantly, this range of interpulse intervals is equivalent to repetitive firing at 10 to 20 Hz, and is within the physiological range recorded in an awake animal (Jones & Wilson, 2005b, a). The combination of PPF and paired-pulse depression (PPD) at the hippocampus SC-CA1 synapse allow these synapses to selectively enhance signals at a specific frequency thereby producing a band-pass filter with a center frequency of about 20 Hz (Partridge & Valenzuela, 2002). Similar band-pass filters are integral to signal processing in many electronic devices enabling them to selectively receive information at specific frequencies while eliminating information (noise) at other frequencies. It is not surprising that the brain appears to use information processing mechanisms that are similar to those common in electronics.

Theta rhythms, which are characterized by oscillatory activity of between 4 and 8 Hz have been observed in the hippocampus and cortex during both sleep states and states of quiet focus, and have been recorded during certain short-term memory tasks (O'Keefe & Dostrovsky, 1971; Wood *et al.*, 1999; Vertes, 2005). Interestingly, a 5Hz signal can be used to induce LTP and the action potential frequencies characteristic of PPF have been shown to be phase locked to the underlying theta waves in the hippocampus. This correlation has been suggested to reflect a role in memory formation and recall (Huhn *et al.*, 2005; Jones & Wilson, 2005a; Burgess *et al.*, 2007).

Calcium domains and release

The manner by which a neuron transfers its signal to another cell was first understood through investigations of neurotransmitter release in the frog neuromuscular junction. In these experiments, the amplitudes of minimal postsynaptic responses were measured and it was found that they occurred in distinct units or quanta (Del Castillo & Katz, 1954a; Boyd & Martin, 1956). Further studies suggested that these quanta reflected the release of individual synaptic vesicles (Del Castillo & Katz, 1954a).

Electron microscopic studies have shown a presynaptic organization of vesicles around an area termed the active zone, which is a specialized structure spanning both the pre and postsynaptic sides of the synapse (Bailey *et al.*, 1981; Landis *et al.*, 1988). In freeze fracture electron micrographs, distinct particles can be observed in the membrane that have been suggested to be the voltage-gated Ca^{2+} channels (VGCCs) that are responsible for the Ca^{2+} influx necessary for vesicle fusion for neurotransmitter release (Landis *et al.*, 1988). The proteins responsible for vesicle release in fast-acting synapses are thought to be within 10 nm (Schneggenburger & Neher, 2000) to 30-300 nm of these VGCCs (Meinrenken *et al.*, 2002). In more slowly releasing terminals, such as those involved in neuropeptide secretion, the vesicle release proteins are not located near VGCCs and thus the distinct active zone necessary for rapid release is lacking (Sudhof, 2004).

The vesicle distribution is dependent on the molecular assembly of proteins in the active zone including synapsin 1 (Landis *et al.*, 1988) and actin (Hirokawa, 1989). These and other presynaptic proteins are important in neurotransmitter release and may also play a role in synaptic plasticity because $[\text{Ca}^{2+}]_i$ can affect their level of phosphorylation (Greengard *et al.*, 1993). For example, the dephosphorylated form of synapsin binds to

both cytoskeletal proteins and to synaptic vesicles. Calcium activates CaM kinase II, which then phosphorylates synapsins, which then release from cytoskeletal elements allowing the movement of synaptic vesicles from the readily releasable pool (RRP) to the active zone (Turner *et al.*, 1999). Synaptotagmin is another abundant membrane protein of the vesicle release complex; it has two Ca^{2+} binding sites and is present in the membrane as a dimer with multiple activation states and it plays a role in the docking and fusion of vesicles. Synaptophysin is the most abundant vesicle membrane protein and it also has both phosphorylation and Ca^{2+} binding sites (Rubenstein *et al.*, 1993; Johnson & Wu, 1995).

Organization of Neurotransmitter Release

In order for fast release of neurotransmitter to occur from a presynaptic terminal to occur a filled vesicle needs to fuse with the presynaptic membrane. This fusion process requires the interaction of soluble *N*-ethylmaleimide-sensitive factor attachment protein receptor (SNARE) proteins, both associated with the target membrane (t-SNARE) and with the vesicle (v-SNARE), (Sollner *et al.*, 1993). It is believed that these two SNARE components form a 4 barrel coiled-coil structure (Sutton *et al.*, 1998) producing a zipper-like interaction with each other that reduces the distance between the plasma membrane and vesicle (Sorensen *et al.*, 2006) thereby allowing the vesicles to fuse and release neurotransmitter into the synaptic cleft. Synaptosomal-associated protein of 25kDa (SNAP-25) is a t-SNARE that has been shown to play a role in Ca^{2+} -dependent vesicular fusion (Sorensen *et al.*, 2002). In hippocampal SC-CA1 synaptic boutons, this fusion is the result of Ca^{2+} binding to synaptotagmin, which allows the complete zippering of SNARE complexes composed of SNAP-25/Syntaxin and vesicle-associated

membrane protein (VAMP). Synaptotagmin thus initiates changes in structural conformation, which in turn allows it to overcome an energy barrier allowing the fusion of the synaptic vesicle membrane and the plasma membranes (Abdulreda *et al.*, 2008).

While the process of filling and releasing a single vesicle can take up to minutes (Heuser & Reese, 1973), neurons can continually release vesicles over extended time periods without depleting the available vesicles. This requires a storage pool of vesicles that can be immediately primed to replace vesicles as they are released. Thus, neurotransmitter-containing vesicles have been found to comprise a number of pools that are based on their probability of release. These pools include the reserve pool, the previously mentioned RRP, the docked pool, and the primed pool (Figure 1.5).

Vesicular pools are developed through the maturation of the fusion competence of the neurotransmitter-containing synaptic vesicles. New vesicles are produced at the trans-Golgi network; however, vesicles are also assembled from retrieved material after membrane fusion. Classically, these fused vesicles are endocytosed from the synaptic membrane in a clathrin-dependent manner that often forms part of the early endosome before the vesicles are available for repackaging (Figure 1.5). These synaptic vesicles are then sorted, filled, and moved to the reserve pool. Another recycling method, which does not require clathrin coating, is 'kiss and run' release where the vesicle does not completely fuse with the membrane. During this form of release, the vesicles do not lose their structure so the recycling process is faster and does not require early endosomal sorting (Sudhof, 2004). The distribution of vesicles in these pools have been shown to be effected by Ca^{2+} signaling (Llinas *et al.*, 1991; Greengard *et al.*, 1993; Mukhamedyarov *et al.*, 2010).

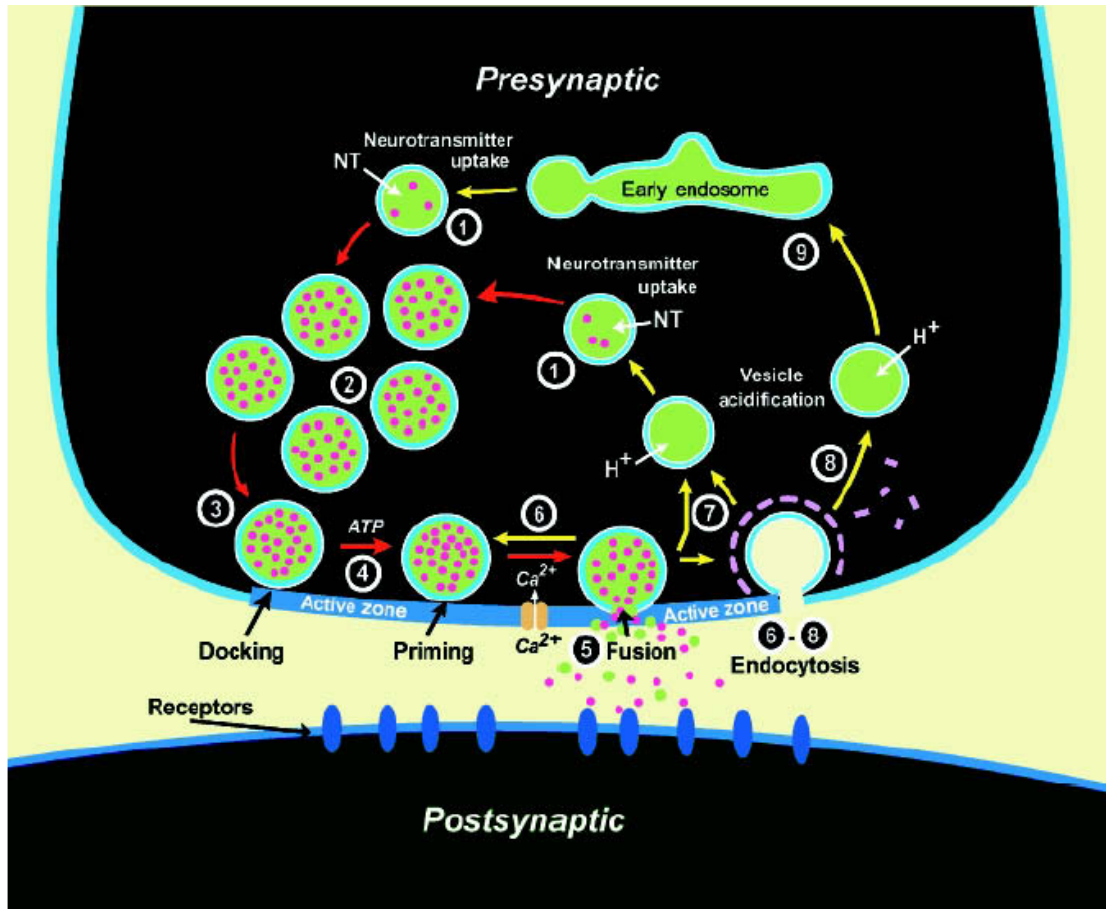


Figure 1.5 Vesicular recycling in the presynaptic terminal.

Diagram of a presynaptic terminal, depicting the stages of the synaptic vesicle cycle, (1) filling/formation of vesicle (2) reserve pool, (3) priming stage, (4) pre-Ca²⁺ binding, (5) fusion pore opening and neurotransmitter release (6) endocytosis (7) recycling (8) clathrin uncoating return to the endosome (Sudhof, 2004).

Calcium hypothesis

The role of Ca²⁺ in an underlying mechanism of presynaptic vesicle fusion and release of neurotransmitter with a subsequent postsynaptic response was first described in motor nerve endings. Katz and Meledi demonstrated that in a 0 mM Ca²⁺ extracellular Ringers solution, a brief pulse of extracellular Ca²⁺ was required to permit a postsynaptic response and it was necessary that this pulse be applied immediately prior to the

stimulation. This provided strong evidence for an essential role for Ca^{2+} in presynaptic release (Katz & Miledi, 1967).

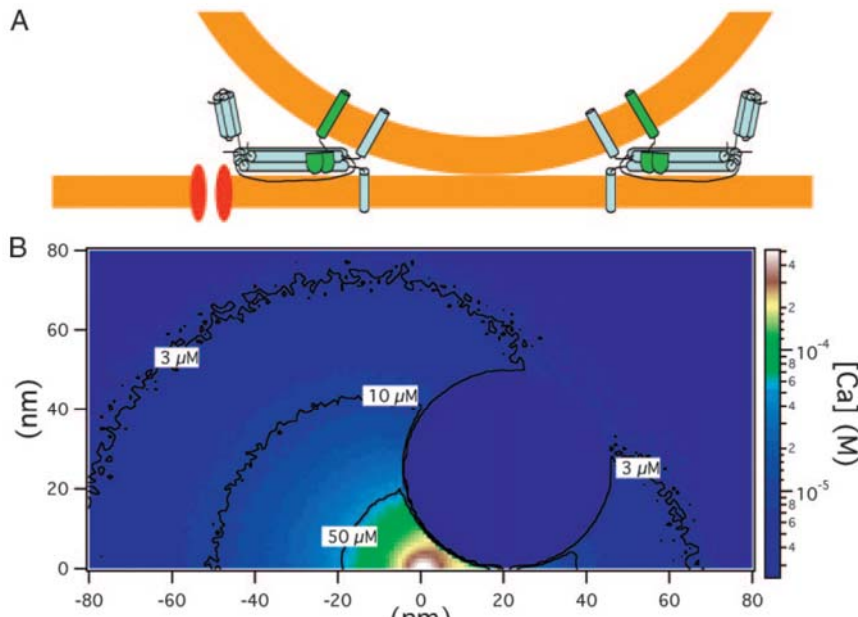


Figure 1.6 Vesicular Ca^{2+} Domains.

Relationship of VGCCs, synaptic vesicles and Ca^{2+} domains. **A**, View of the predicted arrangement of VGCC (red), vesicle (orange), synaptotagmin (green) and SNARE complex (light blue). **B**: Pseudo-colored contour map of predicted nanodomains of $[\text{Ca}^{2+}]$ after opening of the VGCC and constant $[\text{Ca}^{2+}]$ contour profiles for a cross section through the VGCC at (0, 0), the center of the vesicle at (20 nm, 25 nm) (Shahrezaei & Delaney, 2005).

The resting $[\text{Ca}^{2+}]_i$ in a neuron is around 50-100 nM, and a rise in $[\text{Ca}^{2+}]_i$ is needed to trigger release and activate mechanisms of synaptic plasticity. Following activation of VGCCs, $[\text{Ca}^{2+}]$ establishes steep spatial gradients in the cytoplasm that form functional nano- and microdomains (Figure 1.6). As discussed above, in the vicinity of the VGCC $[\text{Ca}^{2+}]_i$ rises to μM levels binding to the low affinity Ca^{2+} sites on proteins responsible for Ca^{2+} dependent vesicular fusion, while the opposite side of the vesicle in the vicinity of the hypothesized facilitatory, high affinity Ca^{2+} binding sites, $[\text{Ca}^{2+}]_{\text{res}}$ rises to no more than a few hundred nM (Johnson & Wu, 1995). Tight regulation of $[\text{Ca}^{2+}]_i$ is important not only at high and low affinity release sites in presynaptic terminals, but for a

multitude of other cellular processes. For example, while vesicle fusion requires activation of a low affinity Ca^{2+} sensor such as synaptotagmin, the movement from the reserve pool to the recycling and RRP requires activation of a high affinity Ca^{2+} sensor, CamKII (Llinas *et al.*, 1991; Greengard *et al.*, 1993; Mukhamedyarov *et al.*, 2010).

Ca^{2+} influx underlying fast vesicular release is primarily due to activation of VGCCs. There are at least four functionally and pharmacologically distinct, broad classes of VGCCs observed in neurons: L-, T-, N-, and P-type VGCC. L-type VGCCs (L for Long lasting) are high-threshold (half-maximum activation -15 mV) and are sensitive to block by Cd^{2+} , nimodipine, and nifedipine. T-type VGCCs (T for Transient) type VGCCs are activated at potentials near rest (half-maximum activation -40 mV), have strong voltage, but not Ca^{2+} -dependent inactivation, and are sensitive to Ni^{2+} , but not dihydropyridines. N-type (N for Neither L or T) are intermediate channels between L- and T-type VGCCs that have a moderate conductance and half-maximum of activation of -25 mV. N-type VGCCs are insensitive to dihydropyridines, but blocked by ω -conotoxin-GVIA and modulated by binding of neurotransmitters. P-type VGCCs (P for Purkinje) have similar conductance to the N-type, however, they have less complete inactivation, are insensitive to both dihydropyridines and ω -conotoxin-GVIA, but are blocked by ω -Agatoxin-IVA. It is thought that P- and N- type VGCCs play a role in fast neurotransmitter release, while L type VGCCs are responsible for slower release of neurotransmitters such as catecholamines and neuropeptides (Catterall, 1999).

Other types of Ca^{2+} channels including Q- and R- type have also been described, but they have not been completely pharmacologically characterized. The R-type Ca^{2+} channel has been shown to play a role in after depolarization and bursting in hippocampal

CA1 pyramidal neurons and is blocked by Ni^{2+} (Metz *et al.*, 2005). The Q-type VGCC has slow kinetics and a high threshold of activation (Wheeler *et al.*, 1994).

Presynaptic modulation such as that by CAMKII activation, $[\text{Ca}^{2+}]$, and protein expression levels can effect Ca^{2+} entry through VGCC (Catterall & Few, 2008). The interaction of SNAP-25 with either P/Q or N-type VGCCs reduces channel opening and shifts the voltage dependence of inactivation toward more negative membrane potentials (Bezprozvanny *et al.*, 1995; Wisner *et al.*, 1996; Zhong *et al.*, 1999). This interaction is thought to occur by binding of SNAP-25 to a synaptic integration site (synprint) (Rettig *et al.*, 1996; Kim & Catterall, 1997; Yokoyama *et al.*, 2005). The synprint site was first identified in N-type VGCCs, but has since been shown to be present on other VGCCs, and it has been shown to be a mechanism by which presynaptic proteins regulate Ca^{2+} influx after stimulation (Catterall, 1999). This interaction is sensitive to protein kinase C and CAMKII phosphorylation of both the VGCC and SNARE proteins (Yokoyama *et al.*, 1997; Pozzi *et al.*, 2008). The inhibitory effects of SNAP-25 on Ca^{2+} entry through VGCCs can be relieved by increasing expression of synaptotagmin-1 (Wisner *et al.*, 1997; Zhong *et al.*, 1999) through formation of a complete synaptotagmin/SNARE complex, which increases Ca^{2+} influx through VGCCs associated with docked synaptic vesicles. It has been suggested that these mechanisms of Ca^{2+} regulation play a role in the regulation of synaptic plasticity (Dittman *et al.*, 2000; Tsujimoto *et al.*, 2002; Sippy *et al.*, 2003; Mochida *et al.*, 2008).

Calcium Regulation and PPF

PPF is generally accepted to be initiated downstream from, and dependent upon, $[\text{Ca}^{2+}]_{\text{res}}$ in the presynaptic terminal (Zucker & Regehr, 2002). The mechanisms by

which $[Ca^{2+}]_{res}$ is regulated are thus very important in determining short-term synaptic plasticity. $[Ca^{2+}]_{res}$ can be regulated by either passive or active processes (Augustine & Neher, 1992). There are a number of mechanisms, which help to regulate the $[Ca^{2+}]_{res}$ after a stimulus. In addition to passive diffusion and buffering, there is the possibility of Ca^{2+} regulation through ATP-dependent processes such as the sarcoplasmic endoplasmic reticular Ca^{2+} -ATPase, the Na/Ca exchanger, the mitochondria Ca^{2+} uniporter, the plasma membrane Ca^{2+} -ATPase, and Ca^{2+} uptake into lysosomes (see Figure 1.7). Contributions to the regulation of $[Ca^{2+}]_{res}$ by presynaptic Ca^{2+} buffers and by uptake and release from the ER have been an important focus in previous studies of the involvement of $[Ca^{2+}]_{res}$ in short-term plasticity in the rodent hippocampus (Scullin & Partridge, 2010).

Diffusion and buffering influence the removal of $[Ca^{2+}]_{res}$ from the presynaptic terminal and consequently short-term plasticity (Wasling *et al.*, 2004; Collin *et al.*, 2005). Although the $[Ca^{2+}]_{res}$ decay kinetics in the adult rodent SC-CA1 synapse are not significantly affected by Ca^{2+} buffer saturation (Blatow *et al.*, 2003), a small but significantly increased role of buffer saturation has been demonstrated in immature SC-CA1 synapses (Wasling *et al.*, 2004). This alteration in buffering capacity suggests that there are developmental changes in the mechanism that regulate the $[Ca^{2+}]_{res}$ in these synapses. In addition to diffusion and buffering, the processes of extrusion, sequestration, and release from internal stores have been postulated to play developmentally-regulated roles in $[Ca^{2+}]_{pre}$ dynamics (Neher & Augustine, 1992; Koester & Sakmann, 2000). Furthermore, there is conflicting evidence regarding the role of internal stores as a source of Ca^{2+} during PPF, which will be discussed further in Chapter 4 (Emptage *et al.*, 2001; Carter *et al.*, 2002; Cabezas & Buno, 2006).

Studies using caged Ca^{2+} in the crayfish neuromuscular junction revealed the likelihood of a second Ca^{2+} binding site that has a higher-affinity than the Ca^{2+} release triggering site, but slower kinetics that could affect the probability of release during the second of paired-pulses (Zucker, 1999). This high affinity Ca^{2+} binding site has been suggested to be the mechanism for the $[\text{Ca}^{2+}]_{\text{res}}$ -based facilitation seen at these short time periods of a few hundred milliseconds (Zucker & Regehr, 2002). In both guinea pigs and rats, it has been shown that the enhancement of the second pulse (R2) over the first pulse (R1) in paired-pulse facilitation in the SC-CA1 synapse is a function of the $[\text{Ca}^{2+}]_{\text{res}}$ from R1 (Wu & Saggau, 1994; Schiess *et al.*, 2006).

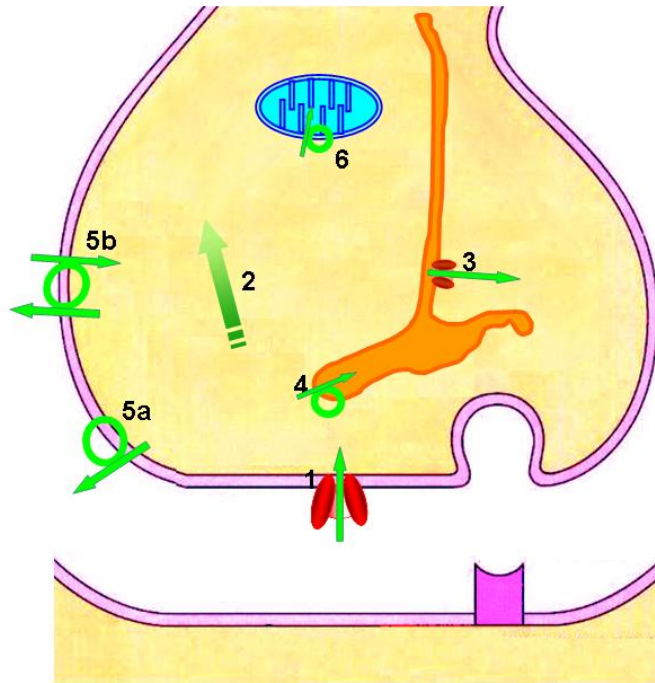


Figure 1.7 Presynaptic Ca^{2+} regulation mechanisms.

Potential major $[\text{Ca}^{2+}]_{\text{res}}$ regulation mechanisms in the presynaptic terminal. (1) VGCCs (2) passive diffusion or buffering (3) ryanodine receptors in the endoplasmic reticulum (4) sarco-endoplasmic reticulum Ca^{2+} -ATPase (5) a) Na/Ca exchanger or the plasma membrane b) Ca^{2+} -ATPase (6) mitochondrial Ca^{2+} uniporter.

Interestingly, changes in Ca^{2+} regulation have been suggested in early and late stages of Alzheimer's disease in both the dentate and CA1 region of the hippocampus due to altered expression of L-type VGCCs (Coon *et al.*, 1999). These potential changes are thought to play a role in deficits in learning both in diseases such as Alzheimer's and during aging (Landfield, 1996), potentially due to an increase in seizure activity (Palop & Mucke, 2009). The known changes in VGCCs due to increased seizure activity suggest that a more intensive investigation of the actual differences in underlying $[\text{Ca}^{2+}]_{\text{res}}$ regulation in the hippocampus is warranted particularly after increased seizure activity.

Development

The early postnatal period of rodent hippocampus development correlates with the adolescent developmental period in humans during which the onset of many neurological disorders are believed to occur, including obsessive compulsive disorder, attention deficit hyperactivity disorder, epilepsy, and schizophrenia (Anderson, 2002; Dumas, 2005).

While little is known about presynaptic development (Hanse *et al.*, 2009), postsynaptically marked developmental changes occur in the rodent hippocampus during the first three weeks after birth both in terms of the differential regulation of proteins and in differentiation and maturation of cell types (Dumas, 2005; Danglot *et al.*, 2006). For example, the subunit composition of NMDA receptors changes from primarily NR1 and NR2B to NR1 and NR2A and this results in shortening of NMDA receptor-mediated responses (Dumas, 2005). There are also changes in the predominant subtype of VGCCs from N- to P/Q-type VGCCs and a simultaneous loss of L-type VGCCs. Additionally, expression levels and isoform expression of proteins with potentially important roles in synaptic plasticity and Ca^{2+} sensitivity have been shown to occur during this maturational

period, including, adenylyl cyclases 1 and 8 (Conti *et al.*, 2007), CDK1/4 (Li *et al.*, 2007), and SNAP-25 (Bark *et al.*, 1995).

These changes in the cellular expression levels of proteins lead to different physiological characteristics of those cells, for example, GABAergic neurons change from excitatory to inhibitory at about the 6th postnatal day (P6) in the rodent hippocampus. Additionally, there is a critical period of synapse formation in the hippocampus during this same time period in rodents and it is during this time period that growth cones change to functional synapses in hippocampus. Figure 1.8 shows this critical period in human hippocampus (Ben-Ari, 2002).

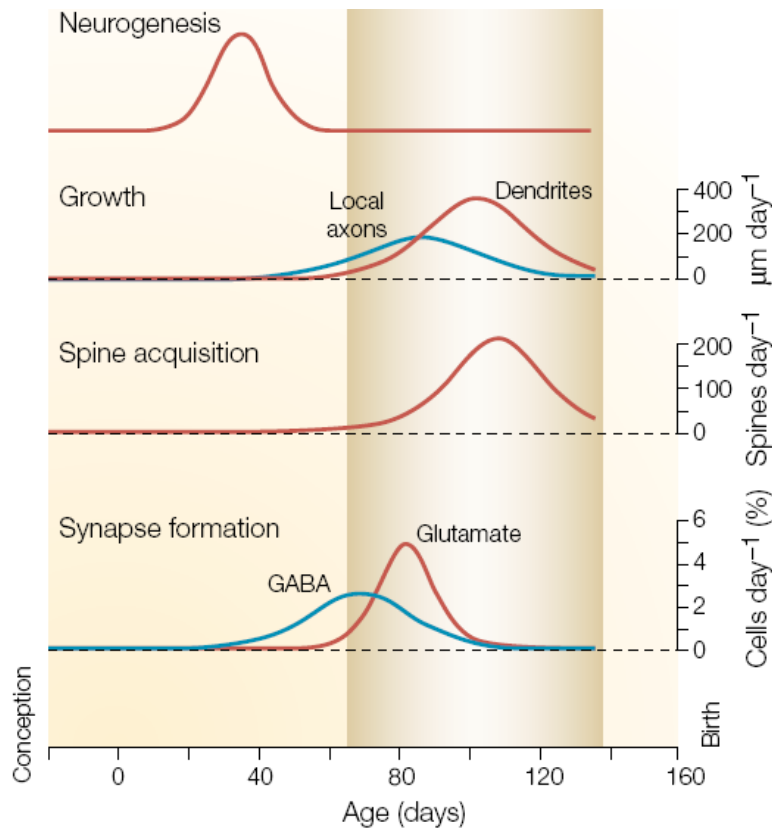


Figure 1.8 Developmental timeline.

Timeline of human hippocampal development showing relative timing of initial neuron formation and axon and synapse formation (Ben-Ari, 2002).

The amount of PPF in hippocampal CA3-CA1 synapses is developmentally regulated in both rats with monotonically increasing amounts of facilitation during the first to second week after birth (Wasling *et al.*, 2004; Dekay *et al.*, 2006) and mice (Schiess *et al.*, 2005). It has been suggested that the increase in plasticity first seen in juveniles is due to a decrease in probability of release of the first pulse in adult animals possibly due to a decrease in Ca^{2+} regulation resulting in less synchronous Ca^{2+} transients (Wasling *et al.*, 2004; Dekay *et al.*, 2006). While these studies compare the probability of release and amount of facilitation developmentally, they do not address the presynaptic contribution to this facilitation. As discussed above, the amount of PPF directly correlates to $[\text{Ca}^{2+}]_{\text{res}}$ in adults (Wu & Saggau, 1994; Schiess *et al.*, 2006). However, the developmental maturation of Ca^{2+} dynamics underlying this alteration of facilitation phenomenon is not well understood. The first aim of this study is to characterize the developmental changes in presynaptic $[\text{Ca}^{2+}]_{\text{res}}$ regulation in the mouse hippocampus.

SNAP-25

As discussed above, SNAP-25 plays a central role in Ca^{2+} -dependent vesicle release, although not in Ca^{2+} -independent release (Washbourne *et al.*, 2002; Bronk *et al.*, 2007). Alterations in polymorphisms and/or expression levels of SNAP-25 have been linked to IQ deficits (Gosso *et al.*, 2006), epilepsy (Geddes *et al.*, 1990; Grumelli *et al.*, 2008)}, schizophrenia (Thompson *et al.*, 1998; Thompson *et al.*, 2003), and attention-deficit hyperactivity disorder (Coghill & Banaschewski, 2009) reviewed in (Corradini *et al.*, 2009). Importantly, multiple mouse models with developmental alterations of expression of SNAP-25 have been shown to lead to a phenotype of seizure susceptibility (Bark *et al.*, 2004; Johansson *et al.*, 2008; Bark, 2009) (also see Appendix A).

Changes in expression levels of SNAP-25 occur during the important time period of synapse formation (Oyler *et al.*, 1989; Catsicas *et al.*, 1991; Oyler *et al.*, 1991) and selective elimination suggest that SNAP-25 could play a role in axonal elongation and growth cones (Osen-Sand *et al.*, 1993). SNAP-25 undergoes a developmental change in isoform expression from primarily SNAP-25a to a mixture of SNAP-25a and SNAP-25b, with the majority in adults being SNAP-25b (Bark *et al.*, 1995). This change may underlie developmental changes in efficacy or plasticity of Ca²⁺-dependent vesicular fusion. In adults, these isoforms have been shown to have differential expression patterns with SNAP-25a primarily found in neuroendocrine cells (Bark *et al.*, 1995), both isoforms found in insulin-producing pancreatic (Gonelle-Gispert *et al.*, 1999) and adrenal cells (Grant *et al.*, 1999). Furthermore, the expression and location of the isoforms has been shown to be developmentally regulated (Boschert *et al.*, 1996).

Detailed investigation of the differences in release kinetics in chromaffin cells suggest that SNAP-25b, in comparison to SNAP-25a, promotes the maintenance of vesicles in a primed state due to a decrease of the inverse rate constant (k_{-1}) of the primed state (Sorensen *et al.*, 2003). SNAP-25a and SNAP-25b are differentially spliced isoforms that differ by only nine out of a total of 206 amino acids (Bark, 1993; Bark & Wilson, 1994; Bark *et al.*, 1995); three of note are amino acids N65D, H66Q, and Q69K, which underlie the kinetic differences between the two isoforms resulting in a larger number of vesicles in the primed state with SNAP-25b (Nagy *et al.*, 2005). There is also a change in the location of one of four cysteines that function as palmitoylation sites and have been shown to be important in the role of SNAP-25 in vesicular release (Graham *et al.*, 2002; Nagy *et al.*, 2005).

The developmental change in SNAP-25 isoform expression also correlates with a developmental change in the RRP size seen in cultured hippocampal neurons (Mozhayeva *et al.*, 2002). Furthermore, SNAP-25 null mutant chromaffin cells, transfected with SNAP-25b, have an increase of the RRP compared to those rescued by SNAP-25a expression (Sorensen *et al.*, 2003; Nagy *et al.*, 2004). Preliminary studies carried out in hippocampal slices of the adult SNAP-25 Tkneo mice, suggest that these mice, which have decreased expression of SNAP-25b and a concomitant increase expression of the SNAP-25a isoform, when compared to WT adult mice, exhibit increased PPF (Bark *et al.*, 2004). These same mice appear to have a larger RRP than WT adults, and a faster rate of release (Denis Bragin and Wolfgang Müller, unpublished), both of these observations are in contrast to results obtained in the transgene rescued chromaffin cells and neurons.

Additionally, SNAP-25 is suggested to play a role in regulating Ca^{2+} influx through N, P/Q, and L- type VGCCs. SNAP-25 that is not associated with the SNARE complex can inhibit P/Q type VGCCs, allowing for the ability to regulate Ca^{2+} influx in those areas with docked synaptic vesicles (Zhong *et al.*, 1997; Catterall & Few, 2008). There is also increased binding of the SNARE complex to the N-type VGCCs at 10-30 μM $[\text{Ca}^{2+}]$, suggesting that these associations could play a role in regulating release (Catterall, 1999). Further, studies suggest that there may be an isoform-dependent regulation of Ca^{2+} flux due to differential phosphorylation of serine 187 (Pozzi *et al.*, 2008). Interestingly, S187 is located near amino acids 66 and 69 that are different between the two isoforms (Tafuya and Wilson, unpublished observation) based on the crystal structure (Sutton *et al.*, 1998). SNAP-25 regulates $[\text{Ca}^{2+}]_{\text{pre}}$; increased expression

of SNAP-25 in GABA neurons is attributed to lower Ca^{2+} responsiveness, and a truncated form of SNAP-25 (1-180) inhibits the Ca^{2+} response sensitivity (Verderio *et al.*, 2004).

The enhancement of PPF at a 50 ms interpulse interval in Tkneo mice SC-CA1 synapses is thus potentially an important tool to better understand the possible link of SNAP-25 to the underlying mechanisms of its role in epilepsy, schizophrenia, Alzheimer's and more generally in synaptic information processing. The increase in PPF, compared with similarly aged WT mice, suggests that the *Snap25*^{Tkneo} synapses could be more immature.

A further possibility is that along with the isoform change there could be differential expression of presynaptic proteins, which could play a primary role in the control of pool size, release plasticity, or Ca^{2+} dynamics that selectively associate with SNAP-25a or SNAP-25b in the SC-CA1 synapses compared to chromaffin cells. Thus, there is a need to further characterize the Ca^{2+} dynamics of Tkneo mice to provide important additional insight into the functional differences between these two isoforms.

In particular, the relationship between Ca^{2+} regulation and SNAP-25 is not well understood and the second part of this study will investigate whether the increase in PPF in Tkneo mice is due to a perturbation of the underlying Ca^{2+} -regulation seen in development or to a secondary mechanism.

Chapter 2 - Specific Aims

Hypothesis

Based on the aforementioned evidence, I propose the following hypothesis:

Changes of Ca^{2+} dynamics and plasticity during synaptic maturation in hippocampal Schaffer collateral-CA1 presynaptic terminals are mediated through alterations in the mechanisms of Ca^{2+} regulation and the mechanisms regulating Ca^{2+} are affected by variations in SNAP-25 isoform expression.

Specific Aims

I will address this hypothesis with the following 3 specific aims:

Aim 1: To describe developmental changes in presynaptic $[Ca^{2+}]_{res}$ dynamics and to investigate the mechanisms responsible for these changes

1a-Characterize the developmental time course of PPF in wild type mice.

1b-Characterize the developmental time course of $[Ca^{2+}]_{res}$ dynamics in wild type mice.

1c-Evaluate the role of ryanodine receptor-sensitive Ca^{2+} stores in presynaptic $[Ca^{2+}]_{res}$ dynamics.

1d-Evaluate the role of SERCA Ca^{2+} transport in presynaptic $[Ca^{2+}]_{res}$ dynamics.

Aim 2: To evaluate the role of SNAP-25 isoform expression in synaptic properties determining short-term plasticity

2a-Characterize PPF in SNAP-25 mutant mice.

2b-Characterize the $[Ca^{2+}]_{res}$ dynamics in SNAP-25 mutant mice.

2c-Account for the observed data with a model based on two vesicle pools with differing probabilities of release.

2d- Investigate the contribution of presynaptic Ca^{2+} buffer sensitivity in presynaptic $[Ca^{2+}]_{res}$ dynamics.

Aim 3: To investigate if the SNAP-25 dependent changes in plasticity and $[Ca^{2+}]_{res}$ kinetics are related to the developmental changes

3a- Evaluate the role of ryanodine receptor-sensitive Ca^{2+} stores in the properties of $[Ca^{2+}]_{pre}$

3b- Evaluate the role of SERCA Ca^{2+} transport in presynaptic $[Ca^{2+}]_{res}$ dynamics.

3c- Evaluate responses to trains of pulses to determine frequency-dependent properties of $[Ca^{2+}]_{pre}$.

These Aims will be specifically addressed in the following three chapters:

Chapter 3 will address modeling undertaken to focus the direction of Aim 1 and Aim 2 and to predict important Ca^{2+} regulatory mechanisms that will be the focus for Aim 1 and to provide a framework for interpreting the results of these Aims.

These models and their supporting data have been published {Schiess, 2006 #67; Scullin, 2010 #646}.

Chapter 4 will address Aim 1 and this chapter has been published (Scullin et al., 2010).

Chapter 5 will addresses Aim 2 and Aim 3 and this material has not been published to date, but is in preparation.

Chapter 3 -Modeling of Presynaptic Mechanisms

Presynaptic and Postsynaptic recordings

To better understand the development of plasticity in the hippocampus, I used published experimental data from the adult rodent (Schiess *et al.*, 2006; Scullin & Partridge, 2010) to extend previous models and to develop new a new model that could provide insight into the important mechanisms that regulate plasticity in the SC-CA1 synapse. In this section, the conclusion from those published experiments important for the modeling will be summarized prior to describing each model. These data were collected using concurrent recordings of presynaptic Ca^{2+} transients measured by a change in fluorescent dye and postsynaptic responses measured using field recordings; this technique is discussed in more detail in the methods Chapter 4 and 5. These data were used to develop two models, one describing the components regulating the presynaptic $[\text{Ca}^{2+}]_i$, and a second that describes the enhancement of vesicle release that occurs between pulses. Both of these models have been published and, the sections describing the two models in the publications are included below with a brief summary of the conclusions found from the experiments, which have, however, been omitted here (Schiess *et al.*, 2006; Scullin & Partridge, 2010).

Release Probability and Vesicle Release

Early studies of the frog neuromuscular junction revealed that synaptic release is stochastic in nature and that a presynaptic action potential does not always result in neurotransmitter release (Del Castillo & Katz, 1954b). This stochastic process can be modeled as a single vesicle pool with a one probability of release, P_R (Del Castillo & Katz, 1954b; Dobrunz & Stevens, 1997). Interestingly, during pairs or trains of pulses,

the P_R can change. It was suggested that the change of P_R of the second pulse response could be due to $[Ca^{2+}]_{res}$ (Del Castillo & Katz, 1954b); however, more recently it has been suggested that this change in P_R can also be influenced by the overall size of the readily releasable pool or by modification or regulation of the components of the synaptic release machinery (Dobrunz, 2002; Hu & Davletov, 2003).

In order to better understand the mechanism for the underlying dependence of the response to the second pulse (R2) on the initial response (R1) during PPF, we undertook modeling studies. To accomplish this we used two separate models, the first focuses specifically on presynaptic mechanisms (Scullin & Partridge, 2010) and the second evaluates overall synaptic transmission as assessed postsynaptically (Schiess *et al.*, 2006). The first model supports the observation that the presynaptic $[Ca^{2+}]_{res}$ clearance was based on the kinetics of efflux and sequestration. We used these model calculations to fit our experimental measurements to published parameters from other cell types (Scullin & Partridge, 2010). The second model was focused on mechanisms downstream from presynaptic $[Ca^{2+}]_{res}$ and was an expansion of a previously published model of PPF, which described the reliance of facilitation on the probability of release and $[Ca^{2+}]_{pre}$ (Bark *et al.*, 2004). We expanded this second model to make the variable, (a) from the original model (see below), a function of $[Ca^{2+}]_{pre}$, by correlating facilitation with the increased probability of release (Schiess *et al.*, 2006). These models predict parameters that are not accessible to direct measurement and thereby provide insight into potential mechanisms of presynaptic Ca^{2+} regulation both during developmental maturation and as a result of the SNAP-25 isoform change.

Model 1-Mechanism of $[Ca^{2+}]_{res}$ Clearance Model

This model has been published (Scullin & Partridge, 2010).

The kinetics of presynaptic $[Ca^{2+}]_{res}$ clearance are an important component of the time course of short-term synaptic plasticity (Burnashev & Rozov, 2005). In other studies, the decay of presynaptic $[Ca^{2+}]_{res}$ transients has been fit as either single or double exponential processes (Augustine & Neher, 1992; Wu & Saggau, 1994; Schiess *et al.*, 2006; Aponte *et al.*, 2008). In our experiments, the $[Ca^{2+}]_{res}$ decay measured by fluorescent indicator dyes in adult rats was best fit with a double exponential, which is consistent with a cooperative clearance mechanism (Schiess *et al.*, 2006). Additionally, there is an increase of the integral of R2 $[Ca^{2+}]_{res}$ after subtraction of R1 $[Ca^{2+}]_{res}$ ($\Delta R2 \int \Delta F/F_0$) in the hippocampal SC-CA1 synapse compared to that of R1 that is primarily due to an increase in τ_s , the slower time constant of decay from a double exponential fit to the decay phase of $[Ca^{2+}]_{res}$ clearance (Schiess *et al.*, 2006).

Measurement of the individual components of $[Ca^{2+}]_{res}$ in the adult rat SC-CA1 synapse produced the following results (Bark *et al.*, 2004): There is a consistent increase in the τ_s of the $\Delta F/F_0$ decay following replacement of $[Ca^{2+}]_o$ with $[Ba^{2+}]_o$ and an increase in $\Delta R2 \int \Delta F/F_0$ with increasing temperature that underscores the importance of active flux contributions to $[Ca^{2+}]_{res}$ clearance (Scullin & Partridge, 2010). Specific membrane flux inhibitors suggest a minimal contribution of L-type VGCCs, plasma membrane Ca^{2+} ATPase, or $Na^+ - Ca^{2+}$ exchange to this process. The mitochondrial role in $[Ca^{2+}]_{res}$ clearance is largely associated with its role in ATP production (Scullin & Partridge, 2010). ER Ca^{2+} stores, while only minimally filled in the basal state (Scullin & Partridge, 2010), are capable of significant Ca^{2+} sequestration and block of sarco- endoplasmic reticulum Ca^{2+} ATPase (SERCA) pumps significantly decreases the τ_s of $[Ca^{2+}]_{res}$

clearance (Scullin & Partridge, 2010). Uptake of Ca^{2+} into lysosomes by the vacuolar proton pump, although an additional Ca^{2+} clearance pathway in axon terminals (McGuinness *et al.*, 2007), has not been evaluated at this synapse.

We hypothesize from these observations that the SERCA-dependent sequestration into the ER plays a major role in presynaptic $[\text{Ca}^{2+}]_{\text{res}}$ clearance and that saturation of this pathway is responsible for the increased τ_s during R2. Lacking the ability to measure ER Ca^{2+} kinetics in presynaptic terminals without permeabilizing the membrane (Solovyova & Verkhratsky, 2002), we resorted to a reduced kinetic model to predict SERCA kinetics based on fits to our paired-pulse $[\text{Ca}^{2+}]_{\text{res}}$ data. While a wide range of initial parameters fit the $[\text{Ca}^{2+}]_{\text{res}}$ decay during R1, the observed increase in τ_s during R2 is most consistently predicted by a reduction of the forward rate constant, k_4 , for cytoplasmic Ca^{2+} binding to SERCA (Figure 3.1A). Additionally, when we used parameters from pairs of pulses to fit to $[\text{Ca}^{2+}]_{\text{res}}$ data from 5 pulses, (Scullin & Partridge, 2010) the model predicted that the free [SERCA] continued to decline and the ER-buffered Ca^{2+} concentration ($[\text{CaB}]$) rose, but did not saturate (Figure 3.1D), which is consistent with our observation that the ER has the capacity to accumulate Ca^{2+} during multiple pulses (Scullin & Partridge, 2010).

Because of the close dependency of short-term plasticity and perhaps working memory on $[\text{Ca}^{2+}]_{\text{res}}$, it is important to understand the mechanisms by which Ca^{2+} ions are cleared from the cytoplasm of the presynaptic terminal during repetitive pulses (Zucker & Regehr, 2002). These modeling studies support our conclusion that in Schaffer collateral terminals in the CA1 field of the hippocampus, SERCA transport into the ER is a major pathway for clearing cytoplasmic Ca^{2+} (Scullin & Partridge, 2010). In the basal state,

there is very little releasable Ca^{2+} in Ca^{2+} -sensitive ER stores, although these stores have considerable capacity to sequester Ca^{2+} (Scullin & Partridge, 2010). Furthermore, we were able to predict from these modeling studies that the cytoplasmic Ca^{2+} binding sites on the SERCA pump are easily saturated so that after only a few pulses this clearance pathway is limited by SERCA turnover limiting the ability of SERCA to remove Ca^{2+} from the synapse, but not by the Ca^{2+} storage capacity of the ER.

Details of Modeling of $[\text{Ca}^{2+}]_{\text{res}}$ Clearance

We have shown that the adult rat $[\text{Ca}^{2+}]_{\text{res}}$ clearance time course is best fit with a double exponential and that SERCA pumps can play a central role in the process and these observations provide important guidelines for creating a simplified model for $[\text{Ca}^{2+}]_{\text{res}}$ clearance, the results and conclusions of which are described below (Scullin & Partridge, 2010).

We approximated transport-independent processes as a single component, which we have estimated from experiments in Ba^{2+} ACSF. We began with a complete kinetic model for $[\text{Ca}^{2+}]_{\text{res}}$ clearance, but then reduced it to only those kinetic components associated with passive diffusion and ER Ca^{2+} flux (Figure 3.1A bold). We assumed that the rate limiting steps of SERCA transport were Ca^{2+} binding in the cytoplasm and ER lumen and not the kinetics of ATP-dependent translocation across the ER membrane (Scullin & Partridge, 2010).

Our kinetic modeling of presynaptic $[\text{Ca}^{2+}]_{\text{res}}$ used a reduced state diagram and was analyzed in a differential form that included k_4 , k_{-4} , k_{-4*} , k_{4*} , k_{BER} , $k_{-\text{BER}}$, k_3 (see Figure 3.1A). Presynaptic Ca^{2+} influx was modeled by a Gaussian curve with a half width of 2.5 ms that was adjusted to fit the derivative of the data scaled to reflect a peak

of 500 nM. $[Ca^{2+}]_{res}$ clearance was evaluated with a model using ordinary differential equations (ODE) and initial conditions (ICs) in a Matlab program with *ode45* 4th or 5th order Runge-Kutta numerical integration. The non-predefined ICs (see Table 3-1) were then fit to the data using a nonlinear least squares analysis, after using an analysis program - Potterswheel (Maiwald & Timmer, 2008) - to determine component sensitivity for all parameters. Parameters found in the literature (see Table 3-1), which robustly affected the fit, were allowed to vary over a pre-specified range (either the range in the literature, or, if no range was found, by an order of magnitude see Table 3-1 and Table 3-2). First the $[Ca^{2+}]_{res}$ data for paired-pulses from Figure 3.1A1 were fit ($R^2 = 0.95$) and the resultant parameters were then applied to a single pulse model, which was compared with single pulse data from the same experiment ($R^2 = 0.93$, Scullin & Partridge, 2010). Next the same parameter range was used to fit an additional 23 paired-pulse $[Ca^{2+}]_{res}$ data sets ($R^2 = 0.86$, Scullin & Partridge, 2010). Finally, we fit $[Ca^{2+}]_{res}$ data from a separate experiment with 5 pulses at 50 ms interpulse interval ($R^2 = 0.94$, Scullin & Partridge, 2010). In this instance the same parameter range was used except that the RyR efflux from the ER was increased to reflect an expected larger Ca^{2+} -dependent component resulting from the increased temporal window.

The $\Delta F/F_0$ data were scaled to the estimated Ca^{2+} influx during a single pulse and average parameters were determined that provided time course information for binding of cytoplasmic Ca^{2+} to SERCA (Figure 3.1C). The $\Delta F/F_0$ data were scaled as in Figure 3.1C in order to predict binding of Ca^{2+} to SERCA and ER buffered Ca^{2+} ($[CaB]_{ER}$).

The applicability of the reduced kinetic model to the process of $[Ca^{2+}]_{res}$ clearance was demonstrated in four ways. First, the model generated a fit to the $[Ca^{2+}]_{res}$ decay data

that was comparable to that of a double exponential. For instance, the decay portion of the $\Delta F/F_0$ data for the single pulse of Figure 1A1 yields an $R^2 = 0.92$ when fit with the model and an $R^2=0.93$ when fit with a double exponential. Second, the model predicted the observed increase of $\Delta R2[\Delta F/F_0]$ over $R1[\Delta F/F_0]$. For example, the modeled $[Ca^{2+}]_{res}$ for a single pulse and $\Delta R2$ in Figure 3.1C gives a ratio of $\Delta R2[\Delta F/F_0]$ to $R1[\Delta F/F_0]$ of 1.34, while the average value of this ratio for the data from each of the 23 individual experiments is 1.33. Third, consistent with our provided data (Scullin & Partridge, 2010), the model predicted a progressive reduction in the availability of SERCA for binding cytoplasmic free Ca^{2+} ($[Ca^{2+}]_{cyt}$) for transport into the ER (Figure 3.1C & D). Fourth, also consistent with our data, the model predicted that ER Ca^{2+} buffer is not saturated over short trains of pulses (Figure 3.1D).

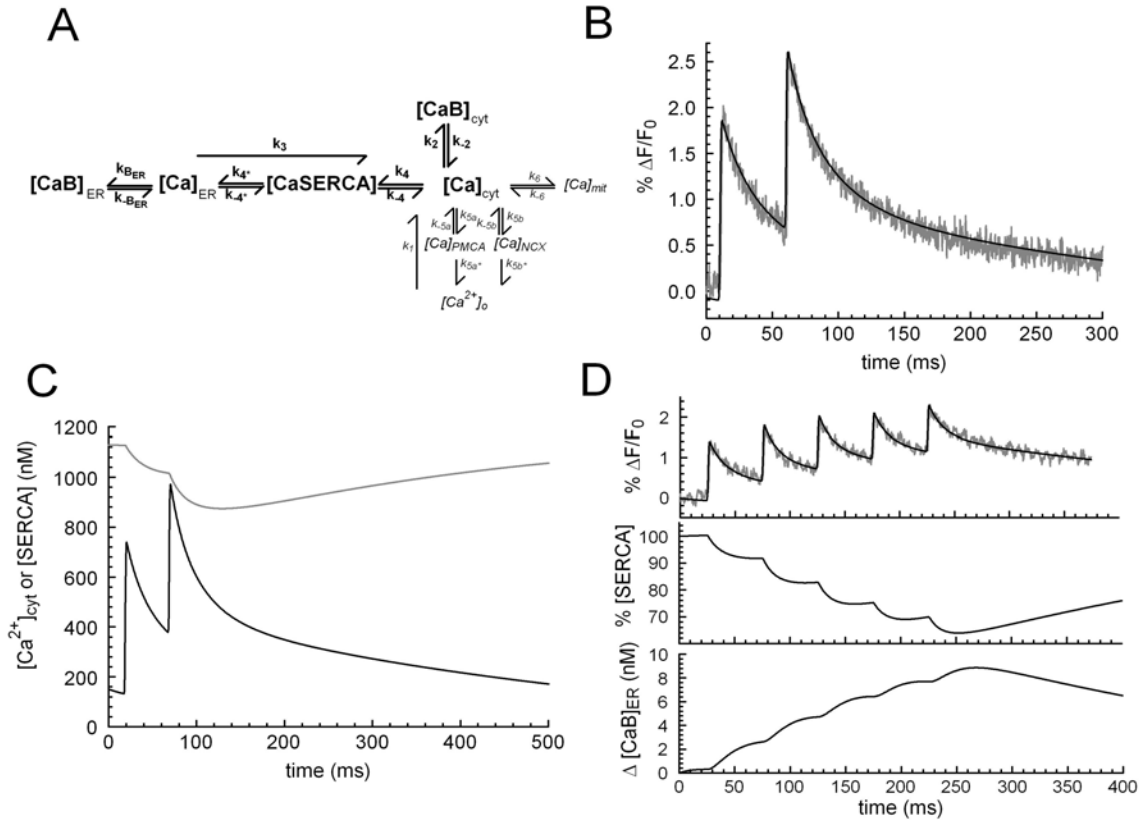


Figure 3.1 Ca^{2+} clearance kinetics.

A. Ca^{2+} clearance pathways that were considered. 1. VGCC, 2. buffering (B) and diffusion, 3. RyR, 4. SERCA, 5a. PMCA, 5b NCX, 6. MCU. Pathways indicated in bold are included in the kinetic model. **B.** Representative trace fit (gray) with the reduced model (black) including only buffer and SERCA/ER components ($R^2 = 0.95$). **C.** Average data from fits to 23 $[\text{Ca}^{2+}]_{\text{res}}$ traces in ACSF. Black, predicted $[\text{Ca}^{2+}]_{\text{cyt}}$; gray, predicted free [SERCA]. **D.** Top panel: fit to $[\text{Ca}^{2+}]_{\text{res}}$ during a train of 5 pulses at 50 ms IPI. ($R^2 = .94$). Middle panel: predicted percent free cytoplasmic SERCA Ca^{2+} binding sites. Bottom panel: predicted change of ER buffered Ca^{2+} (Scullin & Partridge, 2010)

Assumptions for Model:

1. Primary $[Ca^{2+}]_{cyt}$ clearance is an active process with lumped passive kinetics as indicated by the Ba^{2+} experiments (Scullin & Partridge, 2010).
2. Active $[Ca^{2+}]_{cyt}$ clearance is primarily through SERCA uptake into the ER (Scullin & Partridge, 2010).
3. In the basal state, there is a low releasable $[Ca^{2+}]_{ER}$, but the ER is capable of considerable Ca^{2+} uptake (Scullin & Partridge, 2010).
4. All concentrations and rates that were not fit, were taken from published values (see Table 3-1).

$$r_3 = -k_3[Ca]_{ER} \quad [1] \quad \frac{d[Ca]}{dt} = 2r_4 - r_3\gamma + r_{barium} + r_{stimulated} \quad [7]$$

$$r_4 = -k_4\left([Ca]^2[SERCA] - [CaSERCA]Kd_4\right) \quad [2] \quad \frac{d[SERCA]}{dt} = r_4 - r_{4*} \quad [8]$$

$$r_{4*} = -k_{4*}\left([CaSERCA] - \frac{[Ca]_{ER}^2[SERCA]}{Kd_{4*}}\right) \quad [3] \quad \frac{d[CaSERCA]}{dt} = -r_4 + r_{4*} \quad [9]$$

$$r_{BERC} = -k_{BER}\left([Ca]_{ER}[B]_{ER} - [Ca]_{ER}Kd_{4*}\right) \quad [4] \quad \frac{d[Ca]_{ER}}{dt} = -\frac{2r_{4*}}{\gamma} + r_{BERC} + r_3 \quad [10]$$

$$r_{barium} = -k_{barium}[Ca] \quad [5]$$

$$r_{stimulated} = 500e^{-2(t-t_{stim})^2} \quad [6] \quad \frac{d[B]_{ER}}{dt} = r_{BERC} \quad [11]$$

$$\frac{d[CaB]_{ER}}{dt} = -r_{BERC} \quad [12]$$

Table 3-1 Fit Parameters for presynaptic Ca²⁺ Model 1

Model						
parameter	Model value		Published values		Ref	Cell type
[Ca]	133	NM	95	NM	1	Non-excitable
[SERCA]	1062	NM	15 (varied)	μmol/L cyt	5	Non-excitable
[CaSERC						
A]	3	NM				
[CaB] _{ER}	0.120	MM	10	MM	1	Non-excitable
k _{4*}	0.92	ms ⁻¹	0.4	s ⁻¹	5	Non-excitable
			600	s ⁻¹	3	Human SERCA
k ₄	1.097E-07	nM ⁻¹ ms ⁻¹	0.9	μM ⁻¹ s ⁻¹	2	Non-excitable
			67	nM ⁻¹ s ⁻¹	4	PC 12
k ₃	0.0009	ms ⁻¹	2	s ⁻¹	6	Non-excitable
[Ca] _{ER}	40	NM	low		Calculated	
k _{barium}	0.0069	ms ⁻¹	0.002	ms ⁻¹	Calculated	

Table 3-2 Fixed Parameters for presynaptic Ca²⁺ Model 1

Model						
parameter	Model value		Published values		Ref	Cell type
[B] _{ER}	375000	nmol/L ER	375	μmol/L ER	5	Non-excitable
Kd ₄	700000	(nmol/L cyt) ²	0.7	(μmol/L cyt) ²	5	Non-excitable
Kd _{4*}	10	(nmol/L ER) ²	1x10 ⁻⁵	(μmol/L ER) ²	5	Non-excitable
k _{-BER}	0.08	ms ⁻¹	80	s ⁻¹	5	Non-excitable
k _{BER}	0.000001	((nmol/L ER) ⁻¹ ms ⁻¹)	1	((μmol/L ER) ⁻¹ s ⁻¹)	5	Non-excitable
γ	0.185	Vol _{ER} /Vol _{Cyt}	0.185		5	Non-excitable
Kd _{BER}	80000	nmol/L ER				

1. (Baker *et al.*, 2002)
2. (De Young & Keizer, 1992)
3. (Dode *et al.*, 2002)
4. (Duman *et al.*, 2008)
5. (Higgins *et al.*, 2006)
6. (Jafri & Keizer, 1995)

Model 2-Presynaptic Depletion and Probability of Release Model

This model has been published (Schiess *et al.*, 2006).

A limitation of model 1 is that it does not include elements downstream from $[Ca^{2+}]_{res}$ and thus it has no adaptive feature consistent with the prediction of a high affinity Ca^{2+} sensor response to the increased probability of release during facilitation. In previous work in rats, it was suggested that, while there is a linear relationship between R1 $[Ca^{2+}]_{pre}$ and R2 $[Ca^{2+}]_{res}$, there is a non-linear relationship between the R1 fEPSP and the R2 fEPSP (Schiess *et al.*, 2006). This suggests a non-linear process downstream from $[Ca^{2+}]_{res}$ that is important in the facilitation of vesicle release. To better understand this process, I attempted to fit fEPSP data using a model that considers both $[Ca^{2+}]_{res}$ and depletion of the readily releasable pool of vesicles (see Figure. 3.2) that is based on the stochastic nature of vesicular release (Bark *et al.*, 2004). Fits to fEPSP data (based on this model are shown as a continuous red curve in Figure 3.3 (c.d.=0.9508) (Schiess *et al.*, 2006). Thus, while there is a strong correlation between presynaptic $[Ca^{2+}]_{res}$ and synaptic facilitation, the non-linearity and variability in the facilitation of some of the fEPSP population spikes (Schiess *et al.*, 2006) strongly supports published suggestions of a contribution from mechanisms in addition to $[Ca^{2+}]_{res}$ (Wu & Saggau, 1994; Zucker & Regehr, 2002). I thus proceeded to investigate these additional mechanisms by applying and adapting a theoretical model to experimental data.

Details of Presynaptic Depletion and Probability of Release Model

The model that I employed (Bark *et al.*, 2004) defines the relationship between the R1 fEPSP and R2 fEPSP (Figure 3.2) based on $[Ca^{2+}]_{res}$ acting through a second Ca^{2+} -mediated facilitatory site that affects the probability of release (P_R) of a subpopulation of

the readily releasable pool of vesicles. (Other models with similar assumptions have also been proposed for PPF (e.g. (Jiang & Abrams, 1998; Dittman *et al.*, 2000; Rozov *et al.*, 2001)). In experimental recordings from both rat and mouse SC-CA1 synapses we have consistently found that all recording sites showed PPF so that a plot of the R2 fEPSP vs. the R1 fEPSP had a slope greater than 1, was non-linear, and could be accurately fit with the predictions of this model (Figure 3.3, red circles and line). We interpreted by the model as an indication that $[Ca^{2+}]_{res}$ has a significant additional downstream effect possibly at a second facilitatory site due to the non-linearity of the fit, which increases the release probability of a fraction of the vesicles (Atluri & Regehr, 1996).

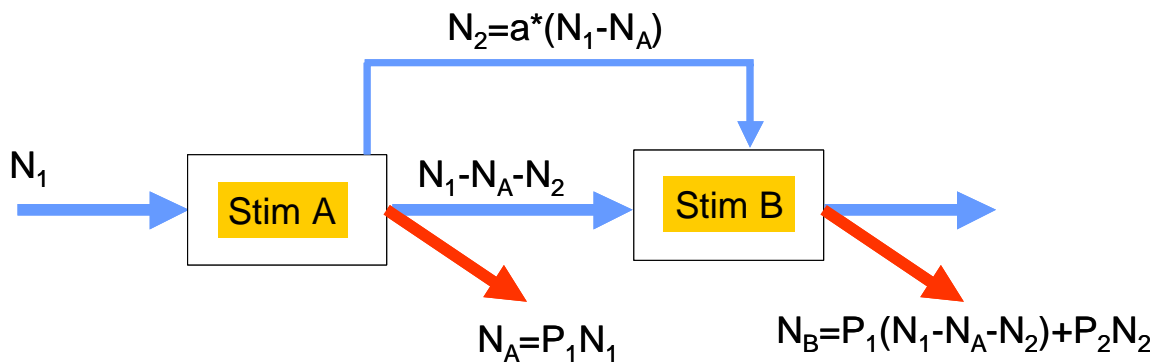


Figure 3.2 Flowchart showing model adapted from (Bark *et al.*, 2004).

According to this model:

$$R1/N_1 = P_1$$

$$R2/N_1 = aP_2(1-P_1) + P_1(1-P_1)(1-a)$$

where $R1/N_1$ and $R2/N_1$ are directly proportional to first and second fEPSP, respectively, and N_1 is proportional to the size of the readily releasable pool; P_1 is the basal release probability and P_2 is the larger, facilitated release probability, and a is the fraction of vesicles influenced by $[Ca^{2+}]_{res}$.

I expanded this model by assuming that the model parameter a was sigmoidally related to P_1 by a Hill function:

$$a = a_{max} / (1 + (K(a)/R1)^{HN})$$

where a_{\max} is a function of the maximum effectiveness of $[\text{Ca}^{2+}]_{\text{res}}$ in facilitating release; $K(a)$ is a function of the sensitivity of R1 in determining a ; and HN , the Hill coefficient, determines the steepness of this relationship. Table 3-1 gives the values of these parameters from least squares fits of the model equations to the shown data.

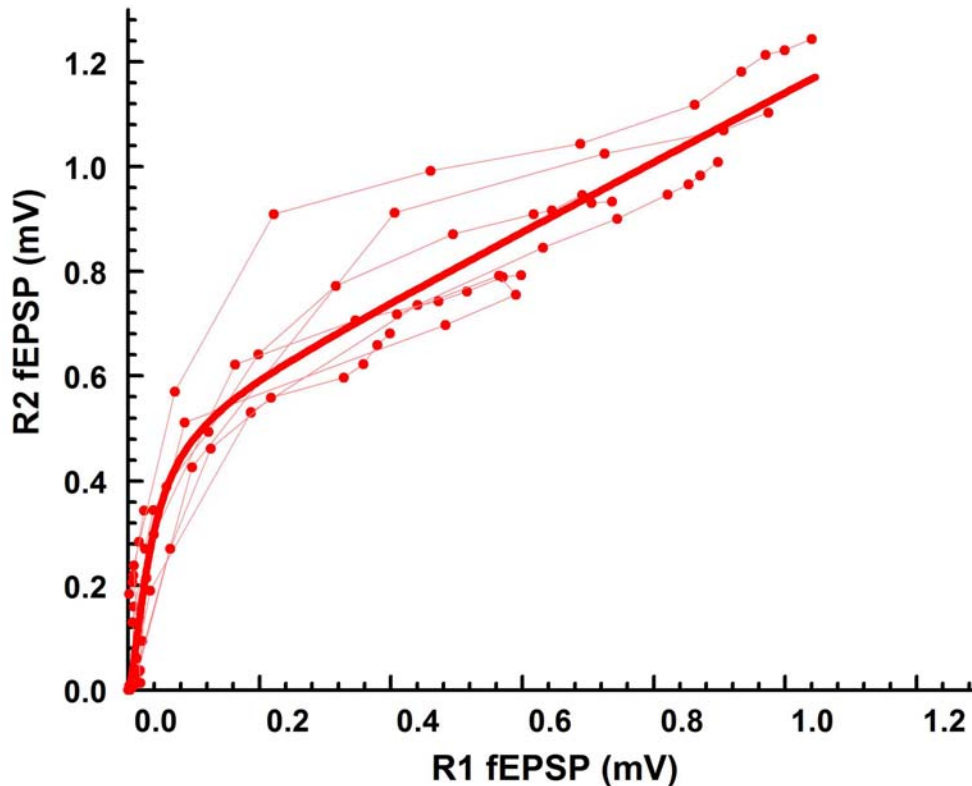


Figure 3.3 Relationship of R1 to R2.

A. Relationship of R2 to R1 at 11 recording sites in adult rat SC – CA1 synapses at stimulus intensities up to that necessary for maximum fEPSP response, continuous line represents least squares regression fit with Model 2 to red circles, slope = 1.30, c.d. = 0.9869; data from fit in Table 3-3, points from individual recording sites are connected with thin lines (Schiess *et al.*, 2006).

Table 3-3 Model 2 Fit Parameters for Figure 3.3

P2	K(a)	N ₁	a _{max}	HN
0.0069	0.0333	208.22	0.331	1.63

Discussion

These models predict that there are multiple parameters that play a role in the regulation of $[Ca^{2+}]_{res}$ and its downstream effects in short-term facilitation. Model 1 describes a presynaptic mechanism for Ca^{2+} regulation during paired-pulses in the basal activation state and suggests that $[Ca^{2+}]_{res}$ clearance is limited by SERCA availability and that the rate of Ca^{2+} binding and release are the rate limiting steps in SERCA activity (Scullin & Partridge, 2010). Model 2 describes an enhancement of facilitation that is non-linearly dependent on the increase of presynaptic $[Ca^{2+}]_{res}$ and suggests a downstream mechanism involved in facilitation (Schiess *et al.*, 2006).

Additionally, these models suggest that there are mechanisms of both depletion and $[Ca^{2+}]_{res}$ regulation that play a role in short-term plasticity. As PPF changes developmentally, Model 1 strengthens our motivation to study the changes in the role of internal stores in $[Ca^{2+}]_{res}$ -dependent synaptic plasticity. Interestingly, components involved in Ca^{2+} regulation such as ryanodine receptors have been shown to have developmental changes in expression (Mori *et al.*, 2000) and to be associated with L-type VGCCs (Kim *et al.*, 2007), which have also been shown to change developmentally in the hippocampus during the first few weeks (Dumas, 2005). Additionally, Model 2 suggests that factors downstream from Ca^{2+} influx could also play a role through a second independent mechanism of regulation so that a difference in presynaptic Ca^{2+} sensitivity, such as changes in Ca^{2+} saturation of presynaptic binding sites, between

pulses would allow different relative amounts of free Ca^{2+} to bind to facilitory sites associated with release proteins thereby creating a nonlinear relationship.

We have used the predictions from these modes to focus the direction of the following studies.

Chapter 4 - Developmental changes in presynaptic Ca²⁺ clearance kinetics and synaptic plasticity in mouse Schaffer collateral terminals

Abstract

Presynaptic Ca²⁺ influx pathways, cytoplasmic Ca²⁺ buffering proteins, and Ca²⁺ extrusion processes undergo considerable change during the first postnatal month in rodent neurons. These changes may be critical in establishing short-term plasticity at maturing presynaptic terminals where neurotransmitter release is directly dependent on the dynamics of cytoplasmic residual Ca²⁺ ([Ca²⁺]_{res}). In particular, the robust paired-pulse facilitation characteristic of adult neurons is almost entirely lacking in newborns. To examine developmental changes in processes controlling [Ca²⁺]_{res}, we measured the timecourse of [Ca²⁺]_{res} decay in presynaptic terminals of Schaffer collateral to CA1 synapses in acute hippocampal slices following single and paired orthodromic stimuli in the *stratum radiatum*. Developmental changes were observed in both the rise time and slow exponential decay components of the response to single stimuli such that this decay was larger and faster in the adult. Furthermore, we observed a greater caffeine-sensitive basal Ca²⁺ store, which was differentially affected when active uptake into the endoplasmic reticulum was blocked, in the presynaptic fields of the Schaffer Collateral to CA1 terminals of P6 and younger mice when compared to adults. These transitions in [Ca²⁺]_{res} dynamics occurred gradually over the first weeks of postnatal life and correlated with changes in short-term plasticity.

This chapter has been published (Scullin *et al.*, 2010).

Introduction

Marked developmental changes occur in the rodent hippocampus during the first three weeks after birth with consequences that affect a wide range of processes extending from the expression and regulation of proteins to the determination of cell morphology and phenotype (Dumas, 2005; Danglot *et al.*, 2006). This early postnatal period of rodent brain development correlates with a parallel developmental period in humans during which the onset of many neurological disorders including obsessive compulsive disorder, attention deficit hyperactivity disorder, and schizophrenia are believed to occur, (Anderson, 2002; Dumas, 2005).

Paired-pulse facilitation (PPF) is a measure of short-term plasticity in which the efficacy of the second of paired synaptic responses is increased in amplitude over that of the first response. PPF is generally accepted to result from presynaptic residual Ca^{2+} ($[\text{Ca}^{2+}]_{\text{res}}$) and its downstream effects (Katz & Miledi, 1968; Wu & Saggau, 1994; Cabezas & Buno, 2006; Schiess *et al.*, 2006) and this suggests that changes in $[\text{Ca}^{2+}]_{\text{res}}$ clearance after stimulation should play an important role in the kinetics of PPF. PPF in the Schaffer collateral to CA1 (SC-CA1) synapse exhibits significant change during the early postnatal period of development, during which time there is an increase in the magnitude of PPF and a predicted change in $[\text{Ca}^{2+}]_{\text{res}}$ regulation (Wasling *et al.*, 2004). Thus the initiation of PPF can provide a criterion that distinguishes the transition between immature and mature synaptic transmission.

Significant changes in the kinetics of presynaptic Ca^{2+} dynamics at SC-CA1 synapses during early postnatal periods are likely to be crucial to the maturation of synaptic plasticity and brain function; however, little is known about the development of

presynaptic components of synaptic plasticity at this synapse (Hanse *et al.*, 2009). In adult rodents, the presynaptic $[Ca^{2+}]_{res}$ clearance in SC-CA1 terminals has been accurately described as a double exponential process (Schiess *et al.*, 2006), which suggests contributions from more than one underlying mechanism. These mechanisms could include buffering, diffusion, uptake into or release from internal stores, and extrusion (Neher & Augustine, 1992; Koester & Sakmann, 2000; Emptage *et al.*, 2001; Carter *et al.*, 2002; Cabezas & Buno, 2006). The $[Ca^{2+}]_{res}$ clearance in SC-CA1 presynaptic terminals of immature animals may be even more complex. While $[Ca^{2+}]_{res}$ clearance is only minimally sensitive to Ca^{2+} buffer saturation in rodent SC-CA1 terminals, immature terminals are somewhat more sensitive than are adult terminals (Blatow *et al.*, 2003). This small change of buffer saturation, however, does not appear to account for the large developmental change in short-term synaptic plasticity (Dekay *et al.*, 2006). One attractive alternative possibility, which could contribute significantly to $[Ca^{2+}]_{res}$ kinetics, but has not been analyzed in this synapse, is developmental changes in the process of Ca^{2+} uptake into, and release from, internal stores. In this study, we have addressed this question and we report modifications in $[Ca^{2+}]_{res}$ clearance kinetic processes that correlate well with developmental changes in short-term synaptic plasticity.

Materials and Methods

Slice preparation

Experiments were performed in coronal hippocampal slices prepared from C57Bl/6 mice at ages described in each experiment; adults used were between 60 and 120 days old; average age 86 days. Animals were deeply anaesthetized by i.p. injection of 250 mg kg⁻¹ ketamine (Fort Dodge Animal Health, Fort Dodge, IA, USA), brains were rapidly removed, and slices were cut at 300 to 400 μm with a vibroslicer (Pelco 101, St Louis, MO, USA) in an ice bath with a cutting solution containing (mM): 220 sucrose, 3 KCl, 1.2 NaH₂PO₄, 26 NaHCO₃, 12 MgSO₄, 0.2 CaCl₂, 10 glucose and 0.01 mg ml⁻¹ ketamine equilibrated with 95%O₂-5%CO₂. Slices were then transferred to a bath containing artificial cerebrospinal fluid (ACSF) containing (mM): 126 NaCl, 3 KCl, 1.25 NaH₂PO₄, 1 MgSO₄, 26 NaHCO₃, 2.5 CaCl₂ and 10 glucose equilibrated with 95%O₂-5%CO₂ at 30°C for 1 h and then maintained at room temperature until transfer to a temperature-controlled recording chamber (Warner Instruments, Hamden, CT, USA or Scientific Systems Design, Mercerville, NJ, USA), which was maintained at 32°C and continuously perfused at 2 ml min⁻¹ with ACSF saturated with 95%O₂-5%CO₂. All experiments were approved by the Institutional Animal Care and Use Committee at the University of New Mexico Health Sciences Center and conformed with NIH guidelines.

Presynaptic Ca²⁺ imaging

Presynaptic fibers were filled with the Ca²⁺ fluorophore, Mg Green AM or Fura2 AM (Molecular Probes, Eugene, OR, USA) using an established technique that measures a spatial and temporal average of [Ca²⁺] in the presynaptic terminal (Regehr & Tank, 1991; Wu & Saggau, 1994; Atluri & Regehr, 1996; Sinha *et al.*, 1997; Kamiya & Ozawa,

1999). This technique provides simultaneous measurements of presynaptic $[Ca^{2+}]_i$ and postsynaptic fEPSP in localized populations of synaptic contacts. In a small number of instances, either the presynaptic or postsynaptic recording was not successful, but the data from the successful component were still included. To minimize the effect of exogenous buffers we used Mg-Green, with a Ca^{2+} binding $K_D = 6 \mu M$ for experiments in which we measured the timecourse of $\Delta F/F_0$ decay (Regehr & Atluri, 1995; Atluri & Regehr, 1996). In some experiments where the rapid decay timecourse was not being assessed, we improved the sensitivity of the $\Delta F/F_0$ measurements by using the higher affinity fluorophore Fura2. Briefly, an ejection electrode (tip diameter 5 – 10 μm) containing the fluorophore (0.9mM Mg Green AM, 10% DMSO, 1% pluronic acid in ACSF or 1 mM Fura2 AM, 10% DMSO, 1% pluronic acid in ACSF) was lowered into the fiber pathway between the stimulating electrode and the presynaptic terminal field to be investigated. While observing the emission image following excitation (490 nm Mg Green AM or 350 nm Fura2 AM) an air pressure pulse was applied with a syringe to the ejection electrode until a small bright spot ($\approx 1 \mu l$) was observed in the fiber pathway.

The slice was then maintained with a 2 ml min^{-1} flow of oxygenated ACSF at $32^\circ C$ for 1 h to allow intracellular diffusion of the dye to the presynaptic imaging site 500 μm away from the ejection site. The excitation light was then reduced to a 100–200 μm diameter spot with a diaphragm in the epi-illumination path, and the emitted light was measured with a photomultiplier tube (PMT). This spot included or was immediately adjacent to the area electrically summed by the field potential recording. A single stimulus or pairs of stimuli were delivered orthodromically at 0.05 or 0.067 Hz by a Master 8 pulse generator (AMPI Instruments, Jerusalem, Israel) under control of the

imaging system (TILL Photonics, Pleasanton, CA, USA). For Mg Green studies, fluorescence responses are reported as the ratio of the change in fluorescence to the pre-stimulus fluorescence ($\Delta F/F_0$). For Fura-2 studies, we first determined the 350 to 380 nm fluorescence ratio and reported the response as the ratio of the change in this ratio to the pre-stimulus ratio ($\Delta R/R_0$). The $\Delta F/F_0$ or $\Delta R/R_0$ signals were corrected for bleaching by subtraction of a linear baseline slope and were inverted so that increasing presynaptic $[Ca^{2+}]_i$ produced an upward deflection. To diminish noise inherent with the low-affinity Ca^{2+} indicator, it was necessary to average five fluorescence responses and to filter the PMT signal at 1 kHz.

We used two tests to demonstrate that the measured $\Delta F/F_0$ signal was consistent with a $[Ca^{2+}]_i$ response predominately from the presynaptic Schaffer collateral axons and axon terminals (Wu & Saggau, 1994; Atluri & Regehr, 1996; Sinha *et al.*, 1997; Kamiya & Ozawa, 1999). First, in the presence of 10 μM CNQX, 25 μM D-AP5, and 20 μM bicuculline, the fEPSP was blocked, while the presynaptic fiber volley and $\Delta F/F_0$ signal were left unchanged, thus the $\Delta F/F_0$ signal was not a postsynaptic response. Second, subsequent addition of 600 nM TTX blocked both the presynaptic fiber volley and the $\Delta F/F_0$ signal arguing against direct stimulation of inadvertently filled postsynaptic dendrites.

Field potential recordings

We used standard electrophysiological techniques for slice fEPSP recordings in the SC-CA1 pyramidal neuron synapse in the *stratum pyramidale* in hippocampal slices (Schiess et al. 2006). Briefly, fEPSPs were recorded with an Axoclamp 2B or Multiclamp 700B amplifier (both from Axon Instruments, Union City, CA, USA) and a

Digidata 1322A interface using pCLAMP 9.2 or 10 software (Axon Instruments) for experimental control and data analysis. fEPSPs were digitized at 20 kHz and filtered at 2 kHz. Presynaptic constant current pulses (150 μ s duration) were applied to Schaffer collateral fibers with an Iso-Flex constant current stimulator (AMPI Instruments, Jerusalem, Israel) through a concentric bipolar electrode (FHC, Bowdoinham, ME, USA) at a current, which was adjusted to produce 40-60% of the maximum fEPSP amplitude. The paired-pulse ratio (PPR) of the fEPSP signal was calculated as the ratio of the slope of second fEPSP at a 50 ms interpulse interval to that of the initial fEPSP. The relationship between $[Ca^{2+}]_{res}$ and PPR was determined using concurrent $\Delta F/F_0$ and fEPSP recordings of paired-pulses at interpulse intervals of 50, 100, 150, 200, 300, and 500 ms. The $[Ca^{2+}]_{res}$ was calculated by measuring the amplitude of the $\Delta F/F_0$ immediately before the second pulse of each pair.

Data analysis

Combining data, even for single developmental days, from the period during which there are rapid changes in $[Ca^{2+}]_{res}$ dynamics is expected to introduce variability into measured parameters. Indeed, our data from early developmental points varied substantially and this variability decreased with increasing age. We have interpreted this to be an indication of the narrow temporal window over which some of these maturation processes occur.

The $\Delta F/F_0$ signal was digitally filtered with a five point center-weighted filter and fit using a least squares regression routine to a single exponential decay beginning 50 ms after the stimulus initiation. In addition, the $\Delta F/F_0$ signal was numerically integrated after being normalized to the $\Delta F/F_0$ peak value ($\int v\Delta F/F_0$). The rise time was measured by

subtracting the time of the $\Delta F/F_0$ peak value and the time of stimulation. Fitting and statistical analysis were carried out with Matlab 7.0 (Mathworks, Natick, MA, USA) using programs as described in Appendix B, Prostat 4.0 (Polysoft International, Pearl River, NY, USA) or Prism (GraphPad Software, La Jolla, CA, USA). Coefficient of Determination (C. O. D.) was used as a measure of goodness of fit for linear regressions. Average data are presented as means \pm s.e.m., and statistical significance was determined at $P < 0.05$. Statistical significance indicated as: * $P < 0.05$, ** $P < 0.01$, *** $P < 0.001$.

Drugs

Drugs were stored frozen in aliquots and diluted to the appropriate concentration in ACSF on the day of the experiment. 6-Cyano-7-nitroquinoxaline-2,3-dione (CNQX), d-(1)-2-amino-5-phosphonopentanoic acid (d-AP5), bicuculline, thapsigargin and tetrodotoxin (TTX) were obtained from Tocris (Ellisville, MO, USA) and all other drugs and reagents were obtained from Sigma-Aldrich (St. Louis, MO, USA). Drugs were applied through a bath perfusion system for a minimum of 10 min (>2.5 bath exchanges) before recording commenced. The timecourse experiments were continuously recorded during bath exchange and the time for complete response was expected to result from a combination of the bath exchange time constant (70 s) and the time necessary for drug permeation into the slice.

Results

Previous studies have shown that there is a developmental increase in hippocampal short-term facilitation during the first few postnatal weeks in rats (Wasling *et al.*, 2004). To determine whether a similar developmental change occurs in mice, we measured the paired-pulse ratio (PPR) of fEPSPs in response to paired stimuli at 50 ms interpulse intervals in hippocampal slice preparations from P1 to adult (>P60) (Figure 4.1A). Similar to the findings in rats, we found a developmental increase in PPR at the SC-CA1 synapse in the mouse between P6 and P9 (Figure 4.1B); however, no significant additional change was observed between P15 and adult animals.

As paired-pulse facilitation (PPF) is believed to be dependent on $[Ca^{2+}]_{res}$, we next chose to measure the kinetics of $[Ca^{2+}]_{res}$ during this developmental period. To characterize the developmental changes of presynaptic Ca^{2+} kinetics in the SC-CA1 synapse, we used Ca^{2+} -sensitive fluorescent dyes to measure presynaptic $[Ca^{2+}]_{res}$ following stimuli in the *stratum radiatum* in brain slices from animals aged between P1 and P120. For this purpose, presynaptic terminals were loaded with AM-derivatives of either Mg Green for millisecond kinetic analysis or Fura-2 for more sensitive analysis of $[Ca^{2+}]_{pre}$ on a timescale of seconds (see Methods). Previous investigations in adult hippocampus in our lab (Regehr & Tank, 1991; Wu & Saggau, 1994; Schiess *et al.*, 2006) and other labs (Regehr & Tank, 1991; Wu & Saggau, 1994; Schiess *et al.*, 2006) have demonstrated that this method reports almost exclusively Ca^{2+} dynamics of presynaptic terminals (see Methods and Discussion). We evaluated quantitatively the changes in $[Ca^{2+}]_{res}$ kinetics by first measuring the change in fluorophore fluorescence of

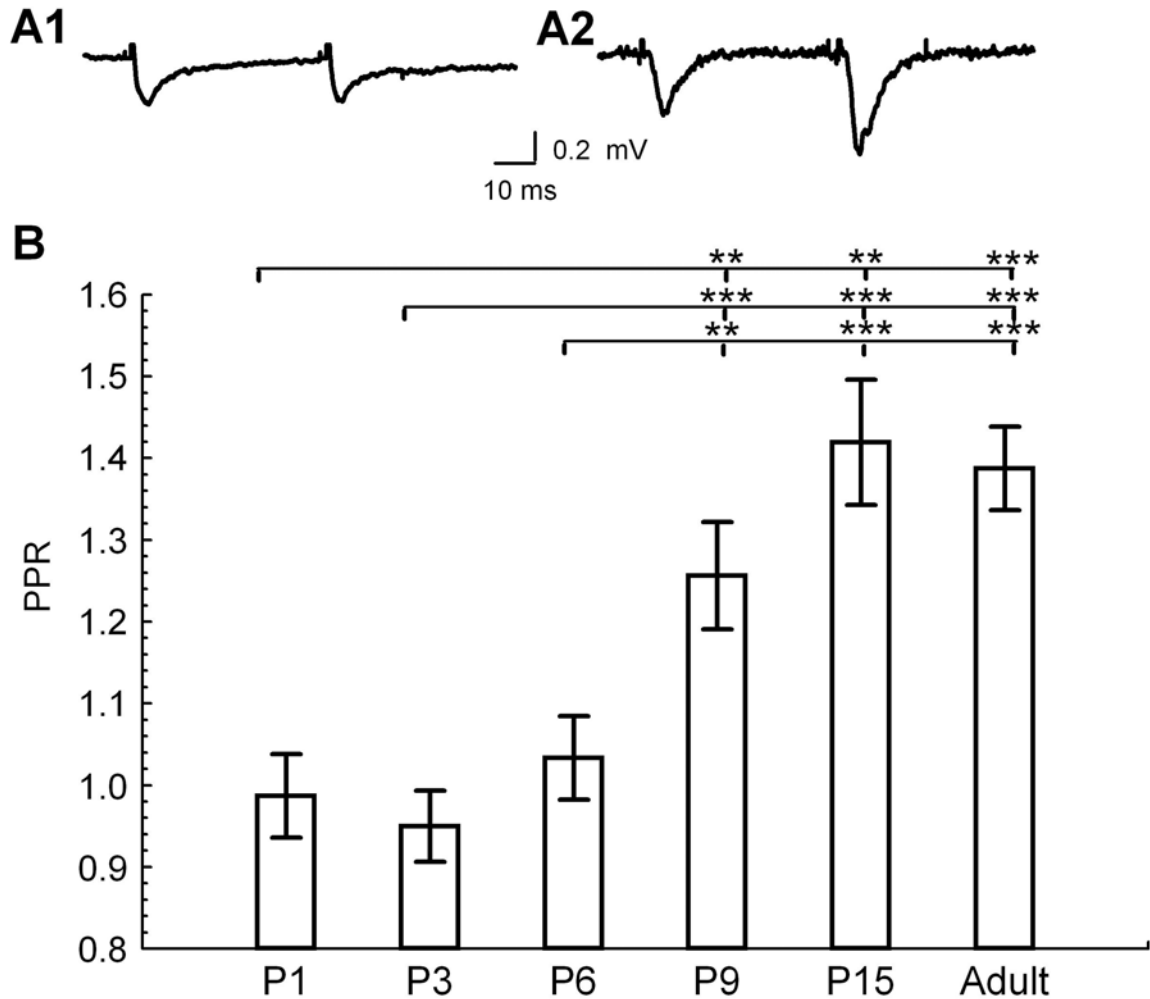


Figure 4.1 Developmental increase in short-term synaptic plasticity.

A. Representative traces of fEPSP slopes at half maximum at two developmental stages during paired stimulation at 50 ms interpulse interval, average of 5 traces (**A1**: immature (P6); **A2**: adult (P114)). **B.** PPR at different developmental ages (ANOVA with Fisher's post-hoc comparison of significance of PPR vs. age between groups ($F_{4,25}=8.71$; $P = 0.0002$; P1, $n=4$; P3, $n=6$; P6, $n=11$; P9, $n=6$; P15, $n=4$; adult, $n=3$ animals) (Scullin *et al.*, 2010).

the Mg Green signal ($\Delta F/F_0$) in response to a single stimulus. To obtain a measure of $[Ca^{2+}]_{res}$ time course that made no assumptions about the specific underlying kinetic processes, we calculated the integral of $\Delta F/F_0$ after it had been normalized to its peak, which provides a measure of the overall kinetic behavior of the $[Ca^{2+}]_{res}$ transient (Figure 4.2A1 & 4-2A2, $\int v\Delta F/F_0$). We found a significant age-dependent decrease in the $\int v\Delta F/F_0$ (Figure 4.2B), which is consistent with a more rapid $[Ca^{2+}]_{res}$ clearance kinetics in older animals.

To assess the relationship between presynaptic Ca^{2+} kinetics and facilitation, we plotted the $\int v\Delta F/F_0$ following a single pulse against the PPR observed in concurrent postsynaptic recordings (Figure 4.2C). Because there appeared to be a distinct transition in PPR between P6-P9, we grouped the data into two groups: P1 to P6 and P9 to adult. We found a negative slope in the P9 to adult group, consistent with the dependence of facilitation on $\int v\Delta F/F_0$ with decreased probability of release and enhanced facilitation (slope = -1.36×10^{-5} , C.O.D. = 0.29). In contrast, however, the P1 to P6 age group did not exhibit a negative slope and the data were more poorly correlated (slope = 0.521×10^{-5} , C.O.D. = 0.14). This suggests a developmental transition between P6 and P9 during which presynaptic $[Ca^{2+}]_{res}$ assumes a role in short-term facilitation. Typically, increased $[Ca^{2+}]_{res}$ correlates with increased facilitation and depletion of vesicles correlates with decreased facilitation (Liley & North, 1953; Takeuchi, 1958; Elmqvist & Quastel, 1965; Thies, 1965; Betz, 1970; Zucker & Regehr, 2002). However, the negative correlation between $\int v\Delta F/F_0$ and PPR suggests $[Ca^{2+}]_{res}$ removal mechanisms are important in the amount of facilitation. Interestingly, a more rapid $[Ca^{2+}]_{res}$ removal is reflected by decreased $\int v\Delta F/F_0$ and this is correlated with increased facilitation. To determine the

processes that contribute to the regulation of $[Ca^{2+}]_{res}$ during this important developmental period, we further investigated the kinetics of $[Ca^{2+}]_{res}$ clearance.

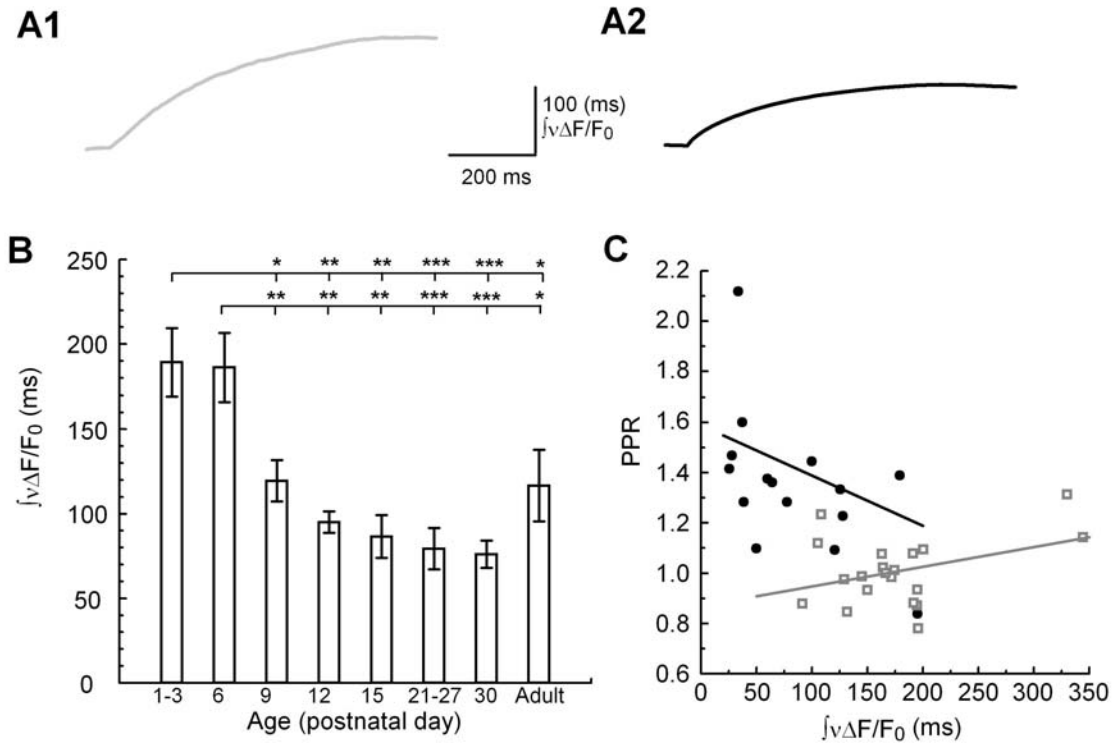


Figure 4.2 Developmental changes in presynaptic $\int v\Delta F/F_0$.

A. Representative traces of $\int v\Delta F/F_0$ at two developmental ages (**A1** P6, **A2** Adult (P85) Mg Green) **B.** Summary data of $\int v\Delta F/F_0$ vs. age. ANOVA with Fisher's post-hoc comparison of significance of $\int v\Delta F/F_0$ vs. age between groups ($F_{40,7}=6.65$; $P = 0.00001$; P1-3, n=8; P6, n=12; P9, n=5; P12, n=4; P15, n=3; P21-27, n=9; P30, n=3; adult, n=4 animals) **C.** Concurrent recordings of fEPSP PPR and $\int v\Delta F/F_0$ (P1-P6 grey open squares, n=20 animals; P9-adult black circles, n=15 animals) fit by least squares linear regression (Scullin *et al.*, 2010).

As shown in Figure 4.3A, there were distinct age-dependent differences in the decay of the Mg Green fluorescence signal, indicative of a change in the rate of $[Ca^{2+}]_{res}$ clearance between P6 and adult mice. We first measured the kinetic components responsible for Ca^{2+} accumulation, peak amplitude of $\Delta F/F_0$, and time to peak of $\Delta F/F_0$. There was an approximate doubling of the peak amplitude of $\Delta F/F_0$ from P1 to adult (Figure 4.3B). Because this could have resulted in part from a difference in Ca^{2+} influx or in the kinetics of an internal store contribution, we also compared the time at which the peak $\Delta F/F_0$ occurred at the different ages. This analysis revealed a dramatic monotonic 20 fold decrease in the time to peak $\Delta F/F_0$ from P1 to adult (Figure 4.3C). Taken together, the age-dependent decrease of the $\int \Delta F/F_0$ signal must therefore reflect an overall increase of the rate of $[Ca^{2+}]_{res}$ clearance, since there was a simultaneous increase in the peak $\Delta F/F_0$ amplitude.

Since the $[Ca^{2+}]_{res}$ has been associated with the degree of PPF, we next compared the relationship between $[Ca^{2+}]_{res}$ and the simultaneously measured PPF in the different age groups by changing the interpulse interval while keeping the stimulation strength constant, (Figure 4.3D). Analysis of these data demonstrated there was a significant positive slope of this relationship in slices from older animals, P9 (slope=0.96 PPR/ % $\Delta F/F_0$, COD = 0.23, $F_{1,25} = 7.47$, $P = 0.011$), P15 (slope = 0.97 PPR/ % $\Delta F/F_0$, COD = 0.27, $F_{1,24} = 8.68$, $P = 0.0071$) and adult mice (slope = 1.17 PPR/ % $\Delta F/F_0$, COD = 0.1752, $F_{1,25} = 5.31$, $P = 0.023$). While the slopes of this relationship were not significantly different (Figure 4.3D, $P = 0.93$) among all age groups, the intercept was

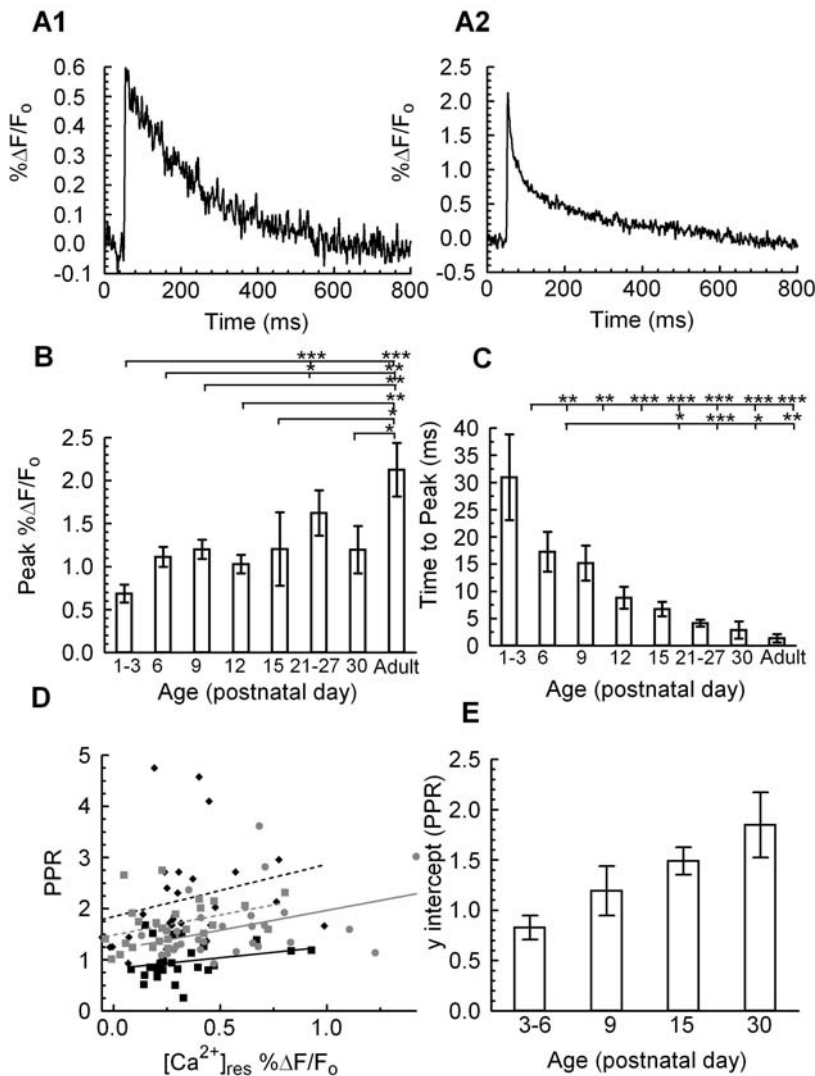


Figure 4.3 Developmental changes in presynaptic $[Ca^{2+}]_{res}$ kinetics.

A. Representative traces of $\Delta F/F_0$ during single stimulus pulses at two developmental ages (top: P6; bottom P14; Mg Green). **B.** Summary data of maximum $\Delta F/F_0$ vs. age. ANOVA with Fisher's post-hoc comparison of significance of peak $\Delta F/F_0$ between age groups ($F_{40,7}=4.12$, $P = 0.0017$) **C.** Time to peak $\Delta F/F_0$ vs. age . ANOVA with Fisher's post-hoc comparison of significance of time to peak between age groups ($F_{40,7}=4.21$, $P = 0.0016$). (P1-3, n=8; P6, n=12; P9, n=5; P12, n=4; P15, n=3; P21-27, n=9; P30, n=3; adult n=4 animals). (Further analysis of this data is shown in Figures 2-4). **D.**

Relationship of PPR vs. $[Ca^{2+}]_{res}$ measured by the $\% \Delta F/F_0$ before stimulation compared to the PPR at IPIs of 50, 100, 150, 200, 300, and 500 ms, least squares linear regression yields a non significant difference in slope between groups (slope= 0.7756; $F_{99,3}=0.18$, $P = 0.91$), (P3-6 black squares, black line n=4, P9 gray squares, gray line n=4, P15 gray circles, dashed gray line n=4, P30 n=4 animals black diamonds, dashed black line slices)

E. y intercept versus age from the linear regression of PPR versus $[Ca^{2+}]_{res}$, significant difference of age versus intercept, ($F_{102,3}=17.97$, $P < 0.0001$) (Scullin *et al.*, 2010).

found to increase significantly with age (Figure 4.3E). By contrast, the slope of this relationship for slices in the younger P3 and P6 mice, which do not exhibit significant PPF, did not differ significantly from zero (P3-6 slope = -0.23, COD = 0.06, $F_{1,26} = 1.78$, $P = 0.19$). This suggests that the mechanisms that underlie the $[Ca^{2+}]_{res}$ -dependent facilitation are not established or are disengaged until the second postnatal week of hippocampal development (see Discussion).

As we reported previously for presynaptic SC-CA1 terminals in adult rats (Schiess *et al.*, 2006), the $\Delta F/F_0$ decay in these terminals in adult mice followed a double exponential timecourse whose time constants differed by about 10 fold (not shown). In contrast, the presynaptic $\Delta F/F_0$ decay in younger mice could not be accurately fit with the sum of two decaying exponential processes and we attributed this to the significantly delayed $\Delta F/F_0$ peak time in the younger animals. In adult mice, the fast $\Delta F/F_0$ clearance process had a time constant of about 20 ms. Consequently, the significantly slower rising kinetic component in the younger animals (time to peak = 30.95 ± 8.31 ms) markedly overlapped this portion of $[Ca^{2+}]_{res}$ clearance (Figure 4.3). Therefore, in order to assess developmental changes in $[Ca^{2+}]_{res}$ clearance kinetics independently of the initial Ca^{2+} accumulation, we measured the decay of $\Delta F/F_0$ beginning 50 ms after its peak when the fast rise and decay contributions were minimal. We reasoned that changes in either the rate or the proportion of this slower component of Ca^{2+} decay would have considerable impact on the overall response. To obtain an estimate of this kinetic component, we fit the slow component of the remaining $\Delta F/F_0$ decay as a single exponential process (Figure 4.4A). The rate of this slow decay component was then extrapolated to the time of the peak of $\Delta F/F_0$ in order to obtain the value indicated as “b” in the rise time in Figure 4.4A.

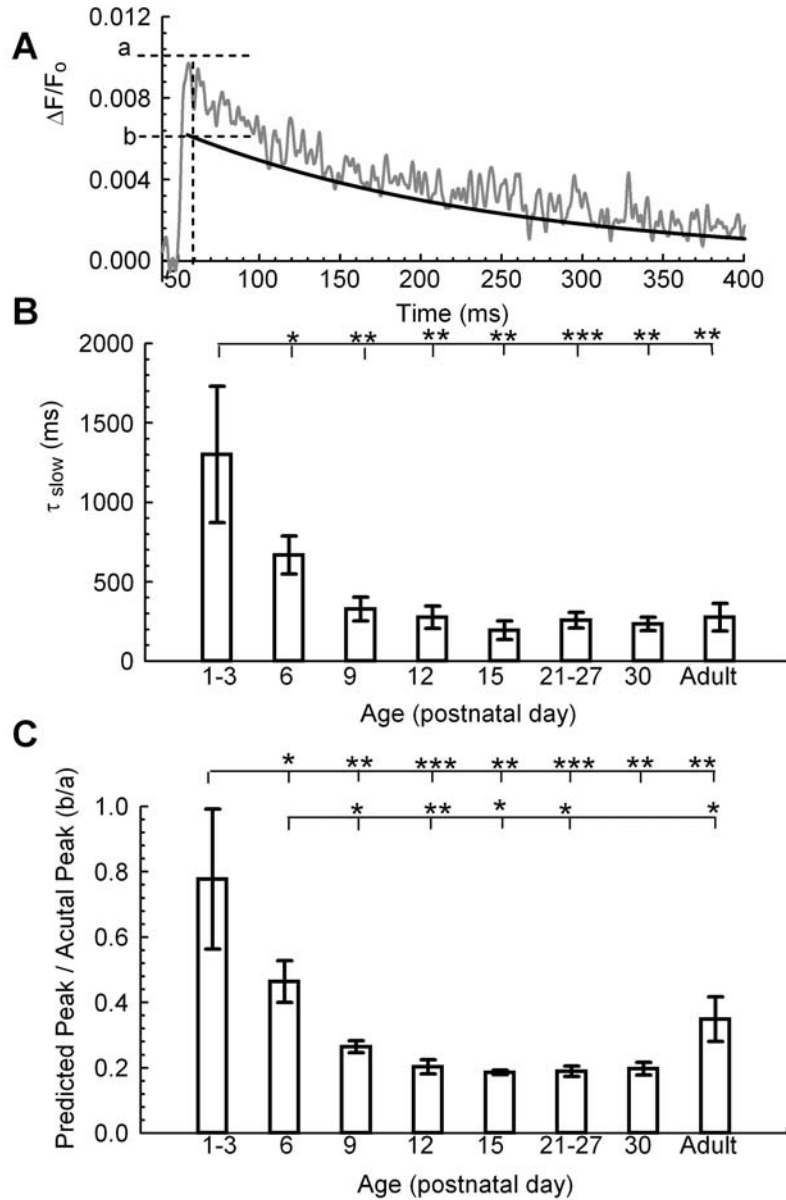


Figure 4.4 Kinetic components of $[Ca^{2+}]_{res}$ evaluated from fits to $\Delta F/F_0$.

A. Example $\Delta F/F_0$ trace (P9), measured peak (a), predicted peak from extrapolated single exponential fit to $\Delta F/F_0$ data beginning 50 ms after the peak, (b). (Mg Green) **B.** Slow time constant (τ_{slow}) measured by exponential fit to $\Delta F/F_0$ trace beginning 50 ms after the peak. ANOVA with Fisher's post-hoc comparison of significance of slow time constant between age groups ($F_{40,7}=3.03$, $P = 0.012$). **C.** Ratio of the extrapolated peak of τ_{slow} to the peak amplitude of the $\Delta F/F_0$ signal. ANOVA with Fisher's post-hoc comparison of significance of between ratio of predicted peak to actual peak between age groups ($F_{40,7}=3.38$, $P = 0.0067$). (P1-3, n=8; P6, n=12; P9, n=5; P12, n=4; P15, n=3; P21-27, n=9; P30, n=3; adult, n=4 animals) (Scullin *et al.*, 2010).

The ratio of this value to the actual peak (“a” in Figure 4.4A) provided an estimate of the contribution of the slow component to the peak $\Delta F/F_0$ signal.

We found an age-dependent decrease in this ratio (b/a, Figure 4.4C) indicating an age-dependent increase of the relative contribution of a process with a fast time constant. Interestingly, the increased peak $\Delta F/F_0$ (Figure 4.3B) and decreased time to peak (Figure 4.3C) offset the decreased slow time constant (Figure 4.4B) to minimize any difference in $\int v\Delta F/F_0$ between the P1 to 3 and P6 age groups (Figure 4.2B). Thus, the most dramatic reduction of $\int v\Delta F/F_0$ occurred between P6 and P9 (Figure 4.2B). These data further indicate that the most dramatic change in $[Ca^{2+}]_{res}$ timecourse occurred over the developmental period of P6 to P9, strongly suggesting a significant transition in the underlying mechanisms of $[Ca^{2+}]_{res}$ clearance during this period. Importantly, the developmental changes that lead to a decrease in total $[Ca^{2+}]_{res}$, as represented by the $\int v\Delta F/F_0$, coincided with the simultaneously recorded increase in the amount of PPF (see Discussion).

We next focused on the possibility that the mechanism that drives the developmental decrease in the $[Ca^{2+}]_{res}$ clearance timecourse could be linked to changes in either release from, or uptake into internal Ca^{2+} stores. A contribution from Ca^{2+} stores would be consistent with the observation that internal stores have a contrasting developmental role in silent and active synapses and that the SERCA pump plays an important role in PPF (Cabezas and Buno, 2006).

To investigate the possibility that Ca^{2+} stores play an important role in the regulation of presynaptic $[Ca^{2+}]_{res}$, we used thapsigargin to block the uptake of Ca^{2+} into the ER by the SERCA pump and measured the effect of SERCA block on the $\int \Delta F/F_0$

signal following stimulation. To compare the timecourse of $\int \Delta F/F_0$ at different ages, we normalized the $\int \Delta F/F_0$ in 3 μM thapsigargin to the response in the same slice in ACSF (Figure 4.5). Interestingly, at P3 thapsigargin caused a decrease in $\int \Delta F/F_0$ while at P5 to P7 it caused no change in $\int \Delta F/F_0$, and it clearly enhanced the $\int \Delta F/F_0$ of adults (Figure 4.5A). To further test whether SERCA clearance is involved in plasticity, we recorded the PPR of fEPSPs and found that application of thapsigargin had no significant effect in the P5-P7 age group, and a trend toward a decrease in the P3 mice. However, application of thapsigargin did cause an increase in the PPR of the adult mice (Figure 4.5C). This suggests that during this time period (P5-P7) there is a rapid transition in the contribution from ER Ca^{2+} stores at synaptic terminals. Furthermore, either release from stores or uptake by the SERCA pump may be reflected in the slow time constant of the $[\text{Ca}^{2+}]_{\text{res}}$ clearance.

In many cell types, thapsigargin unmasks a basal leak of Ca^{2+} from intracellular stores (Verkhatsky, 2005). We reasoned that thapsigargin would produce an increase in the cytoplasmic Ca^{2+} that would be measurable with the high affinity indicator Fura2 ($\Delta R/R_0$ signal) if the SERCA pump normally counteracted a significant leak from Ca^{2+} stores. This could be relevant to our findings because such a leak might contribute to the difference in $[\text{Ca}^{2+}]_{\text{res}}$ timecourse, which we observed between immature and adult SC-CA1 terminals. Importantly, we did not find a significant increase in $\Delta R/R_0$ following thapsigargin application in non-stimulated slices at any age (data not shown). This observation is consistent with the idea that the activity of SERCA does not continually oppose a measurable Ca^{2+} leak from intracellular Ca^{2+} stores in presynaptic terminals from either young or adult animals.

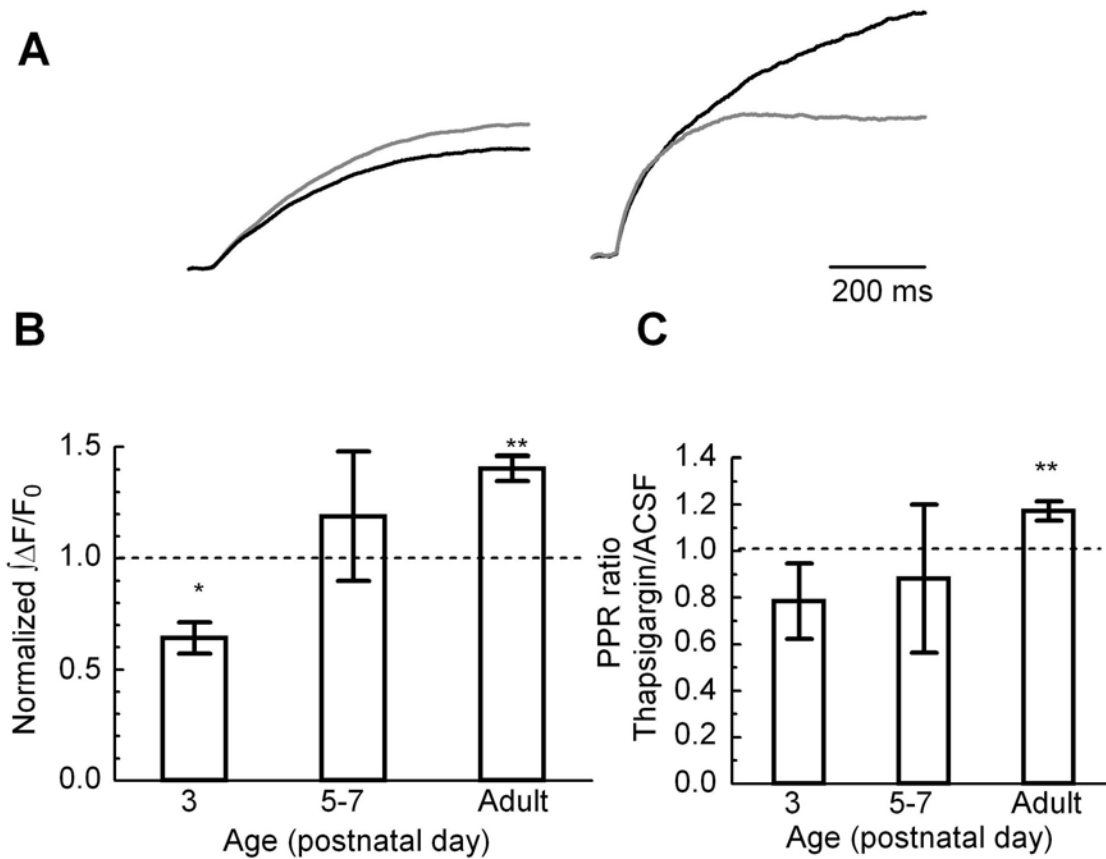


Figure 4.5 Developmental changes in the effect of thapsigargin on $[Ca^{2+}]_{pre}$ clearance.

$\int \Delta F/F_0$ following a single pulse in 3 μ M thapsigargin normalized to the $\int \Delta F/F_0$ response in ACSF. **A.** Representative traces (left, P3; right, adult; gray, ACSF; black thapsigargin) normalized to the respective ACSF traces. **B.** Summary data. (P3, n=3 ; P5-P7, n=4; adult, n=5 animals) (Student's t-test, against theoretical mean of 1) **C.** Effect of application of thapsigargin on PPR between (P3, n=4 $P = 0.11$; P5-7, n=6 $P = 0.34$; adult, n=5 animals) Student's t-test against a theoretical mean of 1 (Scullin *et al.*, 2010).

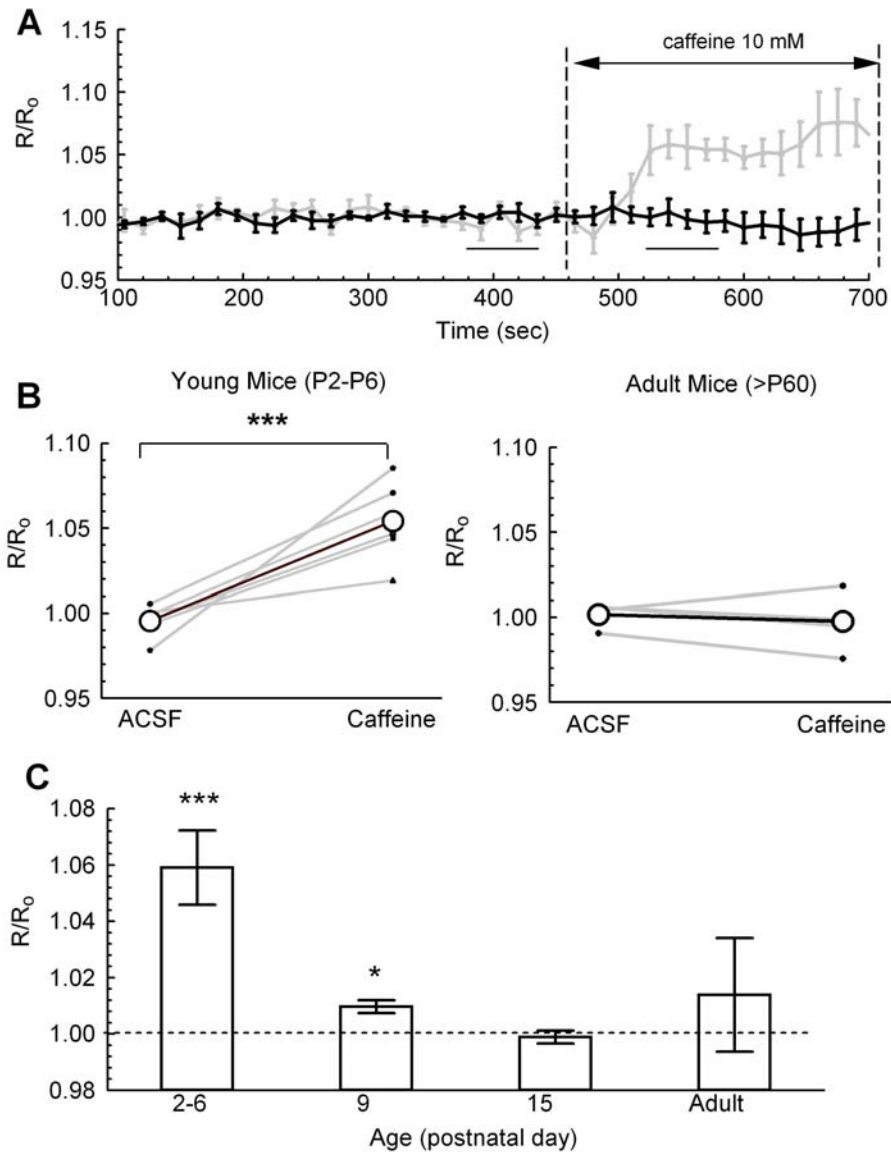


Figure 4.6 Age-dependent differences in basal loading state of Ca^{2+} stores.
A. Timecourse of $\Delta R/R_0$ using Fura-2 in adult (black) and young mice (grey). **B.** Average not normalized $\Delta R/R_0$ in ACSF (4 samples, between 375-435 sec) vs. $\Delta R/R_0$ in 10 mM caffeine (4 samples between, 525-585 sec) Left: Young mice, (P2-6, n=5 animals) Right: adult mice, (>P60, n=5 animals; $P = 0.45$). (Paired Student's t-test) **C.** Caffeine-induced change in $\Delta R/R_0$ normalized to internal control in ACSF (at 375-435 sec), (P2-P6, n= 5; P9, n= 5; P15, n= 5; adult, n= 5; Paired Student's t-test). No significant change in baseline $\Delta R/R_0$ at any age without application of caffeine (P2-P6, $P = 0.38$, n=3; P9, $P = 0.22$, n=3; P15, $P = 0.38$, n=3; adult, $P = 0.30$, n=3); (Paired Student's t-test) (Scullin *et al.*, 2010).

We next examined whether changes in the participation of Ca^{2+} -dependent release from presynaptic Ca^{2+} stores could contribute to the observed age-dependent differences in the $[\text{Ca}^{2+}]_{\text{res}}$ clearance timecourse. Thus, we tested the contribution of these internal stores to $[\text{Ca}^{2+}]_{\text{res}}$ in SC-CA1 terminals from both young and adult mice by measuring the relative change in $\Delta\text{R}/\text{R}_0$ in response to bath application of 10 mM caffeine. Caffeine increases the Ca^{2+} sensitivity of ryanodine receptors and thereby initiates release of Ca^{2+} from Ca^{2+} -sensitive internal stores into the cytoplasm (Verkhratsky, 2005). As shown in Figure 4.6A, there was a consistent, significant increase in $\Delta\text{R}/\text{R}_0$ following application of caffeine in SC-CA1 terminals of young mice (P2-P6); but no equivalent increase in $\Delta\text{R}/\text{R}_0$ in adults (Figure 4.6B). Furthermore, the normalized change in the effectiveness of caffeine occurred during the narrow developmental time period between P6 and P9 (Figure 4.6C). Both the thapsigargin and caffeine data suggest that some of the developmental decrease in the timecourse of $[\text{Ca}^{2+}]_{\text{res}}$ clearance results from a decreasing effectiveness of internal stores involvement during this process.

To investigate the contribution of Ca^{2+} clearance to short-term plasticity, we measured the $\Delta\text{F}/\text{F}_0$ response during paired-pulses at a 50 ms interpulse interval (Figure 4.7A). We computed the ratio of the paired-pulse $\int\Delta\text{F}/\text{F}_0$ to the single pulse $\int\Delta\text{F}/\text{F}_0$ in order to compare the changes in $[\text{Ca}^{2+}]_{\text{res}}$ between the first and second of paired stimuli. We have previously shown in SC-CA1 terminals from adult rats that, after subtracting the residual $\Delta\text{F}/\text{F}_0$ that remains following the first of paired-pulses, there is an increase of $\int\Delta\text{F}/\text{F}_0$ resulting from the second pulse (Schiess *et al.*, 2006). This increase would lead us to anticipate a ratio >2 of the paired-pulse $\int\Delta\text{F}/\text{F}_0$ to the single pulse $\int\Delta\text{F}/\text{F}_0$. As expected, the $\int\Delta\text{F}/\text{F}_0$ ratio was significantly greater than two in the adult mouse indicating an supra-

linear increase of $[Ca^{2+}]_{res}$ during the second pulse (Figure 4.7B). Surprisingly, however, we found that at P1 the $\int \Delta F/F_0$ ratio is significantly less than two and that between P3 and P9 the $\int \Delta F/F_0$ ratio did not differ from two. Thus the short-term effect of $[Ca^{2+}]_{res}$ on subsequent Ca^{2+} clearance reflects unique characteristics at P1 and the adult phenotype is not established until about P15.

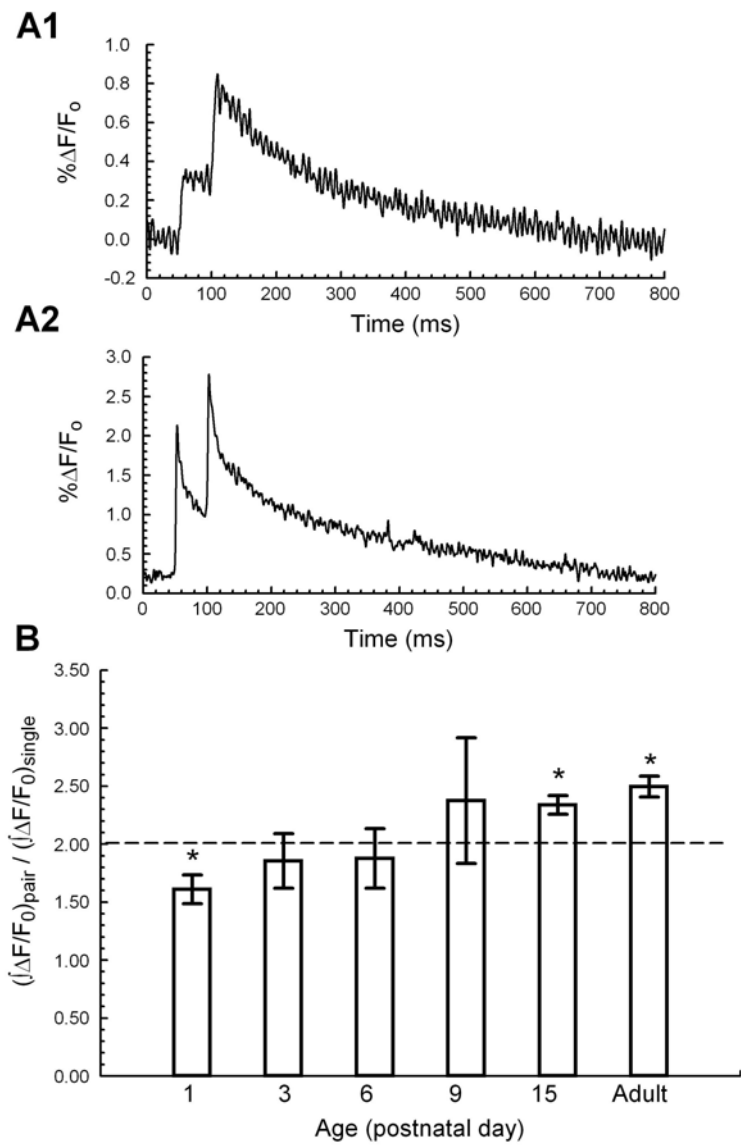


Figure 4.7 Developmental increase in $[Ca^{2+}]_{\text{res}}$ during paired-pulses.

A. Representative traces of $\Delta F/F_0$ during paired stimulation (A1 P6; A2 adult (P85); Mg Green) **B.** Ratio of paired stimulus $\int \Delta F/F_0$ trace versus single stimulus $\int \Delta F/F_0$ trace at different developmental ages, (P1, n=4; P3, n=6; P6, n=11; P9, n=6; P15, n=4; adult, n=5 animals) (Student's t-test against a theoretical mean of 2) (Scullin *et al.*, 2010).

Discussion

Developmental changes in short-term facilitation have been proposed to be correlated with changes in presynaptic Ca^{2+} (Wasling *et al.*, 2004). We demonstrate here that there is a developmental threshold for the involvement of presynaptic $[\text{Ca}^{2+}]_{\text{res}}$ in the regulation of short-term synaptic facilitation. This temporal change occurs between P6 and P9 at which time there is a marked alteration in the $[\text{Ca}^{2+}]_{\text{res}}$ clearance, in the amount of $[\text{Ca}^{2+}]_{\text{res}}$ following a single pulse, and in the accumulation of Ca^{2+} in intracellular stores. This was apparent in the incremental change in the general shape of the $[\text{Ca}^{2+}]_i$ response (Figure 4.3A), in the peak amplitude of this response (Figure 4.3B), and in the time that it takes to reach the peak (Figure 4.3C). The developmental decrease in the $\int v\Delta F/F_0$ (Figure 4.2) further indicates that there are important age-dependent changes in the time course of $[\text{Ca}^{2+}]_{\text{res}}$ clearance and hence the total amount of Ca^{2+} available in the presynaptic terminal.

Paired pulse facilitation at a 50 ms interpulse interval undergoes a significant developmental increase after the first postnatal week (Figure 4.1). Other studies have shown an additional decrease in the PPR between juvenile (P13-18) and young adult (P28-42) rat SC-CA1 terminals (Speed & Dobrunz, 2007). Although we observed a small decline in the PPR between P15 and adult, this decrease was not significant. The difference in these observations could be a result of the broader range of ages of our adult animals, or of species differences between mice and rats. Additionally, while we consistently placed our stimulating electrode in the *stratum radiatum*, where we would expect to stimulate only Schaffer collateral fibers, it is possible that in some instances the stimulus current could have spread to temporoammonic fibers in the *stratum lacunosum-*

moleculare. In contrast to the decrease of PPF between juvenile and adult Schaffer collateral terminals, PPF in temporoammonic fiber terminals increases during this developmental period (Speed & Dobrunz, 2009). It is conceivable therefore, that current spread to *stratum lacunosum-moleculare* in some of our slices could have counteracted the expected age-dependent decrease in the SC-CA1 terminals.

Wasling and colleagues have shown that there is a developmental change in release probability of the first of paired responses that is indicative of this change in facilitation in rats (Wasling *et al.*, 2004). While our determination of spatially and temporally averaged $\Delta F/F_0$ does not directly reflect the $[Ca^{2+}]$ in the release domain nor does it typically reflect influences on release probability of the initial pulse, changes in the measured rise time (Figure 4.3C) do suggest a developmental change in the $[Ca^{2+}]$ that determines release during the first pulse. Although action potentials are a few milliseconds broader in immature than in adult neurons (Lockery & Spitzer, 1992; Gao & Ziskind-Conhaim, 1998), this increased period of depolarization is not expected to increase the duration of Ca^{2+} influx sufficiently to account for the observed slower rise time of $[Ca^{2+}]_{res}$. A possible explanation for the slower clearance of $[Ca^{2+}]_{res}$ in slices from young animals could be maturational changes from growth cones and silent synapses to mature synapses. Growth cones differ from mature synapses in their morphology and volume, their larger number of L-type VGCCs (Ohbayashi *et al.*, 1998), and the role of Ca^{2+} -induced Ca^{2+} release (Tojima *et al.*, 2007). Functionally, influx through L-type VGCCs has been shown to play a role in activation of presynaptic silent synapses (Yao *et al.*, 2006) and in the change from silent to active synapses (Gasparini *et al.*, 2000; Cabezas & Buno, 2006). Any of these factors might be a significant

contributory factor to the observed maturational differences in $[Ca^{2+}]_{res}$ clearance.

However, these alterations in $[Ca^{2+}]_{res}$ kinetics would not be expected to contribute to the observed changes in PPF, since short-term synaptic plasticity must depend on mechanisms specific to presynaptic terminals of functional synapses.

In presynaptic terminals of the adult rodent brain, $[Ca^{2+}]_{res}$ decay kinetics are accurately reflected by the sum of two exponentials (Schiess *et al.*, 2006), which indicates either two separate populations with first order kinetics or a multi-step process. A likely candidate for such a multi-step process is the presynaptic Ca^{2+} clearance by the endoplasmic reticular SERCA pump (Higgins *et al.*, 2006). The decay kinetics for $[Ca^{2+}]_{res}$ in presynaptic terminals of immature SC-CA1 synapses is slower, and is not accurately fit with a double exponential. We thus chose to analyze the timecourse of $[Ca^{2+}]_{res}$ decay in immature synapses by dividing it into the temporally distinct components of peak time, slow time constant, and the ratio of the peak slow component to the peak amplitude. As shown in Figures 3C, 4A, and 4B, each of these components showed an age-dependent decrease. This indicates a developmental change in the underlying kinetic processes, and consequently marked differences in the mechanisms of $[Ca^{2+}]_{res}$ clearance in immature and mature synapses that are coincident with the establishment of the adult phenotype of short-term plasticity (Wasling *et al.*, 2004; Dumas, 2005). Importantly, expression levels and isoform expression of proteins with demonstrated roles in synaptic plasticity and Ca^{2+} sensitivity have been shown to change during this maturational period, including, for example, adenylyl cyclases 1 and 8 (Conti *et al.*, 2007), CDK1/4 (Li *et al.*, 2007), and SNAP-25 (Bark *et al.*, 1995).

As noted above, the multi-step kinetics of $[Ca^{2+}]_{res}$ clearance are consistent with the established multi-step kinetics of Ca^{2+} sequestration by SERCA, making changes in this pathway likely candidates for the mechanism for our observations. There are conflicting findings regarding the role of Ca^{2+} -induced Ca^{2+} release from internal stores in short-term plasticity (Emptage *et al.*, 2001; Carter *et al.*, 2002; Cabezas & Buno, 2006). Furthermore, age-dependent changes in ryanodine receptor expression levels have been shown play a role in endogenous cannabinoid mobilization (Isokawa & Alger, 2006) and the maintenance of presynaptic forms of LTP (Martin & Buno, 2003). We therefore reasoned that developmental changes in the ability to sequester Ca^{2+} in intracellular stores could affect the timecourse of $[Ca^{2+}]_{res}$ clearance directly through $[Ca^{2+}]_{res}$ uptake from the cytoplasm, or indirectly because of a counteracting Ca^{2+} release into the cytoplasm. We found that blocking SERCA-dependent Ca^{2+} sequestration increased the $\int \Delta F/F_0$ in adult presynaptic terminals while causing a decrease at P3 and no difference in the P5 to P6 age group. Even with the more sensitive Fura2 measurements, we were unable to discern a passive Ca^{2+} release from stores induced by thapsigargin in slices from either young or adult animals; however, thapsigargin slowed $[Ca^{2+}]_{res}$ clearance in slices from animals older than P3, but not in slices from those that were younger than P3.

Additionally, we found that caffeine, which can release Ca^{2+} from ryanodine-sensitive stores, caused an increase in presynaptic $[Ca^{2+}]_i$ in the younger, but not in more mature mice. These results suggest that, while SERCA uptake and Ca^{2+} -induced Ca^{2+} release are effective at all ages, there are developmental differences in the passive leak from stores and in the processes that participate in $[Ca^{2+}]_{res}$ clearance. Taken together, these data suggest that the basal filling state of intracellular Ca^{2+} stores could account for

much of the developmental differences in $[Ca^{2+}]_{res}$ clearance. Although SERCA sequestration is effective in both immature and mature terminals, a more effective passive leak in mature neurons would yield a lower basal store of Ca^{2+} in these terminals. As a consequence of the minimal store filling state, SERCA uptake would play a more significant role in speeding $[Ca^{2+}]_{res}$ clearance in mature terminals; yet the more effectively filled stores of immature terminals would allow Ca^{2+} -induced Ca^{2+} release to effectively slow $[Ca^{2+}]_{res}$ clearance. This interpretation is consistent with observations of the involvement of Ca^{2+} -induced Ca^{2+} release in organotypic slice cultures from P8 animals (Emptage *et al.*, 2001) and P15 animals (Cabezas & Buno, 2006) and the contrasting minimal effectiveness of Ca^{2+} -sensitive stores in adult synapses (Carter *et al.*, 2002).

The $[Ca^{2+}]_{res}$ decay kinetics in the adult rodent SC-CA1 synapse have been shown to be unaffected by Ca^{2+} buffer saturation (Blatow *et al.*, 2003). In contrast, regulation of presynaptic $[Ca^{2+}]_i$ in immature SC-CA1 synapses (Dekay *et al.*, 2006) has been reported to be somewhat more sensitive to Ca^{2+} buffer saturation. Our results provide additional support for the notion that the development of mature $[Ca^{2+}]_{res}$ clearance dynamics is not a single mechanistic change, but rather a complex series of modifications that include buffering, SERCA-dependent sequestration, and Ca^{2+} dependent release from intracellular Ca^{2+} stores.

We find that, although SC-CA1 presynaptic terminals of younger mice have greater total integrated $[Ca^{2+}]_{res}$ than adults (Figure 4.2), these synapses exhibit less short-term facilitation (Figure 4.1). Interestingly, although slices from mature animals did exhibit an expected positive correlation between PPF and $[Ca^{2+}]_{res}$ (Figure 4.3D), we

unexpectedly found that the zero $[Ca^{2+}]_i$ intercept in this relationship increased with age (Figure 4.3E), consistent with the notion that this could reflect a maturation of the expression of a high affinity facilitatory site. Additionally, slices from adult and young animals differed markedly in the relationship between PPF and $\int v\Delta F/F_0$ (Figure 4.2C) suggesting a developmental change in the mechanisms that regulate the time course of available Ca^{2+} that influences facilitation.

Clearly, the dependence of short-term facilitation on $[Ca^{2+}]_{res}$ that is characteristic of adult presynaptic terminals, is undeveloped before P9. Since all of our pre- and postsynaptic data result from population measurements, it is impossible to draw conclusions from them about the maturation of individual synapses. It is likely that the developmental process that we observe, does not indicate a homogenous transformation of uniform synapses, but rather reflects trends in a heterogeneous population. However, regardless of their source, our data show that the developmental change in $[Ca^{2+}]_{res}$ kinetics that lead to the mature phenotype of a positive correlation between PPF and $[Ca^{2+}]_{res}$ is not firmly established before P9. Importantly, the lack of a significant positive correlation between PPF and $[Ca^{2+}]_{res}$ (Figure 4.3D) in the P3-6 mice could be due to a change in the relative contributions of PPD and PPF in the population of synapses.

Several underlying mechanisms can be suggested that may mediate the developmental change in the relationship between $[Ca^{2+}]_{res}$ and facilitation. (1) As discussed above, a varying portion of the $[Ca^{2+}]_i$ signal in the slices from immature animals could be from electronically silent growth cones or from silent synapses. (2) The slowed $[Ca^{2+}]_{res}$ clearance in the younger animals could result in a greater $[Ca^{2+}]$

available to deplete the readily releasable pool of vesicles and thus counterbalance a $[Ca^{2+}]_{res}$ -dependent tendency toward increased facilitation (Liley & North, 1953; Takeuchi, 1958; Elmqvist & Quastel, 1965; Thies, 1965; Betz, 1970; Zucker & Regehr, 2002). (3) Age-dependent changes in Ca^{2+} -dependent inhibition of the presynaptic Ca^{2+} currents could contribute to developmental changes in short-term synaptic plasticity (Li *et al.*, 2006; Sullivan, 2007). (4) Expression of an independent modulatory component of the vesicle release machinery such as the high affinity site, which has been suggested to be necessary for facilitation in SC-CA1 synapses, could mature during this time period (P6 to P9) (Atluri & Regehr, 1996; Bark *et al.*, 2004; Schiess *et al.*, 2006). (5) Finally, the change in this relationship could reflect an alteration of the local domain of Ca^{2+} that facilitates release due to a shift of the contribution from internal Ca^{2+} stores. A potential mechanism signaling this change is a difference in the kainate-sensitive glutamate receptor activation, possibly due to BDNF signaling (Lauri *et al.*, 2006; Sallert *et al.*, 2009).

We report here important developmental changes in short-term plasticity and the kinetics of presynaptic $[Ca^{2+}]_{res}$ clearance. These dramatic developmental changes could have important implications for synaptic filtering characteristics and their effects on information processing in the hippocampus (Partridge & Valenzuela, 2002). Understanding the molecular mechanism that drive these changes will be essential to evaluate the neurological impact of presynaptic Ca^{2+} clearance on diseases that have their onset during the transitional period of the juvenile to adult nervous system.

Chapter 5 - Altered regulation of presynaptic residual Ca^{2+} is dependent on SNAP-25 in hippocampal synapses in mice

Abstract

Paired pulse facilitation (PPF) is a form of short-term synaptic plasticity that results from an interaction of residual presynaptic Ca^{2+} ($[\text{Ca}^{2+}]_{\text{res}}$), number of release-competent vesicles, and the sensitivity of the vesicle release mechanisms to Ca^{2+} . While PPF is normally enhanced at Schaffer collateral-CA1 (SC-CA1) synapses, the facilitation is greater in adult mutant mice that exhibit a reduced level of the presynaptic protein SNAP-25 and over-express the SNAP-25a isoform that is predominantly expressed in juvenile animals. This alteration of a key component of the protein machinery required for neurotransmitter release provides a useful tool to investigate mechanisms that influence short-term plasticity. To explore the link between SNAP-25 and PPF, we simultaneously measured postsynaptic potential and presynaptic $[\text{Ca}^{2+}]_{\text{res}}$ during paired-pulses at a 50 ms interpulse interval in adult *Snap25^{tm2M_{cw}}* (Tkneo) mice, *Snap25^{tm1M_{cw}}* heterozygote null (HET) mice and wild type (WT) mice. We demonstrate that enhanced PPF is maintained at mature hippocampal synapses of Tkneo mice and that $[\text{Ca}^{2+}]_{\text{res}}$ saturation during PPF is altered at both Tkneo and HET mice synapses. To relate short-term plasticity to $[\text{Ca}^{2+}]_{\text{res}}$, we applied a vesicular release probability model (Model 2) for neurotransmission that evaluates facilitation based on two states of release probability. These results suggest that the concentration of SNAP-25 and, in particular, the expression of its developmentally regulated isoforms, affects $[\text{Ca}^{2+}]_{\text{res}}$ dynamics and the ability of releasable vesicles to enter into a facilitated state.

Introduction

Paired pulse facilitation (PPF) is a form of plasticity that results from primarily presynaptic mechanisms, which include the actions of presynaptic residual Ca^{2+} ($[\text{Ca}^{2+}]_{\text{res}}$), the number of release-competent vesicles, and the sensitivity of vesicle release mechanisms to Ca^{2+} (Zucker & Regehr, 2002). SNAP-25 is a key component of the exocytotic machinery that mediates neurotransmitter release (Sorensen, 2005) and can act directly on voltage-dependent ion gated channels to alter Ca^{2+} influx that triggers membrane fusion (Catterall, 1999). SNAP-25 is thus well positioned to govern changes of short-term plasticity. The growing evidence that the *SNAP25* gene and protein are associated with neuropsychiatric and neurological disorders (Corradini *et al.*, 2009), emphasizes the importance of understanding how this protein participates in modulating synaptic function. Nevertheless, the precise role of this SNARE protein in influencing the physiology of neurotransmission has been controversial (Matteoli *et al.*, 2009).

Vesicular release of neurotransmitter requires the formation of a ternary complex comprised of members of the SNARE (soluble N-ethylmaleimide factor attachment receptor) protein family (Fukuda *et al.*, 2000). The t-SNARE, SNAP-25, has been shown to play an essential role in action potential-dependent exocytosis at neural synapses (Washbourne *et al.*, 2002). This protein is encoded as two isoforms generated by alternative splicing of tandemly arranged, divergent copies of exon 5 (Bark, 1993; Bark *et al.*, 1995). In neonatal brain, SNAP-25a is the predominant isoform, but after the first postnatal week the relative ratio of the two isoforms is reversed and SNAP-25b constitutes roughly 90% of the total in most regions of the adult rodent nervous system (Catsicas *et al.*, 1991; Bark *et al.*, 1995; Boschert *et al.*, 1996; Jacobsson *et al.*, 1999).

The *Snap25*^{Tkneo} mutation, generated by the insertion of the HSV thymidine kinase neomycin phosphotransferase reporter gene downstream of the alternatively spliced exons 5a and 5b, suppresses the developmental transition of splicing that produces the two isoforms and also reduces the overall expression of SNAP-25 (Bark *et al.*, 2004). Consequentially, homozygous mutant mice (Tkneo) exhibit the isoform and expression level profile typical of juvenile (P4 – P7) mice. (Bark *et al.*, 2004). Electrophysiological analysis has shown that PPF at Schaffer collateral to CA1 pyramidal neuron (SC-CA1) synapses of adolescent Tkneo mice is enhanced compared to wild type (WT) littermates and similar aged heterozygote null (HET) mice. Since SNAP-25 has been suggested to modulate the Ca²⁺ dependency of vesicular release (Graham *et al.*, 2002; Bronk *et al.*, 2007), the increased PPF of Tkneo mice could result from an alteration of this processes. To investigate the relationship between the presynaptic [Ca²⁺]_{res} dynamics and changes in PPF, we carried out Ca²⁺ imaging and field excitatory postsynaptic potential recording (fEPSP) of SC-CA1 synapses in adult *Snap25* Tkneo, HET, and WT mice. These data were fit by Model 2 that describes the [Ca²⁺]_{res}-dependent recruitment of vesicles into a subpopulation that has a higher release probability (Bark *et al.*, 2004; Schiess *et al.*, 2006). This analysis suggests that SNAP-25 isoforms can affect the effectiveness of [Ca²⁺]_{res} in facilitating vesicle release, but the precise mechanism is unknown.

Materials and Methods

Slice preparation

Experiments were performed in coronal hippocampal slices prepared from adult mice (60 to 120 days, average 100 days). Strains bearing the *Snap25^{Tkneo}* (Mouse Genome Informatics allele designation *Snap25^{tm2Mcw}*) (Bark *et al.*, 2004) and *Snap25* null (*Snap25^{-/-}*, MGI allele designation *Snap25^{tm1Mcw}*) (Washbourne *et al.*, 2002) mutations are maintained by brother:sister heterozygote matings after 7 backcross generations to C57Bl/6 at the UNM HSC Animal Resource Facility. Homozygous *Tkneo* (referred to as *Tkneo*) mice, wild type (WT) mice, and heterozygote null mice (referred to as HET) mice were selected after genotyping from litters of the respective heterozygote matings. Genotypes were confirmed for all experimental animals from tail clips taken after removal of the brain for physiological studies. Animals were deeply anaesthetized by i.p. injection of 250 mg kg⁻¹ ketamine, brains were rapidly removed, and slices were cut at 300 µm with a vibroslicer (Pelco 101, St Louis, MO, USA) in an ice bath with a cutting solution containing (mM): 220 sucrose, 3 KCl, 1.2 NaH₂PO₄, 26 NaHCO₃, 12 MgSO₄, 0.2 CaCl₂, 10 glucose and 0.01 mg ml⁻¹ ketamine equilibrated with 95%O₂-5%CO₂. Slices were then transferred to a bath containing artificial cerebrospinal fluid (ACSF) containing (mM): 126 NaCl, 3 KCl, 1.25 NaH₂PO₄, 1 MgSO₄, 26 NaHCO₃, 2.5 CaCl₂ and 10 glucose equilibrated with 95%O₂-5%CO₂ at 30°C for 1 h and then maintained at room temperature until transfer to a temperature-controlled recording chamber (Warner Instruments, Hamden, CT, USA or Scientific Systems Design, Mercerville, NJ, USA), which was maintained at 32°C and continuously perfused at 2 ml min⁻¹ with ACSF saturated with 95%O₂-5%CO₂. All experiments were approved by the Institutional

Animal Care and Use Committee at the University of New Mexico Health Sciences Center Laboratory Animal Care and Use Committee, and the National Institutes of Health.

Presynaptic Ca²⁺ imaging

Presynaptic fibers were filled with the Ca²⁺ fluorophore, Mg Green AM or Fura-2 AM (Molecular Probes, Eugene, OR, USA) using an established technique (Regehr & Tank, 1991; Wu & Saggau, 1994; Atluri & Regehr, 1996; Sinha *et al.*, 1997, Kamiya, 1999 #56). This technique allowed simultaneous measurements of presynaptic [Ca²⁺]_i and postsynaptic fEPSPs. In some instances, either the presynaptic or postsynaptic recording was not successful, but the data from the successful component were still included. To minimize the effect of exogenous buffers we used Mg-Green, with a Ca²⁺ binding K_D = 6 μM for experiments in which we measured the timecourse of ΔF/F₀ decay (Regehr & Atluri, 1995; Atluri & Regehr, 1996). To control for bleaching in longer experiments we measured the fluorescent ratio using Fura-2 at the beginning and end of each stimulus train (40ms 350nm then 40ms 380nm). Briefly, an ejection electrode (tip diameter 5 – 10 μm) containing the fluorophore (0.9mM Mg Green AM or Fura-2 AM, 10% DMSO, 1% pluronic acid in ACSF) was lowered into the fiber pathway between the stimulating electrode and the presynaptic terminal field to be investigated. While observing the emission image following excitation (490 nm) an air pressure pulse was applied with a syringe to the ejection electrode until a small bright spot (≈ 1 μl) was observed in the fiber pathway.

The slice was then maintained with a 2 ml min⁻¹ flow of oxygenated ACSF at 32°C for 1 h to allow intracellular diffusion of the dye to the presynaptic imaging site 500

μm away from the ejection site. The excitation light was then reduced to a 100–200 μm diameter spot with a diaphragm in the epi-illumination path, and the emitted light was measured with a photomultiplier tube (PMT). This spot included or was immediately adjacent to the area electrically summed in the field potential recording. A single stimulus or pairs of stimuli were delivered orthodromically at 0.05 or 0.067 Hz by a Master 8 pulse generator (AMPI Instruments, Jerusalem, Israel) under control of the imaging system (TILL Photonics, Pleasanton, CA, USA). Mg Green fluorescence responses are reported as the ratio of the change in fluorescence to the pre-stimulus fluorescence ($\Delta F/F_0$). The $\Delta F/F_0$ signals were corrected for bleaching by subtraction of a linear baseline slope and were inverted so that increasing presynaptic $[\text{Ca}^{2+}]_i$ produced an upward deflection. To diminish noise inherent with the low-affinity Ca^{2+} indicator, it was necessary to average five fluorescence responses and to filter the PMT signal at 1 kHz. For Fura-2 studies, we first determined the 350 to 380 nm fluorescent ratio and reported the response as the ratio of the change in this ratio to the pre-stimulus ratio ($\Delta R/R_0$). Caffeine time course was measured using Fura-2 ratiometric imaging at 15 s intervals comparing $\Delta R/R_0$ in ACSF to $\Delta R/R_0$ after a minimum of 70 s in 10 mM caffeine only traces in which 40 mM KCl produced a measurable increase in $\Delta R/R_0$ were included in analysis.

We used two tests to demonstrate that the measured $\Delta F/F_0$ signal was consistent with a $[\text{Ca}^{2+}]$ response predominately from the presynaptic Schaffer collateral axons and axon terminals (Wu & Saggau, 1994; Atluri & Regehr, 1996; Sinha *et al.*, 1997; Kamiya & Ozawa, 1999). First, in the presence of 10 μM CNQX, 25 μM D-AP5, and 20 μM bicuculline, the fEPSP was blocked, while the presynaptic fiber volley and $\Delta F/F_0$ signal

were left unchanged confirming that the $\Delta F/F_0$ signal was not a postsynaptic response. Second, subsequent addition of 600 nM TTX blocked both the presynaptic fiber volley and the $\Delta F/F_0$ signal arguing against direct stimulation of inadvertently filled postsynaptic dendrites.

Field potential recordings

We used standard electrophysiological techniques for slice fEPSP recordings in the SC-CA1 pyramidal neuron synapse in the *stratum pyramidale* in hippocampal slices (Schiess et al. 2006). Briefly, fEPSPs were recorded with an Axoclamp 2B or Multiclamp 700B amplifier (both from Axon Instruments, Union City, CA) and a Digidata 1322A interface using pCLAMP 9.2 or 10 software (Axon Instruments) for experimental control and data analysis. fEPSPs were digitized at 50 kHz and filtered at 2 kHz. Presynaptic constant current pulses (150 μ s duration) were applied to Schaffer collateral fibers with an Iso-Flex constant current stimulator (AMPI Instruments, Jerusalem, Israel) through a concentric bipolar electrode (FHC, Bowdoinham, ME) at a current, which was adjusted to produce 40-60% of the maximum fEPSP population spike amplitude. For simplicity we define the response to the first of paired-pulses as R1 and that to the second as R2. R1 to R2 relationships were measured using current steps between 0 and 2 mA. The paired-pulse ratio (PPR) of fEPSP signal was calculated as the ratio of the amplitude of second pulse at a 50 ms interpulse interval to that of the initial pulse. Tetanus was given as 2 seconds of 10 Hz followed by no stimulus for 2 seconds.

Data analysis

The $\Delta F/F_0$ signal was digitally filtered with a five point center-weighted filter and numerically integrated after being normalized to the $\Delta F/F_0$ peak value ($\int v \Delta F/F_0$) yielding

a value proportional to the timecourse of $[Ca^{2+}]_i$ decay. Fitting and statistical analysis were carried out with Matlab 7.0 (Mathworks, Natick, MA) using programs described in Appendix B or Prostat 4.0 (Polysoft International, Pearl River, NY). Coefficient of Determination (C. O. D.) was used as a measure of goodness of fit for linear regressions. Average data are presented as means \pm s.e.m., and statistical significance was determined at $P < 0.05$. Statistical significance indicated as: * $p < 0.05$, ** $p < 0.01$, *** $p < 0.001$.

Drugs

Drugs were stored frozen in aliquots and diluted to the appropriate concentration in ACSF on the day of the experiment. 6-Cyano-7-nitroquinoxaline-2,3-dione (CNQX), d-(1)-2-amino-5-phosphonopentanoic acid (d-AP5), bicuculline, thapsigargin and tetrodotoxin (TTX) were obtained from Tocris (Ellisville, MO, USA). All other reagents were obtained from Sigma-Aldrich (St. Louis, MO, USA). Drugs were applied through a bath perfusion system for a minimum of 10 min (>2.5 bath exchanges) before recording commenced.

Modeling-Adaption of Model 2

Model 2 is described in Chapter 2, but in summary: Model 2 evaluates facilitation based on two states of release probability that consider both $[Ca^{2+}]_{res}$ and depletion of the readily releasable pool of vesicles (Bark *et al.*, 2004; Schiess *et al.*, 2006). Central to Model 2 is a Ca^{2+} -dependent process in which the release state is based on the following factors: the probability of release (P_R) of the first state ($P1$), the P_R of the second facilitated state ($P2$), and the fraction of vesicles (a) that are recruited to the second state with a higher P_R that is a function of the increase in $[Ca^{2+}]_{pre}$. One interpretation of this model is that $[Ca^{2+}]_{res}$ acts through a second facilitatory site on the

release machinery to modulate Ca^{2+} -dependent vesicle release. Other models with similar assumptions have also been proposed for PPF, e.g. (Jiang & Abrams, 1998; Dittman *et al.*, 2000; Rozov *et al.*, 2001). According to this model:

$$R1/N1 = P1$$

$$R2/N1 = aP2(1-P1) + P1(1-P1)(1-a)$$

where $R1/N1$ and $R2/N1$ are directly proportional to the amplitudes of the R1 and R2 fEPSP population spikes; $N1$ is proportional to the size of the readily releasable pool; $P1$ is the basal release probability; $P2$ is the larger, facilitated release probability; and a is the fraction of vesicles influenced by $[\text{Ca}^{2+}]_{\text{res}}$.

We assumed that a is sigmoidally related to $P1$ as a Hill function:

$$a = a_{\text{max}} / (1 + (S * EC / R1)^{HN})$$

where a_{max} is related to the maximum effectiveness of $[\text{Ca}^{2+}]_{\text{res}}$ in facilitating release; S is related to the sensitivity of $R1$; HN , the Hill coefficient, determines the steepness of this relationship; and EC is the half maximum effective concentration or EC_{50} of the Hill equation. Table 5-1 gives the values of these parameters from least squares fits of the model equations to the shown data (Figure 5.3B).

This model was expanded to model the PPR by measuring $\text{PPR}(\text{Ca}^{2+}) = R2/R1(\text{Ca}^{2+})$ with a calculated from Table 5-1, and the $R1$ at different values of $[\text{Ca}^{2+}]_o$ taken from those in Figure 5.4B scaling such that 2.5mM $[\text{Ca}^{2+}]_o$ is 0.5.

Results

To characterize the relationship between SNAP-25 and Ca^{2+} -dependent mechanisms of enhanced short-term synaptic plasticity, we evaluated the dynamics of presynaptic residual Ca^{2+} ($[\text{Ca}^{2+}]_{\text{res}}$) and plasticity in Tkneo, HET, and WT mice (Bark *et al.*, 2004). Tkneo mice were reported to have about a 50% reduction in the overall level of SNAP-25 protein expression. Moreover the adult Tkneo express increased SNAP-25a and reduced SNAP-25b level characteristic of juvenile (P4 – P7) mice (Bark *et al.*, 2004). HET mice bear the targeted ablation of one *Snap25* WT allele and exhibit a 50% reduction of SNAP-25 (Washbourne *et al.*, 2002; Pozzi, *et al.* 2008), but maintain the normal predominate expression of SNAP-25b in RNA (or 95% in hippocampus) as seen in WT see Figure A-2. Since in HET mice, SNAP-25 levels are comparable to those in Tkneo mice, they serve as controls to distinguish between effects due to the decrease in total SNAP-25 and those resulting from increased expression of the SNAP-25a isoform of Tkneo mice (Bark *et al.*, 2004; Bark, 2009). Comparison of the amplitudes of the fEPSP population spikes at half maximum stimulus intensity, however, showed that there were no significant differences in single stimulus responses among the three genotypes (Figure 5.1A & 5.1B). We reported previously that synaptic short-term facilitation at SC-CA1 synapses of adolescent (P21 – P24) Tkneo mice is greater than that of either similarly aged WT littermates or HET mice (Bark *et al.*, 2004). As shown in Fig 1A, B and C, we have confirmed that PPR of fEPSPs is enhanced in adult Tkneo mice (\approx P100) when compared to WT and HET mice. Thus, the phenotype of enhanced plasticity in Tkneo mice is stable from post-weaning adolescence through adulthood.

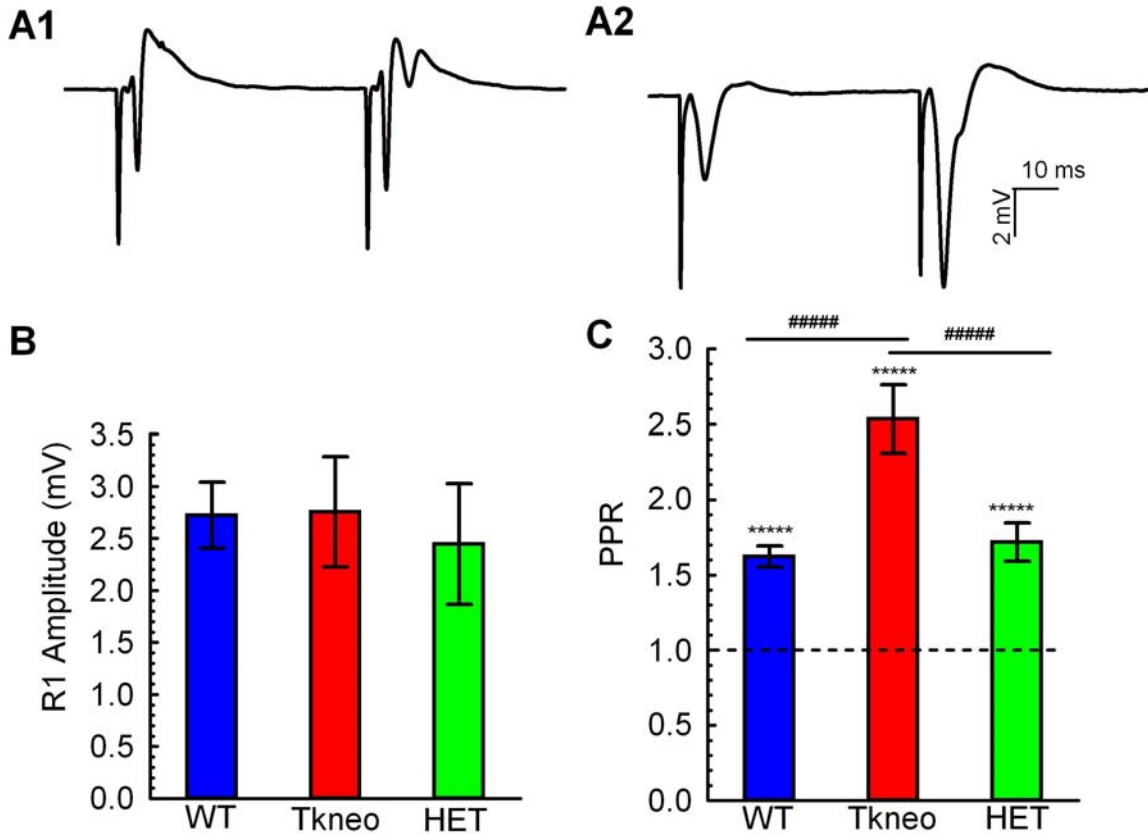


Figure 5.1 Effect of genotype on short-term facilitation.

A. Representative paired-pulse traces (A1 WT, A2 Tkneo). **B.** Amplitude of the fEPSP population spike from the first of paired-pulses at half maximum stimulus intensity. ANOVA of R1 Amplitude vs. genotype shows no significance ($F_{2,77}=1.2394$, $P = 0.2953$). **C.** PPR at 50 ms interpulse interval. ANOVA of PPR versus genotype shows significance ($F_{2,77}=10.9783$ $P < 0.0001$) horizontal bars show Fishers post-hoc test comparing PPR versus genotype, asterisks show Student's t-test against a theoretical mean of 1. (WT, n=30; Tkneo, n=30; HET, n=20).

Relationship of paired-pulse responses

We observed a non-linear relationship between stimulus strength and the amplitude of paired fEPSPs. At lower stimulus strengths, the ratio of R2 to R1 was greater than 1, indicative of PPF. As R1 increased, however, this ratio was reduced, and, in some cases, the ratio became less than 1 reflecting the onset of paired-pulse depression (Figure 5.2A). Because $[Ca^{2+}]_{res}$ is hypothesized to be involved in short-term plasticity (Zucker & Regehr, 2002), we have previously interpreted this non-linear relationship between R1 and R2 fEPSPs to indicate that a mechanism downstream from presynaptic $[Ca^{2+}]_{res}$ contributes to changes in plasticity (Schiess *et al.*, 2006). We describe here distinct genotype differences in the parameters that contribute to this proposed mechanism of synaptic plasticity.

In order to begin to assess how differences in SNAP-25 expression might lead to the greater $[Ca^{2+}]_{res}$ -dependent facilitation observed in Tkneo mice, we fit the non-linear relationship between R1 and R2 fEPSP amplitudes (Figure 5.2A) with a model that accurately reflects PPF and is based on parameters that define Ca^{2+} -dependent vesicle release pools (Schiess *et al.*, 2006). Two important features of this model of presynaptic exocytosis are (i) the existence of an enhanced probability ($P2$) of a second release state and (ii) the parameter a (see Methods) that depends on release during R1 and the amount of $[Ca^{2+}]_{res}$ and reflects the proportion of release-competent vesicles, which can be recruited into the higher probability ($P2$) pool (Bark *et al.*, 2004; Schiess *et al.*, 2006). Since a is dependent on the amplitude of R1 and can be interpreted as representing a facilitatory Ca^{2+} binding site (Schiess *et al.*, 2006), we have described the relationship

between a and $R1$ by a Hill equation that yields the characteristic variables, EC_{50} (EC), Hill coefficient (HN), and a_{max} .

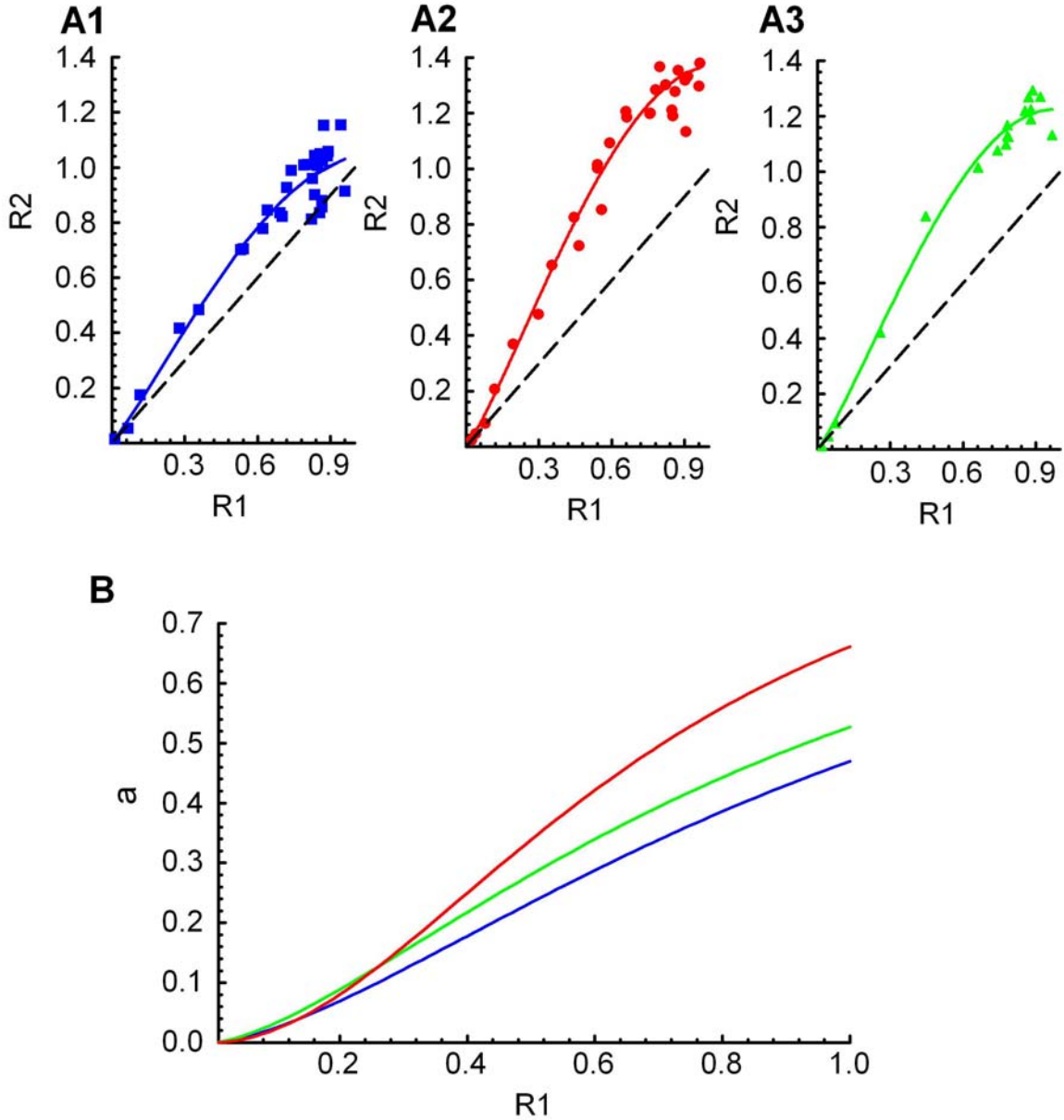


Figure 5.2 Fits of model to paired-pulse fEPSP.

A. Fits of model to paired-pulse fEPSP data (see Table 5.1). **A1.** WT (C.O.D. = 0.9332, $n = 32$); **A2.** Tkneo (C.O.D. = 0.9636, $n = 32$); **A3.** HET (C.O.D. = 0.9371, $n = 18$). Dotted lines indicate equal responses to the first and second pulse. **B.** Model parameter, a , as a function of $R1$ using parameters in Table 5-1. (WT blue, HET green, and Tkneo red).

Table 5-1 Data from fits to following equation

$$R2 = a \times P2 \times (S - R1) + R1 \times \left(1 - \frac{R1}{S}\right) \times a$$

$$a = \left(\frac{YM}{1 + \left(\frac{EC \times S}{R1}\right)^{HN}} \right)$$

where $P2$ is the release probability of the second pulse, S is a scaling factor relating $P1$ and $R1$, and EC , HN and a_{max} are variables in the Hill equation, such that EC reflects the half maximal effective concentration or EC_{50} , HN is the Hill coefficient, and a_{max} = maximum y value for the Hill equation.

	WT	Tkneo	HET
HN	1.539±0.8124	1.969±0.5031	1.515±0.3519
S	8.207±1.536	10.26±1.05	10.26±1.381
EC	0.1318±0.0631	0.0679±0.0081	0.08916±0.0199
a_{max}	1		
$P2$	0.1768		
C.O.D.	0.933	0.967	0.993

Using a non-linear least squares regression, we were able to generate a best fit of the model to the data derived from each of the 3 genotypes (Figure 5.2A1 - A3) and calculate the respective $P2$ and Hill equation parameters for each genotype (Table 5-1). In order to determine the uniqueness of the fits for the three genotypes, we calculated the dependence of the overall probability on the best fit for each of the model parameters. The two variables a_{max} and $P2$, which had the lowest probability of affecting the overall fit, were set to their average values (a_{max} : $F_{2,65}=0.01354$, $P = 0.9866$; $P2$: $F_{2,65}=0.02747$, $P = 0.9729$). This simplified the number of variables in subsequent fitting iterations and greatly increased the reliability of calculating the remaining parameters – EC , S , and HN – derived from fitting the R1 vs. R2 fEPSP data for the 3 genotypes (Table 5-1).

We further tested the applicability of the model by comparing its non-linear fit to a linear regression fit to the same data for all three genotypes. For each group, there was a significantly better fit with the nonlinear regression than with the linear regression (WT: $F_{1,28} = 7.410$, $P = 0.011$; Tkneo: $F_{1,29} = 21.68$, $P < 0.0001$; HET: $F_{1,14} = 22.79$, $P = 0.0003$). Moreover, the fits generated by the model were significantly different among the three genotypes ($F_{2,75} = 105.4$, $p < 0.0001$). The differences among the fits based on the model are best explained by a change in the parameter a where a is a measure of the relative proportion of vesicles that are subject to a probability of release as a result of the first pulse.

Although the statistical differences among the genotypes reflect concurrent changes in all of the parameters, it is instructive to compare the individual parameters of each fit. As shown in Table 5-1, the parameter EC , which reflects the Ca^{2+} -sensitivity of the facilitatory mechanism, was smaller for slices from both Tkneo and HET when compared

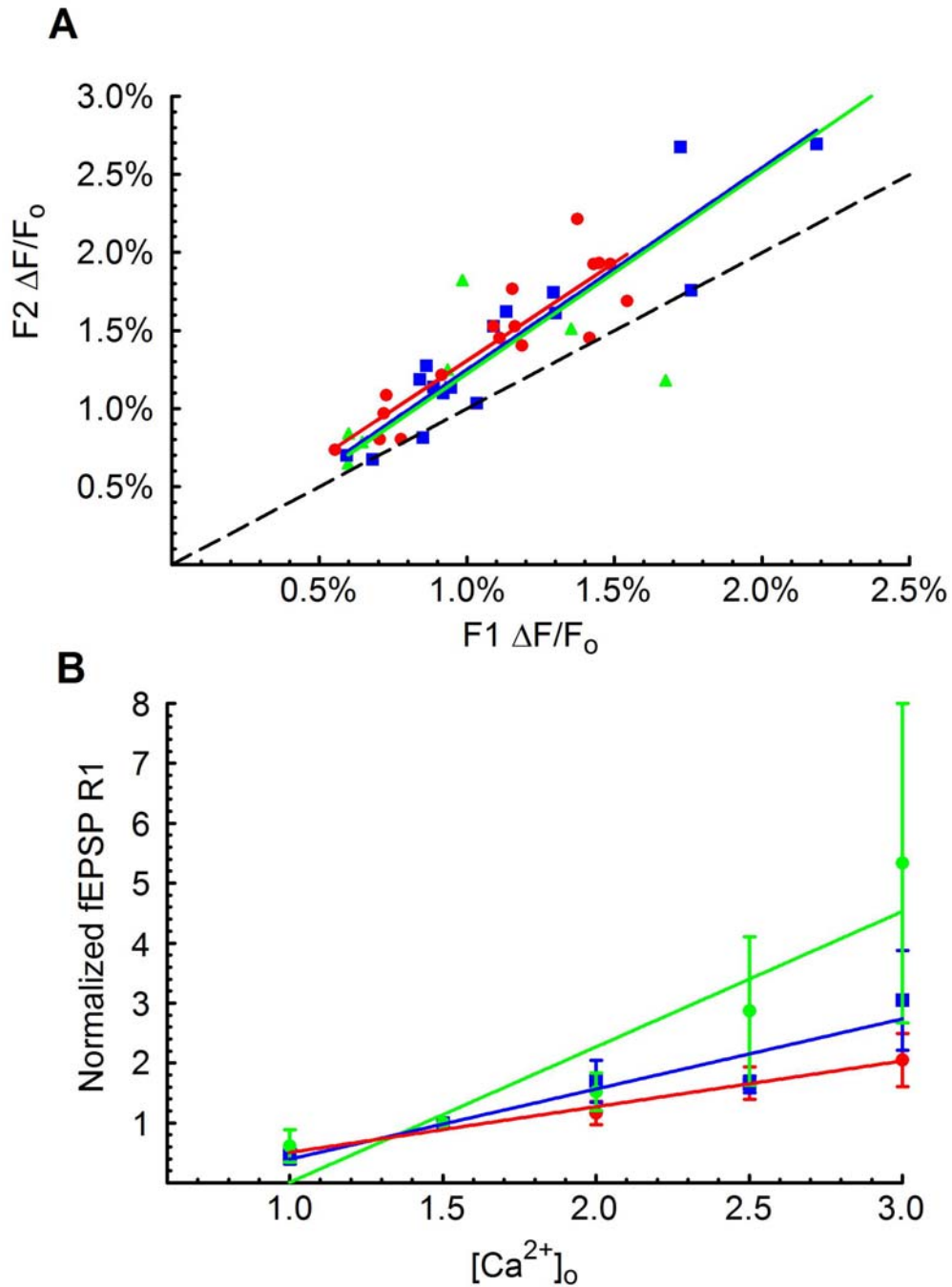


Figure 5.3 Facilitation during paired-pulses.

A. Linear regression fit to paired-pulse $\Delta F/F_0$ responses (WT, slope = 1.259, C.O.D. = 0.8576 blue; Tkneo, slope = 1.2974, C.O.D. = 0.8059 red; HET, slope = 1.2951, C.O.D. = 0.9461, green). Dotted line indicates unity slope. **B.** Relationship between R1 and $[Ca^{2+}]_o$. (WT, slope = 0.763, C.O.D. = 0.9832, n=10 animals, blue; Tkneo, slope = 1.1705, C.O.D. = 0.9018, n = 10 animals, red; HET, slope = 2.2607, C.O.D. = 0.87163, n = 7 animals, green).

to WT mice. This is consistent with an increased contribution of the facilitated state during the second response in Tkneo and HET mice, which have a reduced amount of SNAP-25. Our model additionally allows us to make a novel prediction of the synaptic scaling factor, S (see Methods), which was larger in slices from both Tkneo and HET when compared to WT mice. Overall, these modeling results suggest that a decrease in the amount of SNAP-25 may lead to greater sensitivity of the facilitatory mechanism to $[Ca^{2+}]_{res}$ and this is reflected in the relationship of the parameter a to R1 (Figure 5.2B). This indicates a difference in saturation of $[Ca^{2+}]_{res}$ clearance among the three genotypes that could result from a SNAP-25-dependent increase in cytoplasmic buffering or in an active Ca^{2+} transport process. Importantly, the Ca^{2+} saturation effect on the facilitatory process, as measured by changing $[Ca^{2+}]_o$, could not alone account for the greater PPF in Tkneo when compared to either HET or WT mice. We therefore sought to further investigate additional factors that might contribute to this enhanced plasticity.

Ca²⁺ regulation

As synaptic facilitation has been shown to be correlated with presynaptic $[Ca^{2+}]_{res}$ and our model suggests an increase in Ca^{2+} sensitivity of this process (Regehr & Tank, 1991; Wu & Saggau, 1994; Schiess *et al.*, 2006), we measured presynaptic Ca^{2+} after filling SC-CA1 presynaptic terminals with the fluorescent Ca^{2+} -sensitive indicator, MgGreen-AM. By measuring the relative change in fluorescence ($\Delta F/F_0$), we were able to determine the kinetics of the $[Ca^{2+}]_{res}$ transients that accompanied PPF {Regehr, 1991 #135; Wu, 1994 #88; Schiess, 2006 #67; Scullin, 2010 #645; Scullin, 2010 #646}.

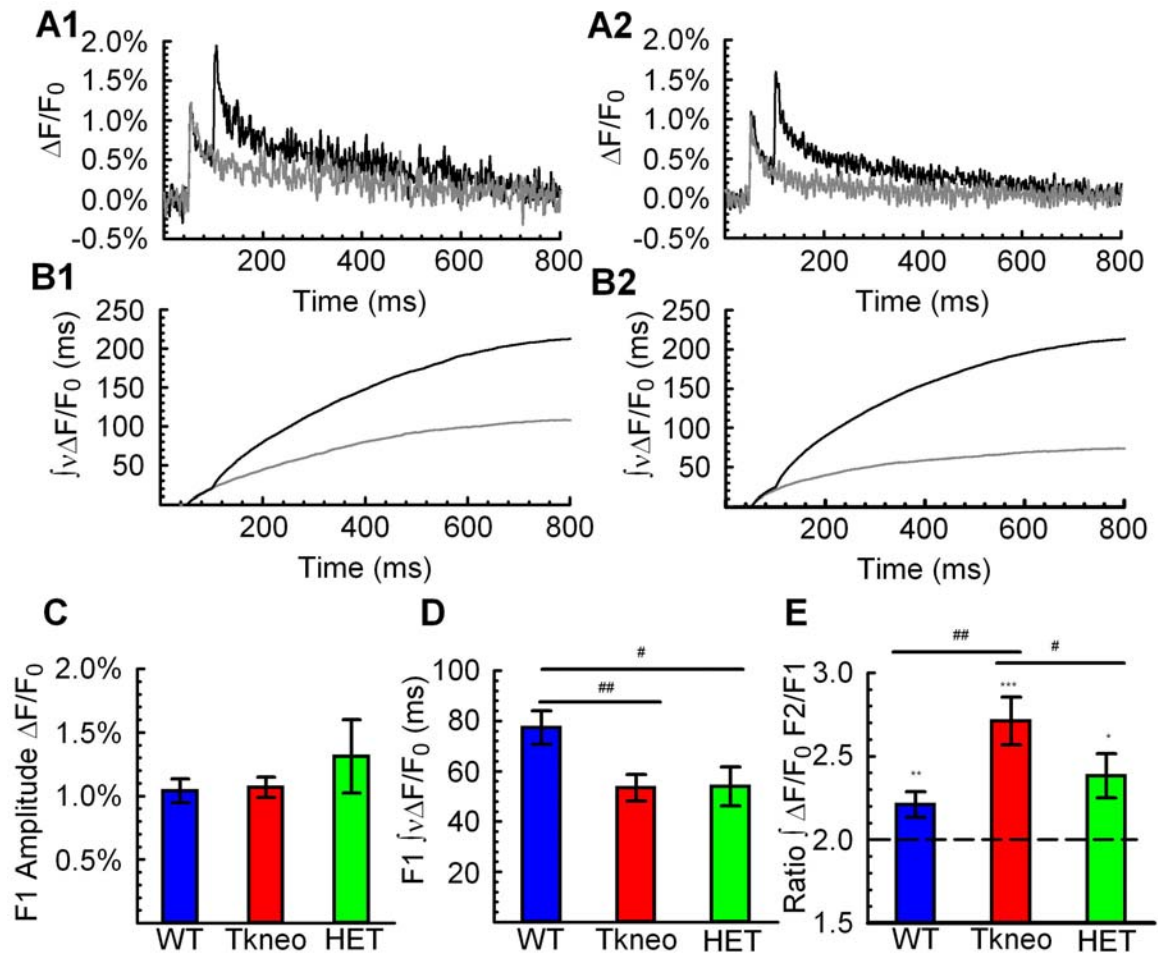


Figure 5.4 Presynaptic $[Ca^{2+}]_{res}$ kinetics during paired-pulses at 50 ms interpulse intervals.

A. Representative $\Delta F/F_0$ traces (**A1**. WT; **A2**. Tkneo). Representative $\int v\Delta F/F_0$ traces. (R1 gray and R2 black) (**B1**. WT; **B2**. Tkneo). **C.** Peak amplitude of $\Delta F/F_0$ for the three genotypes. ANOVA comparing F1 amplitude vs. genotype is not significantly different ($F_{2,39} = 0.9699$, $P = 0.3881$). **D.** $\int v\Delta F/F_0$ for the three genotypes. ANOVA comparing F1 $\int v\Delta F/F_0$ vs. genotype is significantly different ($F_{2,39} = 4.8772$, $P = 0.012$). Horizontal bars show results of post-hoc comparison. Note, following normalization of $\Delta F/F_0$ to F1, R2 $\int v\Delta F/F_0$ vs. genotype is not significantly (ANOVA $F_{2,39} = 1.6273$, $P = 0.2095$, not shown) **E.** Ratio of F2 to F1 $\int v\Delta F/F_0$ following paired stimuli for the three genotypes (ANOVA of Ratio $\int v\Delta F/F_0$ vs. genotype ($F_{2,39} = 5.6064$, $P = 0.0072$) horizontal bars show result of post-hoc comparison. Asterisks show Student's t-test against a theoretical mean of 2. (For C, D, and E: WT, n=16; Tkneo, n=17; HET, n= 9 animals.).

We then compared the amplitudes of the $\Delta F/F_0$ responses of R1 and R2. As expected from our previous measurements in rats (Schiess *et al.*, 2006), we found a linear relationship between these presynaptic Ca^{2+} transients with a greater than unity slope. Furthermore, we found no difference in the slope among the three genotypes (Figure 5.3A, $P = 0.9838$), consistent with there being no effect of genotype on the initial presynaptic $[Ca^{2+}]_{res}$. We next determined the dependence of R1 on extracellular $[Ca^{2+}]_o$ for the three genotypes. As shown in Figure 5.3B, the amplitude of the R1 fEPSP for all three genotypes followed the expected increase in response to increased $[Ca^{2+}]_o$ (Blatow *et al.*, 2003; Wasling *et al.*, 2004).

As a further indication of the role of presynaptic Ca^{2+} kinetics in synaptic efficacy, we determined the integral of $\Delta F/F_0$ (Figure 5.4A) after normalizing it to the $\Delta F/F_0$ peak value of a single pulse. This value, $\int v\Delta F/F_0$ (Figure 5.4B & D), has units of time and thereby provides a measure of the rate of $[Ca^{2+}]_{res}$ clearance, but it is distinct from $\int \Delta F/F_0$, which reflects the total amount of Ca^{2+} . While the peak $\Delta F/F_0$ response to a single stimulus was not significantly different among the three genotypes (Figure 5.4C, $P = 0.3881$), the value of $\int v\Delta F/F_0$ for both Tkneo and HET mice was significantly less than that of WT mice (Figure 5.4D). This suggests a SNAP-25 expression level effects the $[Ca^{2+}]_{res}$ regulation that could contribute to the previously observed differences in the parameter a (Figure 5.2B).

Because some proportion of the $[Ca^{2+}]_{res}$ signal during paired-pulses results from the summation of $[Ca^{2+}]_{res}$, it is difficult to accurately measure $\Delta F/F_0$ caused by the influx of Ca^{2+} during R2. However, if we consider that the $\int \Delta F/F_0$ for successive pulses is independent, the sum for a pair of pulses should be twice the size of that for a single

pulse. We have previously demonstrated that there is significant supra-linear summation of the Ca^{2+} signals resulting from paired-pulses in the adult rat hippocampus (Schiess *et al.*, 2006) such that the ratio of $\int \Delta F/F_0$ for paired-pulses to that for a single pulse is, in fact, greater than two. When we performed the same analysis on the data derived from slices of Tkneo, HET, and WT mice, we found as expected that this ratio was larger than two for all three genotypes. Moreover, this ratio was significantly greater for Tkneo than in either HET or WT mice. This increased facilitation of $[\text{Ca}^{2+}]_{\text{res}}$ in Tkneo presynaptic terminals (Figure 5.4E), therefore, was comparable to the greater facilitation of fEPSPs recorded from this genotype. As discussed below, one possible explanation for this observation is that the SNAP-25a isoform influences the saturation of the $[\text{Ca}^{2+}]_{\text{res}}$ clearance mechanisms.

Predicting the $[\text{Ca}^{2+}]_{\text{res}}$ sensitivity of PPF

We further addressed the relationship of the *Snap25* genotype to the Ca^{2+} sensitivity of facilitation through the modeled parameters of P_R and the components of a described in Table 5-1, by predicting the effect of $[\text{Ca}^{2+}]_o$ on short-term facilitation. We based these predictions on the well-established method of determining the $[\text{Ca}^{2+}]_o$ dependence of PPR (Blatow *et al.*, 2003; Wasling *et al.*, 2004; Schiess *et al.*, 2006). We used the values derived from a linear fit between R1 and $[\text{Ca}^{2+}]_o$ (Figure 5.3B), and the modeled relationship between R1 and R2 (Figure 5.2A) for the condition of a half maximum response of R1 at 2.5 mM $[\text{Ca}^{2+}]_o$ to determine the dependence of short-term plasticity on $[\text{Ca}^{2+}]_o$ (Figure 5.5A). Consistent with previous reports for SC-CA1 synapses in both rats and mice (Blatow *et al.*, 2003; Schiess *et al.*, 2006), these calculations yield an inverse and linear relationship of PPR to $[\text{Ca}^{2+}]_o$ for WT mice.

However, equivalent calculations for both Tkneo and HET mice yield a markedly different relationship between PPR and $[Ca^{2+}]_o$ that had a generally positive slope at low $[Ca^{2+}]_o$ that peaked at about 2 mM and was then replaced by a negative slope at higher $[Ca^{2+}]_o$ (Figure 5.5B). Our calculations thus predict that both Tkneo and HET mice exhibit a different Ca^{2+} sensitivity of facilitation than is seen in WT mice.

To test the preceding modeling predictions further, we then measured PPR experimentally as a function of $[Ca^{2+}]_o$ in the three genotypes. As depicted in Figure 5.5B & C, the data generally emulated the PPR response predicted by our calculated results in Figure 5.5A. As expected, slices from WT mice, showed a significant negative slope of -0.8393 ($F_{1,42} = 4.208$, $P = 0.0465$) (Figure 5.5B). In contrast, we observed a clearly different response to increasing $[Ca^{2+}]_o$ for slices from Tkneo and HET mice. For both of these genotypes, this curve had a significant positive slope between 1 and 2 mM $[Ca^{2+}]_o$ similar to that predicted in Figure 5.5A (overall significance $F_{2,72} = 3.855$, $P = 0.0257$; Tkneo: $F_{1,29} = 7.963$, slope = 0.8590, $P = 0.0085$; HET: $F_{1,19} = 4.915$, slope 1.270, $P = 0.039$). Between 2 and 3 mM $[Ca^{2+}]_o$, although there was a tendency for a decrease in PPF with increasing $[Ca^{2+}]_o$, the slope was not significantly different from 0 for either Tkneo or HET (Tkneo: $F_{1,51} = 0.4621$, $P = 0.6686$; HET: $F_{1,33} = 0.4621$, $P = 0.5014$). Importantly, the qualitative agreement between the predicted and experimentally observed data presented in Figure 5.5A and B help to validate the model described here and originally developed in Bark et al. (Bark *et al.*, 2004). As expected, the greater variability in the PPF values obtained for WT mice at 1mM $[Ca^{2+}]_o$ results from reduced amplitude of R1 fEPSP and the enhanced facilitation (Figure 5.5B) is consistent with previous reports from our laboratory and from other groups (Blatow *et*

al., 2003; Wasling *et al.*, 2004; Schiess *et al.*, 2006) and suggests that there are significant variations in the electrophysiological responses at low values of $[Ca^{2+}]_o$.

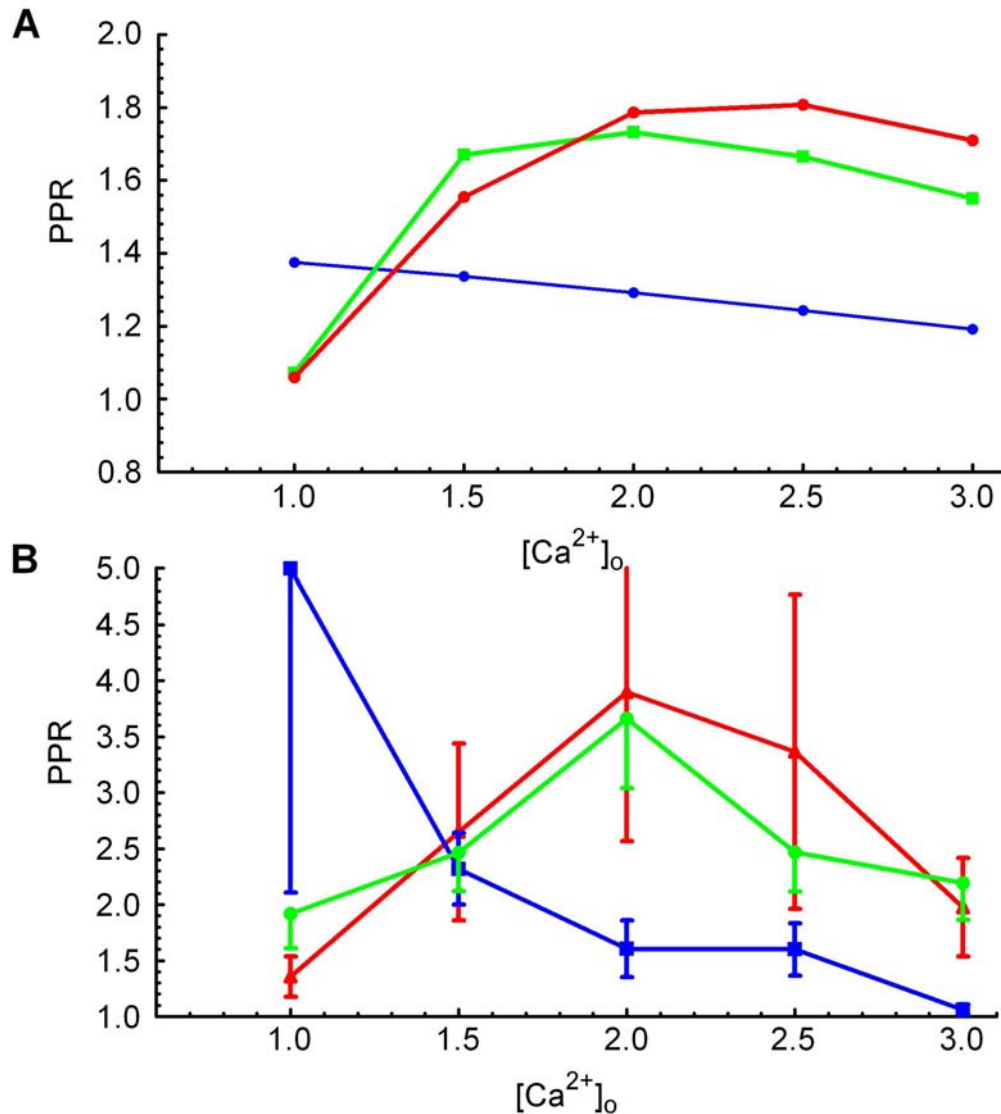


Figure 5.5 Determination of Ca^{2+} buffering.

A. Modeling predictions using a and the relationship of $[Ca^{2+}]_o$ on R1. (Details of model in Methods). **B.** PPR vs. $[Ca^{2+}]_o$ (WT, $n = 10$ animals, blue; Tkeo, $n = 10$ animals, red; HET, $n = 7$ animals, green).

Although our calculations predicted the general shape of the curves for the three genotypes, they resulted in a generally lower level of PPR than was experimentally observed. This was possibly due to the different ratio of $[Ca^{2+}]_o$ to $[Mg^{2+}]_o$ in the modeled values than in the experiments where the R1 and R2 fEPSPs were measured. In our experimental tests, we determined the relationship between R1 and R2 by changing the stimulus strength, which has the effect of changing the number of synapses that respond and should not increase the driving force on Ca^{2+} (Blatow *et al.*, 2003). By contrast, changing the extracellular divalent cation ratio (Figure 5.3B) changes the amplitude of the initial response by increasing or decreasing the relative Ca^{2+} flux. Differences in $[Ca^{2+}]_i$ are likely to account for the differences in PPR resulting from our calculations and our experimental results (Figure 5.5A and B).

Potential Mechanisms of Genotype Differences

Because our $\int v\Delta F/F_0$ data (Figure 5.4D) were consistent with a SNAP-25-dependent change in $[Ca^{2+}]_{res}$ clearance, we assessed the contribution of differences between the genotypes in the ER in presynaptic Ca^{2+} regulation. Since the ratio of SNAP-25a to SNAP-25b of the adult Tkneo mice is similar to that of P4 - P7 mice, we investigated two mechanisms of $[Ca^{2+}]_{res}$ regulation that are known to change between P2 - P6 and adult (Scullin *et al.*, 2010). First, we assessed the contribution of the SERCA pump to the uptake of presynaptic $[Ca^{2+}]_{res}$ into the ER (Scullin & Partridge, 2010). To this end, we used thapsigargin to effectively block SERCA pump activity (Verkhatsky, 2005). As expected, application of 3 μ M thapsigargin significantly increased $\int v\Delta F/F_0$ following a single pulse in the WT and, importantly, led to a similar increase in Tkneo mice (Students t-test, $n = 4$ animals per group, $P = 0.324$, data not shown). This

suggested that differences in SERCA uptake do not play a major role in shaping the difference in $[Ca^{2+}]_{res}$ clearance between Tkneo and WT mice. Second, we determined the role of Ca^{2+} -dependent Ca^{2+} release from the ER by application of 10 mM caffeine. As previously reported (Scullin *et al.*, 2010), caffeine did not induce significant amounts of Ca^{2+} release in SC presynaptic terminals ($\Delta R/R_0$) in WT mice (paired Student's t-test, $n=10$, $P = 0.13$, data not shown). Furthermore, there was no increase of $\Delta R/R_0$ following caffeine application in Tkneo adults (paired Student's t-test, $n = 6$, $P = 0.84$, data not shown), which again supports our findings with the thapsigargin and suggests that a difference of intracellular Ca^{2+} stores does not account for the observed differences in Ca^{2+} regulation.

Finally, we extended our findings of the differences of $[Ca^{2+}]_{res}$ clearance among the 3 genotypes during paired-pulses to $[Ca^{2+}]_{res}$ accumulation during longer stimulus trains. We used Fura2 ratiometric imaging and a paradigm of repeated 2 s, 10 Hz pulse trains to approximate physiological burst firing and long-term plasticity paradigms (Grover *et al.*, 2009). While there was not a significant difference in the initial Fura-2 ratio response between genotypes ($F_{2,9} = 1.0856$, $P = 0.3781$; Tkneo = 0.8195 ± 0.0708 ; HET = 0.716703 ± 0.017 ; WT = 0.73357 ± 0.062 ; data not shown), there was a significantly greater accumulation of background Ca^{2+} early in the stimulus train in Tkneo compared to HET and WT mice; however, this difference diminished later in the stimulus train (Figure 5.6). These data suggest a diminished degree of negative feedback modulation on Ca^{2+} influx in Tkneo mice.

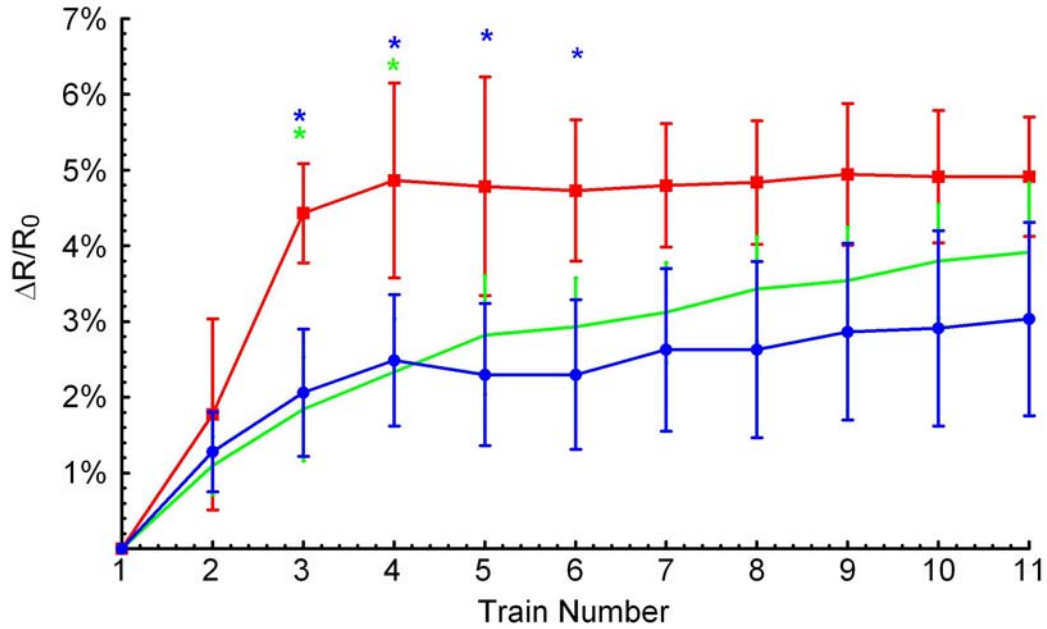


Figure 5.6 Accumulation of background Ca^{2+} during stimulus trains.

Fura-2 images of $[\text{Ca}^{2+}]_i$ prior to repeated stimulation by trains of 2 s at 10 Hz separated by 2 seconds. Background $[\text{Ca}^{2+}]_{\text{pre}}$ accumulation is significantly different among the three genotypes (ANOVA, $F_{32,99} = 3.0375$, $P < 0.0001$, Fishers post-hoc) (WT blue n=5, Tkneo red n=4, HET green n = 4). Significance between the WT and Tkneo in blue asterisks and between Tkneo and HET green asterisks.

Discussion

The shift from SNAP-25a to SNAP-25b may underlie a refinement of the Ca^{2+} -dependent vesicular fusion process responsible for the mature phenotype of synaptic plasticity (Bark *et al.*, 2004; Johansson *et al.*, 2008; Pozzi *et al.*, 2008). Indeed, detailed investigation of the kinetics of neuroexocytosis in reconstituted null mutant chromaffin cells and cultured neurons has suggested that SNAP-25b is more effective than 25a or the constitutive cellular homologue SNAP-23 in maintaining vesicles in the primed state, which leads to a greater size of the readily releasable pool (Sorensen *et al.*, 2003; Delgado-Martinez *et al.*, 2007). This functional distinction between the SNAP-25 isoforms appears to be due to three of the 9 amino acid differences encoded by the alternative copies of exons 5a and 5b (Nagy *et al.*, 2005). In addition, there is evidence to suggest that the two isoforms are phosphorylated (Shimazaki *et al.*, 1996; Kataoka *et al.*, 2006) to a different extent at a conserved site that may affect the regulation of Ca^{2+} flux via voltage-gated ion channels by changing their binding affinities (Pozzi *et al.*, 2008).

Here we report that the level of SNAP-25 expression affects distinct properties of presynaptic $[\text{Ca}^{2+}]_{\text{res}}$ in adult SC-CA1 synapses and that differential expression of the two SNAP-25 isoforms is involved in determining the amount of facilitation at these synapses. Our results further suggest the possibility that both parameters of expression may have combined effects on PPF and $[\text{Ca}^{2+}]_{\text{res}}$ regulation. This indicates that the regulated expression of SNAP-25 is likely to be essential in sculpting the properties of specific synapses as they contribute to nervous system circuits.

SNAP-25 and the regulation of PPF

We have reported previously that PPF is enhanced in Tkneo mutant SC-CA1 synapses of adolescent (P21 - P23) when compared to WT mice, but that there is no similar enhancement of facilitation in HET mice (Bark *et al.*, 2004). We have now confirmed that this enhanced facilitation is maintained in adult Tkneo mice. This indicates that alterations of SNAP-25 do play a role in regulating plasticity.

However, HET mice, which have reduced expression of SNAP-25, provide conflicting evidence about this role (Matteoli *et al.*, 2009). While we did not observe enhanced plasticity in HET mice, studies reported by Pozzi *et al.* 2008 reported enhanced PPF at SC-CA1 synapses of the same HET mice at intervals of 10 ms or less, but not at 20 ms intervals or more. The mechanism for facilitation at this shorter interpulse interval is more difficult to interpret because it reflects not only the differences in $[Ca^{2+}]_{res}$ regulation, but also the contribution of recurrent GABA inhibition that is not a significant factor at longer interpulse intervals (Steffensen *et al.*, 2006). Our experiments, however, have focused on PPF at a 50 ms interpulse interval, that is generally accepted to measure homosynaptic presynaptic plasticity (Partridge & Valenzuela, 2002). Bark and colleagues have reported that mice with a targeted mutation of the *Snap25* gene that entirely eliminates the expression of the SNAP-25b isoform, but not SNAP-25a (without affecting the level of total SNAP-25), exhibit reduced PPF (Johansson *et al.*, 2008). These measurements of PPF, however, were performed at room temperature whereas both our experiments reported here and previously (Bark *et al.*, 2004) were conducted at near physiological temperatures (32°C). Indeed, we have recently demonstrated that PPF is affected by age by temperature interactions and that this plasticity could be masked, or even expressed as depression, depending on the experimental conditions (Schiess *et al.*,

2010). It is evident, therefore, that while SNAP-25 must play an intimate part in mediating short-term plasticity, how that plasticity is resolved can be dependent on the experimental protocol. This stresses the need to directly compare these properties under precisely the same and most appropriate conditions.

SNAP-25 effects Ca²⁺ regulation

Previously we found that reduced expression or the complete absence of SNAP-25 did not significantly affect the amplitude of Ca²⁺ transients elicited by K⁺-triggered depolarization in the soma of cultured hippocampal neurons (Tafoya *et al.*, 2008). In contrast, Pozzi and co-workers showed that Ca²⁺ transients were enhanced largely in neurite processes of hippocampal neuron cultures from these mutants, which may be attributed to the loss of SNAP-25-mediated control of the inactivation kinetics of VGCCs (Pozzi *et al.*, 2008). Interestingly, the regulation of Ca²⁺ transients was restored by expression of exogenous SNAP-25b, and not SNAP-25a, which is consistent with a maturation process that is not readily reflected by the rather immature state of neuronal cultures.

We now show by imaging stimulus-driven presynaptic [Ca²⁺]_{res} transients that mature SC-CA1 presynaptic terminals of Tkneo and HET mice, which express comparably reduced levels of SNAP-25, exhibit similar alterations of Ca²⁺ dynamics with respect to WT mice. For example, although there was no difference on the amplitude of the Ca²⁺ signal between genotypes, both Tkneo and HET mice were found to have a decrease in the total presynaptic Ca²⁺ transient in response to a single stimulus compared to WT mice (Figure 5.4D). This suggests a faster clearance of [Ca²⁺]_{res}, which could be dependent on both diffusion and buffering (Wasling *et al.*, 2004; Collin *et al.*, 2005).

Moreover while the $[Ca^{2+}]_{res}$ decay kinetics in the adult rodent SC-CA1 synapse do not appear to be significantly affected by Ca^{2+} buffer saturation (Blatow *et al.*, 2003), an increased role of buffer saturation has been reported in the immature P6 – P12 synapse (Wasling *et al.*, 2004) that reflects a developmental period when the level of SNAP-25 expression increases. The increase in SNAP-25b that normally occurs during this period might therefore coincide with an increasing buffering capacity of the presynaptic terminal. Consistent with this interpretation, we found that adult WT presynaptic SC-CA1 terminals exhibit the expected non-saturating buffer characteristics, whereas both Tkneo and HET synaptic terminals exhibit some degree of buffer saturation. The terminals of both Tkneo and HET mice have positive slopes of the relationship of PPR to $[Ca^{2+}]_o$ between 1 mM and 2 mM and a similar overall shape (Figure 5.5B). These data indicate that the buffer saturation could be dependent upon the isoform amounts of SNAP-25 or it could be the result of a compensatory mechanism secondary to or in addition to these amounts in the presynaptic terminal during development. However, this effect is apparently insufficient to lead to an enhancement of PPR at a 50 ms interval in HET as is observed in Tkneo mice.

The modification of $[Ca^{2+}]_{res}$ dynamics that results from altered expression of SNAP-25 isoforms is observed in both fEPSPs and $[Ca^{2+}]_{res}$ transients following paired stimuli in Tkneo mice. While the initial amplitude of the fEPSP and the $[Ca^{2+}]_{res}$ transient following a single pulse (Figure 5.1B and 4C) was not correlated with the SNAP-25 isoform, there was a significant difference in the second $[Ca^{2+}]_{res}$ transient in synapses from Tkneo mice (Figure 5.4E) suggesting a decrease in the rate of influx following a repeated stimulus or removal of $[Ca^{2+}]_{res}$. The greater accumulation of

$[Ca^{2+}]_{res}$ in Tkneo synapses during our repeated pulse train paradigm is also consistent with additional mechanisms affected either directly or indirectly by how SNAP-25 isoforms might differently regulate $[Ca^{2+}]_{res}$ influx or removal following repetitive stimuli (Figure 5.6). The difference in the clearance of $[Ca^{2+}]_{res}$ between Tkneo and both WT and HET mice may thereby contribute to the genotype-dependent differences in plasticity among these synapses. This suggests that the effect of SNAP-25 levels in the regulation of Ca^{2+} dynamics particularly the change in Ca^{2+} saturation sensitivity may be distinct from the isoform effects, and that this affect could be dependent on compensatory maturation of the synaptic circuitry.

Modeling synaptic vesicle pools

The differences in $[Ca^{2+}]_{res}$ clearance in the SC-CA1 terminal fields among Tkneo, HET, and WT mice do not fully describe the enhanced PPF at this synapse. This increased short-term plasticity may reflect an additional mechanism that leads to increased P_R in Tkneo synapses during repetitive stimulation. Based on the rate of activity-dependent blockade of NMDA receptors by MK801, neither the P_R nor the amplitude of the R1 fEPSP at half-maximum stimulation differs between Tkneo, WT, or HET synapses when measured at P21 - P25 (Bark *et al.*, 2004). This is consistent with our modeling results that suggest that the primary mechanism underlying increased facilitation in Tkneo mice is an increased sensitivity of release mechanisms to Ca^{2+} during R2 that is fueled by a greater recruitment of vesicles to a facilitated state during the initial pulse. The model used here, which is based on the existence of two vesicle pools with different P_{RS} , successfully predicts several aspects of facilitation (see Methods) (Bark *et al.*, 2004; Schiess *et al.*, 2006). For example, this model predicts an

increase in both T_{kneo} and HET of the synaptic scaling factor, S , that could implicate an increased RRP. In chromaffin cells, SNAP-25b has been found to be responsible for an increase in the size of the readily releasable pool in rescued *Snap25* null mutants (Sorensen *et al.*, 2003; Nagy *et al.*, 2004; Delgado-Martinez *et al.*, 2007). Furthermore, the transition between SNAP-25 isoforms appears to be temporally correlated with a developmental increase in size of the RRP in cultured hippocampal neurons (Mozhayeva *et al.*, 2002). Importantly, S reflects not only the value of N_1 , which is a subpopulation of the RRP. (see Methods), but may also include postsynaptic factors, such as changes in postsynaptic receptors. While several reports have implicated SNAP-25 in the availability of glutamate receptors in the postsynaptic plasma membrane (Selak *et al.*, 2009; Lau *et al.*, 2010), other recent studies have attributed this trafficking to the homologue SNAP-23 (Suh *et al.*, 2010). Never the less, it is important to note that alteration in receptor number could influence synaptic scaling without affecting PPF.

The changes in the Hill equation parameters that are predicted by our model suggest increased Ca^{2+} sensitivity at a site that facilitates neurotransmitter release. These modeled parameters implicate a SNAP-25-dependent alteration in either $[Ca^{2+}]_{res}$ buffering or the affinity of this facilitatory site. Another potential mechanism for the influence of this SNARE protein on presynaptic $[Ca^{2+}]_{res}$ regulation is that SNAP-25 associates with VGCCs through a synaptic protein interaction (synprint) site to provide a feedback mechanism that modulates the dynamics of Ca^{2+} influx and intracellular Ca^{2+} kinetics via regulation of VGCCs (Catterall, 1999; Pozzi *et al.*, 2008). Furthermore, stimulation frequency dependent alterations in PPF have been reported at these synapses in an exon 5b ablated mutant that expresses solely SNAP-25a (Johansson *et al.*, 2008).

This may reflect a change in the regulation of presynaptic $[Ca^{2+}]_i$ due to continued expression of SNAP-25a, which has reduced phosphorylation and thus reduced inhibition of VGCCs. Thus, while $[Ca^{2+}]_{res}$ plays an important role in short-term plasticity, our data suggest that multiple converging factors, which may be influenced by SNAP-25, ultimately act to regulate $[Ca^{2+}]_{res}$ and thereby help govern synaptic facilitation.

It is well-established that $[Ca^{2+}]_{res}$ has an important role in the regulation of presynaptic plasticity (Zucker & Regehr, 2002). As we have shown here, either the amount or concentration of isoform expression of SNAP-25 are crucial to the regulation of $[Ca^{2+}]_{res}$. We propose that changes in the isoform ratio result in enhanced plasticity that affects multiple factors including those that regulate $[Ca^{2+}]_{res}$ and those that regulate the sensitivity of vesicular release proteins to Ca^{2+} , in a feedback loop. Further understanding of the mechanisms that control $[Ca^{2+}]_{res}$ sensitivity in the presynaptic terminal will increase our understanding of synaptic plasticity as mediated through short-term facilitation and the central role of presynaptic $[Ca^{2+}]_i$ in this phenomenon. This insight should provide the basis for targeting research on the spectrum of developmental disorders that can be attributed to deficits in synaptic plasticity encoded by protein interactions at the presynaptic nerve terminal.

Chapter 6 - Discussion

As discussed in Chapter 3, synaptic vesicular release is inherently stochastic, and is characterized by the probability of transmitter release (P_R). P_R is not fixed, but it is sensitive to many conditions that influence the presynaptic component of synaptic transmission. One important example in which P_R changes is during the time course of paired-pulse facilitation (Dobrunz & Stevens, 1997; Schiess *et al.*, 2010), indicating that there are factors that play a role in determining P_R , which can be altered during the short interval between two closely spaced pulses. Specifically, changes of P_R have been suggested to correlate with the amount of facilitation with a high initial P_R predicting depression and a low initial P_R predicting facilitation (Xu-Friedman & Regehr, 2004). Interestingly however, the relationship between P_R and facilitation is complicated, since P_R increases during development and it parallels the development of facilitation (Wasling *et al.*, 2004; Dekay *et al.*, 2006). This developmental change in facilitation was shown not to be primarily due to a change in P_R , vesicle pool size, or post-synaptic excitability, therefore it has been hypothesized to be due to a change in the presynaptic Ca^{2+} dynamics (Wasling *et al.*, 2004; Dekay *et al.*, 2006). In this study, I have attempted to ascertain whether the development of a presynaptic facilitatory mechanism results from an alteration of presynaptic Ca^{2+} regulation. In addition, I investigated whether a similar mechanism was responsible for the enhanced plasticity previously observed in Tkneo SC-CA1 synapses. The results presented here suggest that at the SC-CA1 synapses there are complex interactions between $[Ca^{2+}]_{res}$ and presynaptic vesicular release proteins and the way in which these interactions underlie P_R and plasticity is an essential prerequisite in understanding important components in synaptic information processing.

Major Findings

Modeling presynaptic $[Ca^{2+}]_i$:

In order to better understand the regulation of presynaptic $[Ca^{2+}]_i$, I took advantage of experimental data from our previous study that characterized the individual components of Ca^{2+} regulatory mechanisms from the adult rat and a resultant model of the kinetics of $[Ca^{2+}]_{res}$ transients during paired pulses. This modeling resulted in the hypothesis that the major active component of $[Ca^{2+}]_{res}$ clearance during paired stimuli is Ca^{2+} binding to SERCA and its subsequent removal from the cytoplasm by sequestration in the ER (Scullin & Partridge, 2010).

Development

In this study, I first characterized developmental changes in presynaptic $[Ca^{2+}]_{res}$ clearance kinetics by measuring the Ca^{2+} transients after both a single and paired stimuli at different developmental ages. These data revealed that, coincident with a developmental change in the degree of PPF, there was a concurrent change in presynaptic $[Ca^{2+}]_{res}$ regulation. Because of both these developmental changes in $[Ca^{2+}]_{res}$ regulation and the previous modeling data, I then investigated changes in the role of internal stores during development.

In the adult rat, we had shown that thapsigargin caused an increase in the slow time constant of $[Ca^{2+}]_i$ clearance following a single pulse and this was found to be consistent with my observation of an increased $\int [Ca^{2+}]_{res}$ in the adult mouse. Since the fits to the data showed that $[Ca^{2+}]_{res}$ removal from the presynaptic cytoplasm is not either a simple single or even a double exponential process, I measured the $[Ca^{2+}]_{res}$ clearance simply as the $\int [Ca^{2+}]_{res}$. When I related this integral to PPF at the same age, I found that

there was a change in relationship between PPF and $\int[\text{Ca}^{2+}]_{\text{res}}$ between P1-P6 and P9-adult. Interestingly, this was also related to developmental changes in Ca^{2+} stores, since in the younger animals, addition of thapsigargin decreased the $\int[\text{Ca}^{2+}]_{\text{res}}$ following a single pulse, rather than increasing it as was the case in the adult. These results suggest a different role for internal stores in the younger neurons than is found in mature neurons. Additionally, the application of caffeine in the adult mouse did not result in a measurable change in $[\text{Ca}^{2+}]_i$ accumulation, although it was shown that caffeine produces a significant increase in $[\text{Ca}^{2+}]_i$ accumulation at younger ages.

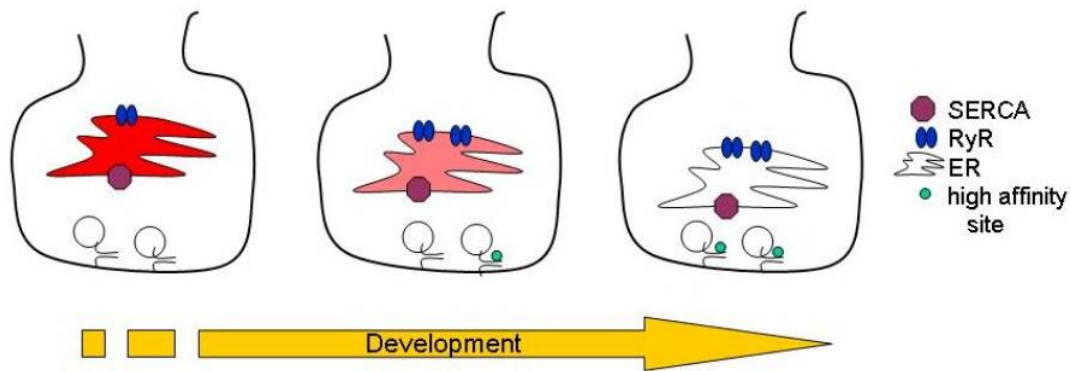


Figure 6.1 Schematic of developmental changes of the presynaptic terminal.

Three important changes that occur during development are summarized here: There is an increased involvement of SERCA binding as represented here by a reduced distance between vesicle binding sites and SERCA location. There is a decreased involvement of Ca^{2+} -induced Ca^{2+} release from the ER as shown here by reduced $[\text{Ca}^{2+}]_i$ levels in the ER (red shading indicating higher levels of $[\text{Ca}^{2+}]_i$), and increased number of RyR receptors. Additionally we propose that there is an increased expression or maturation of a high affinity (facilitatory) Ca^{2+} sensor, which is shown here as an increase in the number of these sites.

These findings suggest that during this developmental period there is a change in presynaptic $[\text{Ca}^{2+}]_i$ regulation resulting from an alteration in the role of internal stores. Most likely this results from decreased involvement of Ca^{2+} -induced Ca^{2+} release (CICR) in the mature animals, which could potentially result in lower levels of maintained $[\text{Ca}^{2+}]_i$

that could play a role in both decreasing the probability of release and decreased regulation of proteins after synapse maturation is complete. Also, maturation of expression of a protein with a high affinity (facilitatory) site could account for the developmental change in the ability of $[Ca^{2+}]_{res}$ to increase the probability of release during a second of paired-pulses (Figure 6.1).

SNAP-25

The second part of this study was an investigation of the role of genetic manipulation of SNAP-25, an important vesicle release protein that is known to affect PPF, and to identify whether this effect is the result of a developmental change in $[Ca^{2+}]_i$ regulation. The first approach was to measure the $\int[Ca^{2+}]_{res}$ for both single and paired-pulses. Tkneo mice, which have enhanced PPF, show an increase in the ratio of the $\int[Ca^{2+}]_{res}$ between the first and second pulses, when compared to both WT and HET adult mice. Analysis of the $\int[Ca^{2+}]_{res}$ following a single pulse shows a significant decrease of $[Ca^{2+}]_{res}$ in Tkneo mice suggesting that $[Ca^{2+}]_{res}$ is more effectively removed during this first pulse in Tkneo synapses. However, the amplitude of actual influx of Ca^{2+} during the first pulse is not significantly different among the three groups. Interestingly, each of these groups maintains a ratio of ~ 1.3 of peak $[Ca^{2+}]_{res}$ of first pulse to that of the second pulse, which suggests an enhanced Ca^{2+} binding during the first response not a change in Ca^{2+} entry. The $\int[Ca^{2+}]_{res}$ following the second pulse is not significantly different among the three groups, further suggesting that the difference between Tkneo and controls is the Ca^{2+} regulation during the first pulse, which results in an increased ratio of $\int[Ca^{2+}]_{res}$ of F1 to F2 in Tkneo compared to either the WT or HET mice.

I then used Model 2 to elucidate potential mechanisms of enhanced facilitation between the first and second pulses. The model suggested a change in Ca^{2+} sensitivity of the facilitatory mechanism, as predicted by the parameter a among Tkneo, HET, and WT mice. The model was further adapted to predict the Ca^{2+} sensitivity of a facilitatory site and the predicted Ca^{2+} sensitivity was then tested with measurements that compared PPR at varying $[\text{Ca}^{2+}]_o$. It was found that the predicted change in Ca^{2+} sensitivity, a , was adequate to produce the differences found during the Ca^{2+} sensitivity experiments. Furthermore, these results suggest a change in Ca^{2+} buffering or in proteins that interact with the SNARE proteins to determine Ca^{2+} binding.

The contribution of internal stores to cytoplasmic Ca^{2+} regulation is the major modification regulating Ca^{2+} developmentally, and this change coincides with the time period of significant changes in PPF, therefore I investigated the role of internal stores in the increased plasticity observed in Tkneo mice. Consistent with normal development, there was no difference in the fluorescence response of the measured Ca^{2+} kinetics between WT and Tkneo mice with either thapsigargin or caffeine application, suggesting that the SNAP-25 related mechanism regulating $[\text{Ca}^{2+}]_i$ is not due to a developmental change in internal Ca^{2+} stores. Thus, the change in $[\text{Ca}^{2+}]_{\text{res}}$ in Tkneo and HET synapses seems to be dependent on the Ca^{2+} buffering and not on a change in the developmental regulation of the role of internal stores in regulating $[\text{Ca}^{2+}]_i$. While the cytoplasmic Ca^{2+} buffering is distinctly different between Tkneo and WT, there is a much smaller difference between the HET and Tkneo, suggesting that there is a major effect due to the reduction of SNAP-25 levels, while a minor, but important, difference due to a change in isoforms.

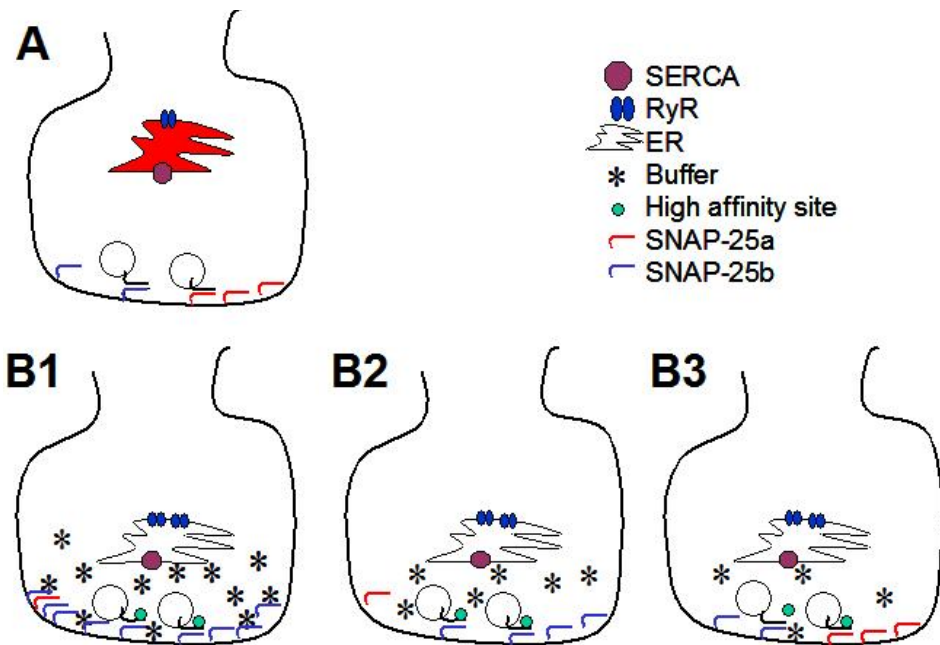


Figure 6.2 Schematic of SNAP-25 effect at the presynaptic terminal.

A. Schematic of P2-P6 presynaptic terminal. **B.** Schematic of the presynaptic terminal among the three genotypes (**B1.** WT, **B2.** HET, **B3.** Tkneo). Decreasing buffer capacity between the WT, HET, to Tkneo mice is shown by different amount of buffer. All of the adult animals have similar Ca^{2+} stores regulation of $[\text{Ca}^{2+}]_i$.

Summary

While there is a developmental change in presynaptic Ca^{2+} regulation due to alterations of the involvement of internal Ca^{2+} stores, this does not appear to involve the same mechanism that causes enhanced facilitation in Tkneo SC-CA1 synapses (Figure 6.2). The developmental changes in $[\text{Ca}^{2+}]_{\text{res}}$ result mainly from a change in the influence of ER in Ca^{2+} regulation and increased expression of a high affinity site (Figure 6.1). The second focus of this study suggests that there is a change in $[\text{Ca}^{2+}]_{\text{res}}$ regulation, which depends on SNAP-25, that results from an alteration of the regulation of Ca^{2+} in the presynaptic terminal. Thus, Tkneo mice have increased removal of $[\text{Ca}^{2+}]_{\text{res}}$ from the

presynaptic terminal during the first pulse due to a change in the buffering of presynaptic Ca^{2+} .

Limitations/Future Directions

One of the major limitations of this study is that the techniques used here measure presynaptic Ca^{2+} and postsynaptic potential of a population of cells and synapses. While these data provide important insight into the overall function of synaptic fields, it is impossible to draw conclusions from them about the characterization of individual synapses. Importantly, our data show that the developmental change in $[\text{Ca}^{2+}]_{\text{res}}$ kinetics, which underlies the mature phenotype of a positive correlation between PPF and $[\text{Ca}^{2+}]_{\text{res}}$, is not firmly established before P9. It is likely that the developmental process that we have observed, does not result from a homogenous transformation of uniform synapses, but rather reflects trends in a heterogeneous population. The lack of a significant positive correlation between PPF and $[\text{Ca}^{2+}]_{\text{res}}$ (Figure 4.3D) in the P3-6 mice could be due to a change in the relative contributions of PPD and PPF in the population of synapses. Furthermore, the enhanced plasticity found in Tkneo SC-CA1 synapses could also result from a change to an increased proportion of facilitatory synapses in the distribution of PPD and PPF among synapses. One possible method for determining the plasticity in individual synapses is through the use of the minimal stimulation technique (Cabezas & Buno, 2006; Schiess *et al.*, 2010), while this would not allow both the Ca^{2+} recordings and post-synaptic responses, it would provide a measure of the distribution of plasticity of randomly chosen individual release sites at functional synapses and could be used to help interpret the population measurements.

Furthermore, our determination of spatially and temporally averaged $\Delta F/F_0$ does not directly reflect the $[Ca^{2+}]$ in the release domain nor does it typically reflect influences on release probability of the initial pulse. However, changes of rise time, peak F1 $\Delta F/F_0$, or F1 $\int \Delta F/F_0$ do suggest that the $[Ca^{2+}]$ that determines release during the first pulse could be altered both developmentally and in Tkneo mice. One possible explanation for the slower clearance of $[Ca^{2+}]_{res}$ in slices from young animals could be maturational changes from growth cones and silent synapses to mature synapses. As discussed previously, growth cones differ from mature synapses in their morphology and volume, their larger number of L-type VGCCs (Ohbayashi *et al.*, 1998), and the role of Ca^{2+} -induced Ca^{2+} release (Tojima *et al.*, 2007). Functionally, influx through L-type VGCC has been shown to play a role in activation of presynaptic silent synapses (Yao *et al.*, 2006) and in the change from silent to active synapses (Gasparini *et al.*, 2000; Cabezas & Buno, 2006). Any of these factors might be a significant contributory factor to the observed maturational differences in $[Ca^{2+}]_{res}$ clearance. However, the alterations in $[Ca^{2+}]_{res}$ kinetics that we have observed would not be expected to contribute to the observed changes in PPF, since short-term synaptic plasticity must depend on mechanisms specific to presynaptic terminals of functional synapses. Furthermore any growth cone contribution, as measured by L-type VGCC current, could be evaluated by blocking L-type VGCCs, since this current has been shown to have little effect in the mature SC-CA1 synapses of the adult rodent (Scullin & Partridge, 2010)

A measure of unitary presynaptic $[Ca^{2+}]_{res}$, similar to minimal stimulation post-synaptic recordings, would resolve the question of whether there are separate populations of presynaptic terminals with different mechanisms of Ca^{2+} regulation. One possible

technique to evaluate Ca^{2+} dynamics of individual synapses is the use of two-photon microscopy with fluorescent indicators as has been successfully applied to organotypic cultures in adults (Emptage *et al.*, 2001) or acute slices (Carter *et al.*, 2002). Another recent option to monitor individual synapse dynamics is the use of quantum dots, (QDs) and the recent use of nanotechnology in biological research is opening up opportunities for the measurement of the kinetics of individual vesicles in living cells (Zhang *et al.*, 2009). However, the specific parameters for conducting these experiments have yet to be established in hippocampal slices and there are not yet appropriate QDs commercially available. Research into the development and design of pH-sensitive QDs using components that are commercially available could provide a method to measure the release properties of individual vesicles in slices (see Appendix C) and would greatly improve the ability to measure the effect of developmental and genetic changes in the presynaptic terminal. QDs have also shown a potential for use in the measurement of changes in membrane potential (see Appendix C) and thus could be used to provide further insight into the network properties of the hippocampus and potentially the role of PPF in the signal processing of these networks in living tissue.

Developmental changes of endogenous cannabinoid signaling (Isokawa & Alger, 2006) and developmental changes in adenylate cyclase (Conti *et al.*, 2007) are both confounds in the use of caffeine for measurements of CICR effects on $[\text{Ca}^{2+}]_{\text{res}}$ kinetics. However, when we used caffeine in the adult rat preparation, we did not observe an increase of fluorescence unless the stores were preloaded and this suggested to us that these stores are not loaded in the basal state (Scullin & Partridge, 2010). This finding is in marked contrast to the basally loaded condition that we found in the younger animals,

which makes a strong argument for a developmental change in the mechanisms of $[Ca^{2+}]_i$ uptake. However, any further conclusions about presynaptic Ca^{2+} stores based on the use of caffeine are complicated by the drug's effect on endogenous cannabinoid release, which changes developmentally and has been shown to modify synaptic transmission (Isokawa & Alger, 2006; Berrout & Isokawa, 2009; Hoffman *et al.*, 2010).

While SNAP-25b undergoes expression changes during the same period that PPF undergoes developmental changes, the expected characteristics of Ca^{2+} regulation attributable to immature presynaptic terminals are not observed in Tkneo or HET mice. A more parsimonious explanation for the change in plasticity in these mutants is an increase in Ca^{2+} buffer sensitivity. The underlying mechanisms responsible for a change in buffering in Tkneo mice are difficult to differentiate. Some possibilities are a reduction in amount of buffer, a lower buffer K_D , a change in the amount SERCA or endoplasmic reticulum localized to the presynaptic terminal, or a change in the volume of the terminal. Any of these could affect the localized $[Ca^{2+}]_i$ at the facilitatory site. Alternatively, a change in phosphorylation (Pozzi *et al.*, 2008) or amount of SNAP-25 could result in a different organization or association of proteins in the presynaptic terminal (Catterall & Few, 2008) resulting in the observed change in kinetics.

Snap25 null hippocampal neurons rescued by either expressing SNAP-25a or SNAP-25b show no isoform-dependent change in P_R of vesicles; however, dye-loading and unloading studies with both electrical stimulation and sucrose challenge indicated that SNAP-25a rescued neurons have a smaller RRP size (Delgado-Martinez *et al.*, 2007). Furthermore, experiments performed in adolescent Tkneo hippocampal slices measuring the block of NMDA currents using the open channel NMDAR blocker MK-

801 support the findings of no change in P_R as a result of differences in isoform expression (Bark *et al.*, 2004). Both a smaller RRP and the lack of a change in single pulse P_R would typically predict a decreased PPR, thus our observation of an increase in short-term plasticity in Tkneo mice comes as a surprise. However, our modeling predicts an increase in the synaptic scaling factor, which could reflect an increase in RRP size. Additionally, preliminary experiments by Denis Bragin and Wolfgang Müller (using two-photon fluorescent dye loading and unloading during stimulation, unpublished) also indicate an increase in RRP size of Tkneo SC-CA1 terminals. An increased RRP could result from the existence of a compensatory mechanism that counteracts the predicted decrease in RRP size perhaps from a change in $[Ca^{2+}]_{res}$ regulation. Interestingly, my experiments with the multiple stimulation protocol, (also used in the Bragin and Müller experiments to measure pool size and release rate), resulted in faster Ca^{2+} accumulation in Tkneo compared to WT adult or HET mice (Figure 5.6). The increased $[Ca^{2+}]_{res}$ could easily influence the determination of RRP size or result in increased recruitment to the RRP. Thus, additional measures of the vesicular pools, such as with EM studies of the vesicular pools in intact SC-CA1 presynaptic terminals of WT and Tkneo mice, could provide important resolution and insight into the relationship between SNAP-25 isoform and RRP size. Also, since increased phosphorylation of SNAP-25, with consequent effects on its ability to bind to VGCCs and reduce Ca^{2+} entry, has been suggested to be dependent on the SNAP-25b isoform (Pozzi *et al.*, 2008), further analysis of the effect of phosphorylation on the Ca^{2+} accumulation during high frequency stimuli and its effect on Ca^{2+} buffer saturation would further elucidate the role of SNAP-25 isoform in presynaptic Ca^{2+} signaling.

Interestingly, while SNAP-25 has been suggested to have its primary role in Ca²⁺ dependent neurotransmission, recent studies have suggested a controversial role for SNAP-25 in postsynaptic NMDAR trafficking (Selak *et al.*, 2009; Lau *et al.*, 2010), although others have suggested that SNAP-23 is the primary SNARE involved in NMDAR trafficking and that SNAP-25 should have little effect (Suh *et al.*, 2010). My study focused primarily on short-term synaptic plasticity that, due to its time course, should reflect primarily presynaptic mechanisms. Long-term effects leading to LTP induction could contribute to the predicted compensatory mechanisms involving changes in retrograde messengers such as BDNF released from the post-synaptic terminal to effect synaptic signaling (Lauri *et al.*, 2006; Sallert *et al.*, 2009). Thus, it would be interesting to evaluate potential postsynaptic changes in the numbers of NMDARs or their subunit composition.

While we are interested in the differential roles of SNAP-25 isoforms, we have compared functional differences among genetically engineered mice, which are likely to have undergone compensatory responses. In particular, Tkneo mice exhibit seizures and SNAP-25 expression levels and phosphorylation have been shown to change due to kainate-induced seizures (Kataoka *et al.*, 2006; Grumelli *et al.*, 2008). Thus, the change in plasticity in these mice could be due in part to recurring seizures that alter the levels of SNAP-25 or change phosphorylation levels. Furthermore, alterations of SNAP-25 resulting in increased plasticity could change negative or positive feedback dynamics that could change synaptic properties. Thus, the ability to distinguish whether the changes found in Tkneo or HET mice are the direct result of SNAP-25 level or isoform expression or concentration is difficult to ascertain. One way to address this issue more directly is to

use conditional genetic manipulation (Liu *et al.*, 2003) or RNAi studies (Hammond *et al.*, 2001), to avoid developmental compensatory mechanisms or long term effects from repeating seizures.

Impact

While the properties regulating plasticity are well understood at larger synapses such as the Calyx of Held, less is known about the mechanisms regulating plasticity at smaller synapses such as the SC-CA1 synapse (Lisman *et al.*, 2007), the focus of this study. The mechanisms that affect release and plasticity in the presynaptic terminal are not commonly studied at these smaller synapses because of the difficulty in directly applying techniques such as fluorescent microscopy and electrophysiology (Hanse *et al.*, 2009).

I have shown that the correlation between Ca^{2+} , P_R , and facilitation is not as simple as previously discussed (Xu-Friedman & Regehr, 2004; Dekay *et al.*, 2006), and this relationship is different at various developmental stages. I have succeeded in identifying several underlying components of presynaptic Ca^{2+} regulation that change during this period of development and support the idea that there are multiple presynaptic regulation pathways that are involved in short-term facilitation. The identified changes in PPF that are due to the alterations in the expression of SNAP-25 further support this complexity.

One interesting hypothesis about how memories are forgotten is the ‘neurogenesis-memory clearance hypothesis,’ which suggests that, in adult rodents, birth of new neurons and their subsequent death provide a storage and removal system for

memories (Feng *et al.*, 2001). The new neurons survive for approximately 3 weeks, and their death results in the removal of short-term memories as a result the development of new active synapses may play a role at all stages of brain development. This hypothesis supports the idea that the SNAP-25a isoform might be important for initiating neuronal connections by playing a role in axonal outgrowth (Oyler *et al.*, 1991; Osen-Sand *et al.*, 1993; Boschert *et al.*, 1996), which is important at all stages of life, and SNAP-25b could then play a role regulating synaptic transmission after these connections have been established and help to regulate excitability and Ca^{2+} at established functional synapses (Pozzi *et al.*, 2008).

Genetic polymorphisms and altered expression of SNAP-25 have been linked to neurological diseases that have their onset during adolescence, when SNAP-25b expression levels increase (Gosso *et al.*, 2006; Zhang *et al.*, 2008; Corradini *et al.*, 2009; Gao *et al.*, 2009). Mice with alterations in either the isoform ratio or expression level of SNAP-25 have a phenotype of increased seizures and significant behavioral abnormalities (Bark *et al.*, 2004; Johansson *et al.*, 2008; Corradini *et al.*, 2009). Understanding the potential differences in the role of presynaptic proteins in plasticity could help to better understand the basis of important neurological and psychiatric pathologies.

Our understanding of the mechanisms of plasticity used by the brain, particularly of the smaller, less-studied synapses, emphasizes the complexity and regional specificity of plasticity (Lisman *et al.*, 2007; Hanse *et al.*, 2009). Knowledge of this region-specific plasticity and its development provides the basic background to begin to make predictions about mechanisms of learning and memory, or simpler functions, such as grid

cell organization, that are hypothesized to underlie cognition (Hafting *et al.*, 2005; Burgess *et al.*, 2007; Fyhn *et al.*, 2008; de Almeida *et al.*, 2009). These efforts at comprehension of plasticity are integral to identifying important alterations in basic functional characteristics of a disease state and provide a guide for possible therapies.

Appendix A

Snap25^{tm2Mcw} mice

Snap25^{tm1Mcw} mice (homozygous referred to as Tkneo) have a targeted mutation as described in (Bark *et al.*, 2004) and briefly described below. This mutation impairs the developmental shift between the SNAP-25a and SNAP-25b isoforms. The directed mutation was carried out using a targeting vector construct for homologous recombination in the *Snap25* locus. The vector was inserted into embryo stem cells using G418 resistance. The insertion was an attempt to replace exon 5b with a chicken exon 5a, which was intended to result in a mouse that has no exon 5b. Additionally, a Tkneo gene surrounded by loxP sites was introduced in the intron upstream of exon 6 in the targeting vector. After the initial transfection, chimeric mice were crossed for seven generations onto a C57BL/6J background before use in this study. However, instead of the whole target gene being inserted, only the loxP sites and Tkneo gene were inserted leaving exon 5b intact (Figure A.1).

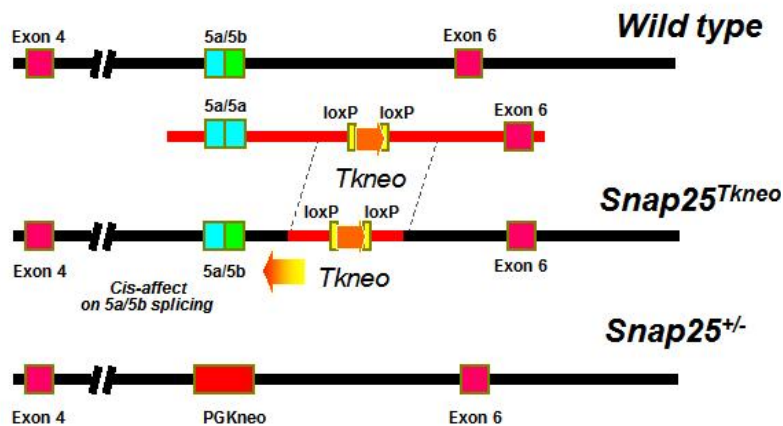


Figure A.1 Splicing Strategy

Shows splicing strategy for Tkneo, HET and WT mice adapted from (Bark *et al.*, 2004) and (Washbourne *et al.*, 2002).

The insertion of the Tkneo gene disrupted the developmental regulation of alternative splicing between exon 5a and 5b. Although these mice have no apparent deficits in hippocampal development or morphogenesis, they have increased SNAP-25a RNA expression in both the cerebellum and hippocampus and increased paired-pulse facilitation at 50 ms. This increased expression of SNAP-25a RNA is maintained in adult Tkneo mice (Figure A.2). Initial study of the homozygous mice showed that the adolescent mice have a 72-82% smaller body weight and a high postnatal lethality between P14 and P60 (Bark *et al.*, 2004). For this study we used homozygous adults with an average age of 110 days that weighed 92% of their wild type counterparts. Importantly, because most of these mice die between 3 and 5 weeks of age, the adults used in this study could be a select subpopulation of the mutant mice.

***Snap25*^{tm1Mcw} mice**

Heterozygote *Snap25* null mice (referred to as HET, MGI designation *Snap25*^{tm1Mcw} as originally described in (Washbourne *et al.*, 2002)) are maintained by brother : sister mating after 7 backcross generations to C57Bl/6 at the UNM HSC Animal Resource Facility. For this mouse, a targeting construct was generated from a genomic clone containing SNAP25 exons 5 and 6 in which the region containing both exon 5a and 5b, defined by *NsiI* and *AvrII* sites, was replaced by PGKneo. This resulted in a null mutant that showed a dose-dependent deficit in SNAP-25 protein levels, with the heterozygote mutants having approximately half the protein level of SNAP-25 of whole hippocampus. However, assaying other presynaptic proteins showed that there is no significant difference in expression (Washbourne *et al.*, 2002).

The heterozygote knockout mice have been shown to have similar paired-pulse facilitation to that of wild type at 50 ms interpulse interval and similar stimulus sensitivity as shown by similar input/output curves. The homozygotes die at birth; respiratory failure is likely cause of death since SNAP-25 is essential for the release of acetylcholine at the phrenic nerve terminals on the diaphragm, which is necessary for muscle contraction of the diaphragm. They have the same isoform RNA expression ratio as the WT, but reduced total levels of SNAP25 RNA (Figure A.2).

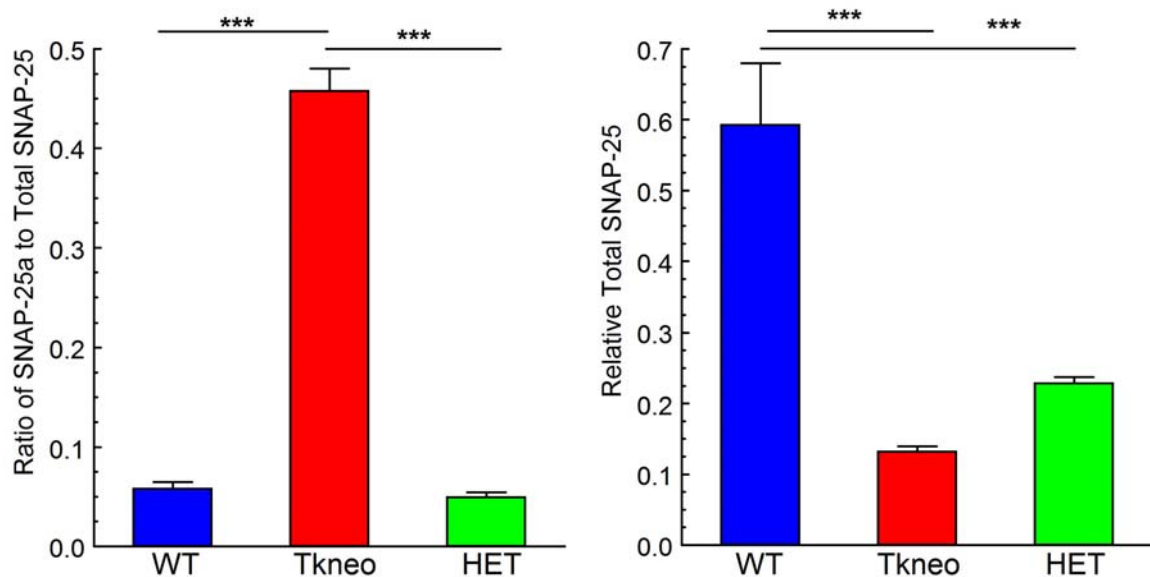


Figure A.2 Quantitative real time PCR.

Left panel: Ratio of SNAP-25a mRNA to the total level of SNAP-25 mRNA, calculated as the sum of SNAP-25a and SNAP-25b for the three different genotypes. **Right panel:** Relative total SNAP-25 mRNA for the three different genotypes, measured by summation of SNAP-25a and SNAP-25b calculated as the ΔC_t with β -actin. WT n = 3, Tkneo n = 8 HET n = 4 adult bilateral hippocampus preparations, quantitative RT-PCR using SYBRGREEN with SNAP-25a, SNAP-25b and β -actin specific primers (Tafoya *et al.*, 2008). Asterisks show Bonferonni post-hoc *** = $P < 0.001$.

Appendix B -Programs for $[Ca^{2+}]_i$ Analysis

The following were the most important programs for analysis of imaging and electrical records. **Import_abf10a**, reads the header and data of the binary file created by Clampex version 10 *.abf into Matlab. **Reada** creates a directory in matlab of all of the abf files in the specified directory. **Testplot** takes the resultant directory and opens it and does analysis on the fluorescent data file. **Double exponential fit**, is a program that takes any model and performs a non-linear least squares fit between the specified model and provided data.

For the high frequency experiments:

Additional programs that were written, but not shown, are as follows: **import_abf** was written for the version of pClamp on the patch rig and was adapted from a published program by Carsten Hohnkes. Electrophysiological analysis programs were written for both slope and amplitude, and minimal stimulation analysis.

Import_abf10a

```
% reads data from abf 10, adapted from pclamp 9 version written by Carsten Hohnke
function [data] = import_abf10a(file, en, dt)
if nargin < 2
    error('Function requires two input argument (the ABF filename and the en)');
elseif ~isstr(file)
    error('Input must be a string representing an ABF filename');
end

fid = fopen(file);          % Opens the file
if fid==-1
    error(sprintf('File %s has not been found or permission denied',file));
    return;
end

fseek(fid,12,'bof');
h.lActualEpisodes=fread(fid,1,'int');
h.size=5000;
s.size=632;
```

```

h.nADCNumChannels=2;

fseek(fid,244,'bof');
h.lActualAcqLengthF=fread(fid,1,'int');
fseek(fid,12,'bof');
h.lActualEpisodes=fread(fid,1,'int');
h.fHeaderVersionNumber=2;
h.nDataFormat=0;

fseek(fid,622,'bof');
h.fADCRange=fread(fid,1,'float');
fseek(fid,630,'bof');
h.lADCResolution=fread(fid,1,'int');
fseek(fid,1064,'bof');%1064,1192
h.fInstrumentScaleFactor(1)=fread(fid,1,'float');
fseek(fid,1192,'bof');%1064,1192
h.fInstrumentScaleFactor(2)=fread(fid,1,'float');
h.x_fAutosampleAdditGain=1;
fseek(fid,1052,'bof');%1052,1180
h.fADCProgrammableGain(1)=fread(fid,1,'float');
fseek(fid,1180,'bof');%1052,1180
h.fADCProgrammableGain(2)=fread(fid,1,'float');

fseek(fid,1072,'bof');%1072,1200
h.fSignalGain(1)=fread(fid,1,'float');
fseek(fid,1200,'bof');%1072,1200
h.fSignalGain(2)=fread(fid,1,'float');

fseek(fid,1076,'bof');%1076,1204
h.fSignalOffset(1)=fread(fid,1,'float');
fseek(fid,1204,'bof');%1076,1204
h.fSignalOffset(2)=fread(fid,1,'float');
ne = h.lActualEpisodes; % Get the number of episodes contained in the data file...
if en < 1 | en > ne, % and check if valid
    error('Invalid episode number.');
```

```

end

Nchan = h.nADCNumChannels;
ns = h.lActualAcqLength / h.lActualEpisodes;

if (h.fHeaderVersionNumber >= 1.6)
    fseek(fid, (h.size+s.size) + (en-1)*2*ns, 'bof');
else
    fseek(fid, (2048+s.size)+370 + (en-1) * 2 * ns, 'bof');
end

```

```

if (h.nDataFormat == 0) % Data representation. 0 = 2-byte integer; 1 = IEEE 4 byte float.
    xdata = fread(fid, ns, 'short');
else
    xdata = fread(fid, ns, 'int');
end

eval('xdata = reshape(xdata, Nchan, length(xdata)/Nchan)';, '');
data    = [];
data    = zeros(size(xdata,1),Nchan+1);
data(:,1) = dt*(0:size(xdata,1)-1);

for chan=1:Nchan,
    gain(chan) = h.fADCRange / h.lADCResolution / (h.fInstrumentScaleFactor(chan) *
h.x_fAutosampleAdditGain * h.fADCProgrammableGain(chan) * h.fSignalGain(chan));
    offset(chan) = h.fSignalOffset(chan);
    data(:,chan+1) = xdata(:,chan) * gain(chan) + offset(chan);
end
fclose(fid);

```

Reada/summarize

```

% reads data from subfolders that divide traces into slices and makes a directory of traces
file=cd;
dirlist=dir;
[a,b]=size(dirlist);
count1=1;
for n=3:a;
    if (dirlist(n).isdir==1)
        founddir(count1).name=strcat(file,'\ ',dirlist(n).name);
        count1=count1+1;
    end;
end;
clear a n count1;
m=1;
[a,b]=size(founddir);
for n=1:b;
    dirlist2=dir(founddir(n).name);
    [c,d]=size(dirlist2);
    for n2=1:c;
        if (strcmp(dirlist2(n2).name,'A1'))
            basal(m).directory=strcat(founddir(n).name,'\ ', 'A1\ ');
            m=m+1;
        end;
        if (strcmp(dirlist2(n2).name,'A2'))
            basal(m).directory=strcat(founddir(n).name,'\ ', 'A2\ ');

```

```

    m=m+1;
    end;
    if (strcmp(dirlist2(n2).name,'A3'))
        basal(m).directory=strcat(founddir(n).name,'\','A3\');
        m=m+1;
    end;
end;
end;
clear m n n2 a b c d dirlist dirlist2;
%start of summarize
m=1;
[a,b]=size(basal);
for n=1:b;
    dirlist2=dir(basal(n).directory);
    [c,d]=size(dirlist2);
    for n2=1:c;
        if (strcmp(dirlist2(n2).name,'a'))
            traces(m).directory=strcat(basal(n).directory,'a\');
            m=m+1;
        end;
        if (strcmp(dirlist2(n2).name,'a2'))
            traces(m).directory=strcat(basal(n).directory,'a2\');
            m=m+1;
        end;
    end;
end;
end;
clear a b c d m n n2 dirlist2 basal founddir file;

recordingrate=.05;
[a,b]=size(traces)
e=1;
value=0;
for n=1:b;
    n
    abfdir=strcat(traces(n).directory,'*.abf')
    file=dir(abfdir)
    [a,b]=size(file)
    for m=1:a;
        dat(e).name=file(m).name
        dat(e).dat=import_abf10a(strcat(traces(n).directory,file(m).name),1,recordingrate);
        plot(dat(e).dat(:,1),dat(e).dat(:,2))
        %value=input('single 1 paired 2 or none 0');
        if isempty(value);
            value=999;
        end;
        type(e)=value;
    end;
end;

```



```

    e=e+1;
end;
end;
type=type';
for tag=1:(e-1);
name(tag,:)=dat(tag).name;
end;

```

Testplot

Makes all of the calculation for the fluorescent signals from a previously read in set, (subprograms not shown)

```

for e=1:size(sets);
    g=sets(e,1);
    h=sets(e,2);
    i=sets(e,3);
    tempsing=dat(g).dat(:,2);
    if (h==0)
        h=g;
        tempdoub(:,1)=.0000000000000001;
    else
        tempdoub=dat(h).dat(:,2);
    end;
    if (i==0)
        i=g;
        tempnor(:,1)=0.0000000000000001;
    else
        tempnor=dat(i).dat(:,2);
    end;
    %plot(time,dat(g).dat(:,2),time,dat(h).dat(:,2),time, dat(i).dat(:,2));
    e,
    sets(e,4),
    tempsingnor=(tempsing(:,1)-tempsing(1,1))/tempsing(1,1);
    tempdoubnor=(tempdoub(:,1)-tempdoub(1,1))/tempdoub(1,1);
    tempnorun=(tempnor(:,1)-tempnor(1,1))/tempnor(1,1);
    tempnornor=smooth(tempnorun,321);
    [sing(:,e),doub(:,e)]=subtrace(time,tempsingnor,tempdoubnor,tempnornor);
    [fluordoub(e,:),fluordoubx(e,:),fluorsubdoub(:,e)]=fluorset(time,doub(:,e),'p',.05);
    [fluorsing(e,:),fluorsingx(e,:),fluorsubsing(:,e)]=fluorset(time,sing(:,e),'p',.05);
    %plot(time,fluorsubsing(:,e),time,fluorsubdoub(:,e)); ginput;

    fluorsubsingdivmax(:,e)=fluorsubsing(:,e)/max(fluorsubsing(:,e));
    if (min(fluorsubsingdivmax(1:3000,e))<-0.5);
        fluorsubsingdivmax(:,e)=fluorsubsingdivmax(:,e)*0;
    end;

```

```

cumsfssdm=cumsum(floursubsingdivmax);
if (cumsfssdm(16000,e)>100);
    table(e,:)=[sets(e,4),cumsfssdm(16000,e)];
else table(e,2)=0;
end;
end;
end;
[peaksing,peaktime]=max(floursubsing);
timetopeak=peaktime*.05-50;
clear e g h i tempdoub tempsing tempnor tempsingnor tempdoubnor tempnor;

```

Double Exponential Fit

```

function [fresult, gof]=doubleexponentialfit (fluorx,fluory)
x = fluorx;
y = fluory;
sigma = 2.5;
sig = ones(size(x))*sigma;
modelstr = 'a*(b*exp(-x/c)+(1-b)*exp(-x/d))+e';
model=fittype(modelstr);
value='NonlinearLeastSquares';
opts =fitoptions('method', value);
opts.StartPoint=[.01 .4 10 150 0];
[fresult, gof, output]= fit(x,y,model,opts);
ci=confint(fresult, .95);
figure (1); % opens figure 1 and makes it active
clf; % clears the active figure
subplot(2,1,1);
hold on;
axis([x(1),x(length(x)), min(y)-.1*min(y), 1.1*max(y)]);
plot(fresult,x,y,'fit');
subplot(2,1,2); % Makes the bottom row of figure 1 active;
hold on;
plot(fresult,x,y,'residuals');

```

Appendix C – Potential Biomedical Applications of Coated Colloidal Nanocrystals

The development of new technology for biomedical research applications is an important means to overcome limitations of current research techniques (Hanse *et al.*, 2009). We have described and investigated the potential use of nanocrystal quantum dots (QDs) in neurons (Figure C.1) with the goal of devising a more localized measurement tool for local membrane potential (Figure C.2-C.4) and for pH in synaptic vesicles (Figure C.5-C.12). We first describe the novel idea of manipulating the coating of QDs to target them to the hydrophobic plasma membrane and suggest their use to measure transmembrane potential as described in the published Patent Application #12/364,562, with supporting data (Figure C.2-C.4). Secondly, the investigation of synthesizing pH sensitive QDs in synaptic vesicles using a FRET based construct to create pH sensitive QDs that could eventually be used to track individual vesicles (Figure C.5-C.12). The following two sections are the patent for the possible membrane potential sensing QDs and the work on a FRET-based QD pH sensor.

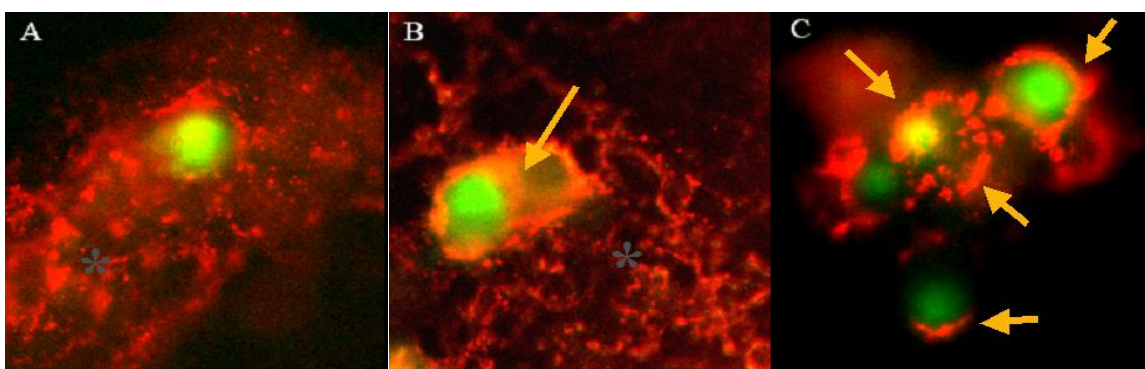


Figure C.1 QD exposed mouse hippocampal neurons.

Mouse hippocampal cultured neurons, exposed to ~1mmol QD dissolved in 55mM KCl. Picture shows that cultured neurons have the potential to uptake QD (red), co-staining using Alexa 488 NeuN antibodies (green). **A.** 10 min KCl and QD stimulation followed by fixation. **B.** 10 min stimulation with KCl and QD, 1 hr chase post stimulation followed by fixation. **C.** 5 hrs chase post stimulation followed by fixation (Fan *et al.*, 2005).

A. Quantum Dots as sensors of membrane potential

Our use of QDs to measure membrane potential is described in a patent application: *Biofunctionalized quantum dots for cell membrane potential sensing -Patent Application #12/364,562*. Briefly, the focus of this patent is to synthesize QDs that are capable of being inserted into the membranes of living cells. QD synthesis was carried out in the laboratory of Hongyou Fan at the Advanced Material Labs, in a collaboration between the University of New Mexico and Sandia National Labs in Albuquerque, New Mexico.

Monodisperse CdSe and CdSe/CdS core/shell QDs were synthesized through a “hot soap” injection process. Phospholipids were used to encapsulate the QDs within a micelle core to form water-soluble and biocompatible QD micelles (Figure C.2) using an interfacially-driven micro-emulsion process developed at Sandia National Labs. Neurons were cultured for 10 days using a standard protocol (Tafoya *et al.*, 2006) and synthesized QDs were applied to these cultures for 30 minutes at a 1:200 dilution of QDs to ACSF. Fluorescent microscopy demonstrated that the neurons appear to have QDs associated with their membrane (Figure C.3A). The next step was to evaluate whether the QDs were sufficiently embedded into the membrane so that they would respond to a change in trans-membrane field.

Sensing neuronal transmembrane potential changes is determined from the fluorescent intensity changes of those QDs that are close to or within neuronal membranes. Initial tests utilizing a QD micelle solution applied to cultured hippocampal pyramidal neurons demonstrated that there is insertion of QDs into the neuron (Figure

C.3A). The next step was to evaluate whether the QDs were appropriately located within the transmembrane field such that they would respond to a change in membrane voltage.

The resting membrane potential of hippocampal pyramidal neurons is largely determined by the equilibrium potential for K^+ and is typically -75mV . From the Nernst Equation, adding 40 mM KCl to the solution bathing the neurons should change the membrane potential of the cell from -75mV to approximately -21 mV . Live cell experiments using the QD-treated cultured neurons, showed a factor of 7 increase in fluorescent intensity in response to this approximately 50 mV membrane depolarization (Figure C.3B). We also used this technique in rat hippocampal slices using trains of stimuli to produce changes in the membrane potential (Figure C.4).

The present synthesis technique indicates the potential of incorporating QDs sufficiently close to the membrane to be sensitive to changes in transmembrane field. QDs are distinctly advantageous over traditional voltage-indicating fluorescent dyes because of their high quantum yield and photostability.

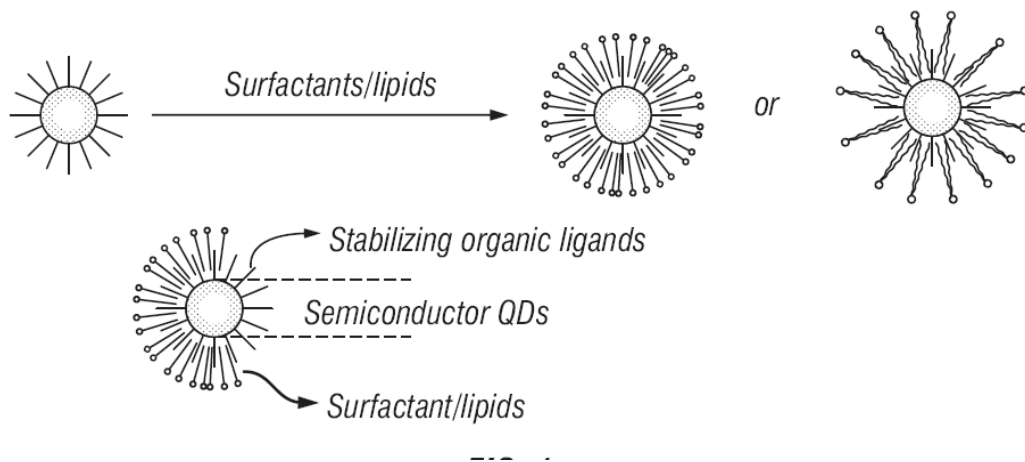


Figure C.2 Water-soluble Micelles.

Principle of water-soluble and biocompatible QD micelles of the present innovation.

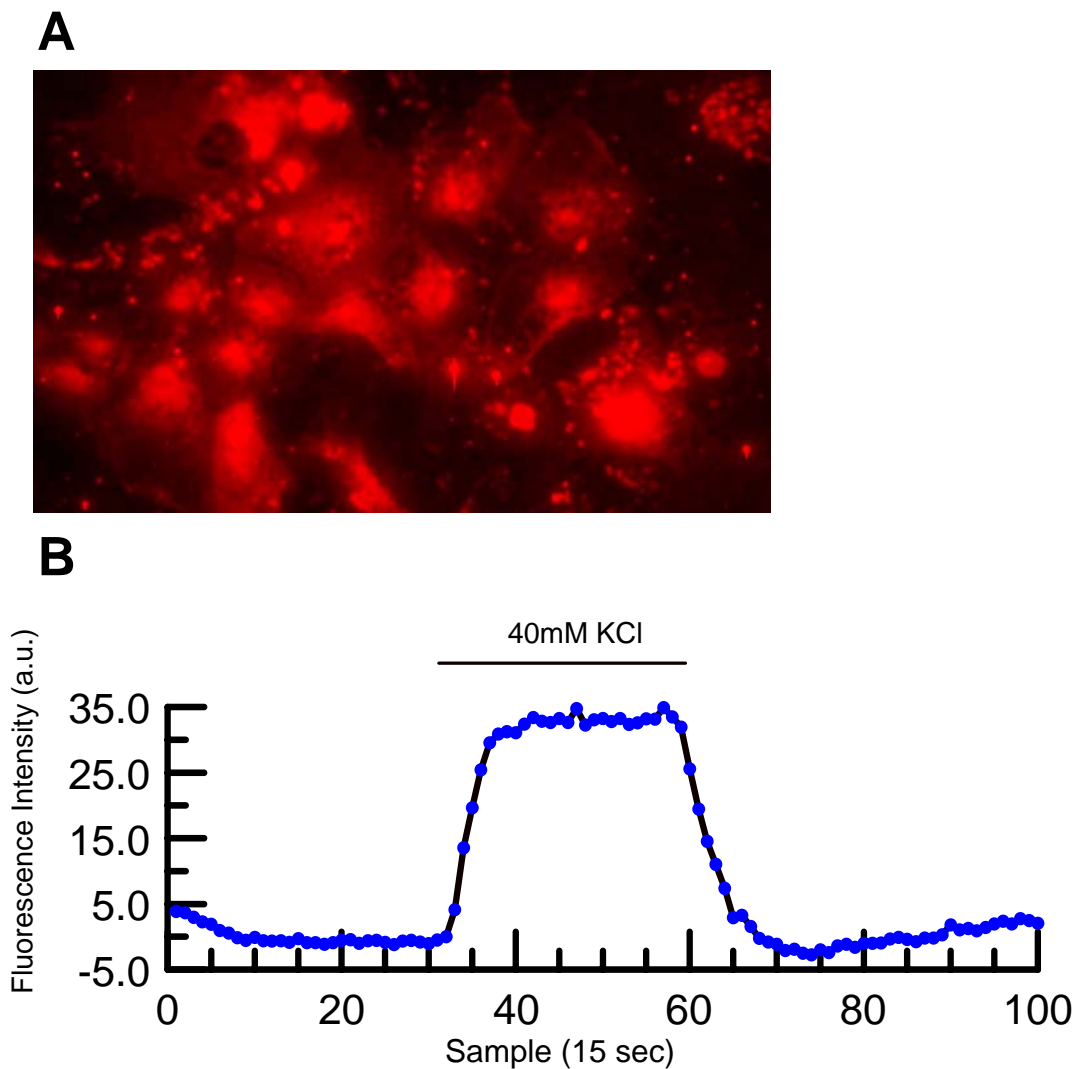


Figure C.3 Potential sensing QD in cultured hippocampal neurons.

A. Coverslip of cultured hippocampal neurons from postnatal day 1 (division 9) mouse brain were exposed to 10 min of 1:200 dilution of stock QD to culture media, then the media was exchanged with normal culture media and incubated for ~1hr, then the coverslip was fixed and mounted and imaged with an Olympus BX-40 microscope (40x objective; Rhodamine/Cy3 cube), scale bar =10 μ m.

B. Fluorescence intensity trace from QD exposed cultured neurons placed in a flow chamber of the imaging system (T.I.L.L. Photonics, Pleasanton, CA). The average fluorescence intensity was recorded at 15 s time intervals. The fluorescence was allowed to stabilize in normal ACSF for sample numbers 1-30, then 40 mM KCl was applied to the neurons between sample number 30-60, then washed with normal ACSF for sample numbers 60-100 (bar shows application of KCl). The QD were excited at 516nm and recorded using the Rhodamine/Cy3 cube. Trace shows response from one region of interest that was picked over a cell body, and baseline fluorescence was subtracted, not shown.

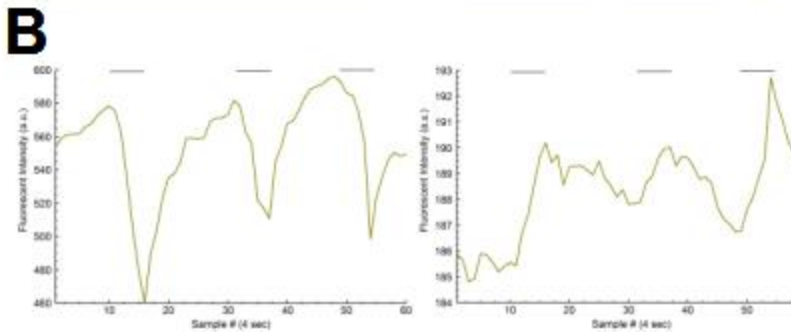
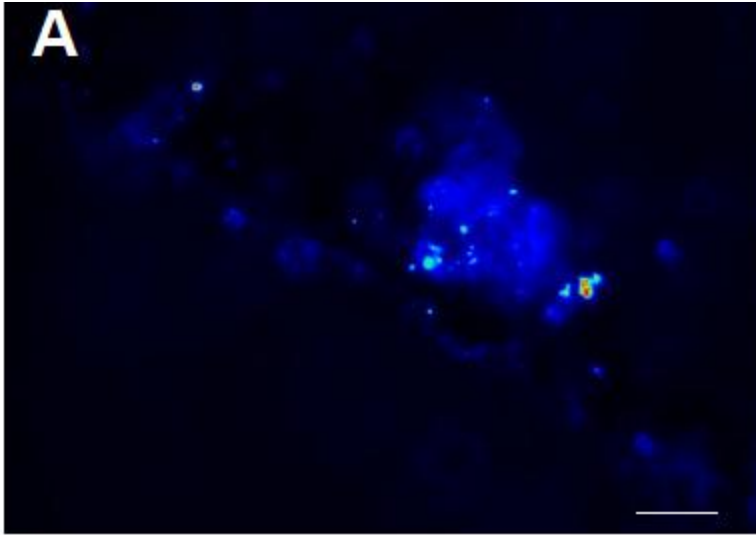


Figure C.4 Potential sensing QD in rat hippocampal slices.

A. Rat hippocampal slice of CA1 pyramidal cell layer showing accumulation of PC-12 QDs shown in pseudo color scaling red reflecting high intensity to blue reflecting low intensity, scale bar = 40 μm . **B.** Relative fluorescence intensities of two different areas of interest during intervals of repetitive stimulation (solid bars).

B. Quantum Dots as sensors of pH

Abstract

Nanocrystals have been found to be useful as fluorophores for a variety of labeling experiments and their use has increased the sensitivity of protein tracking to the point of allowing the identification of single molecules. However, technical advances that take advantage of other intrinsic controllable properties of QDs have, to date, been limited. With the goal of making a consistent high intensity probe for pH changes, we have successfully developed a method, which utilizes FRET with a combination of commercially available Adirondack Green Quantum dots and SNARF-1 pH sensitive fluorophores. This new tool has the potential for use in monitoring the pH changes in the immediate environment of the QD in important biological applications such as synaptic vesicular tracking or endocytic compartmental analysis.

Introduction:

Fluorescent semiconductor nanocrystals (quantum dots, QDs) have certain properties that have led to their use over traditional fluorophores. These advantages include broad excitation spectrum, tunable emission spectra, resistance to photobleaching and blinking (Xing *et al.*, 2009). These properties have led to the use of QDs in a variety of different biological applications that have traditionally resisted the use of traditional fluorophores. These applications include tracking membrane receptors and determining the kinetics of single vesicles in neuronal cultures (Zhang & Johnson, 2007; Zhang *et al.*, 2009). However, use of other intrinsic properties of QDs for biological measurements

has been more limited and has often required that each batch be characterized before use (Wu *et al.*, 2007a; Wu *et al.*, 2007b) due to batch-to batch variability (Wu *et al.*, 2007a).

One of the limitations of the use of the intrinsic sensitivities of QDs is the stability and reproducibility of these properties. We investigated various commercially available QDs, which were described as being insensitive to pH, since they had been coated in order to protect them from environmental effects such as pH. However, due to changes that occur during shipping and storage, the effectiveness of this coating is not consistently stable even between batches of the same lots of QDs (Wu *et al.*, 2007a). Furthermore, the potential breach of the coating raises concerns about the toxicity of these QDs in biological tissue (Hoshino *et al.*, 2007). We thus sought, by conjugating a pH sensitive dye to QDs, to produce pH sensitive QDs that can potentially be used to measure pH while retaining an intact coating making them stable in a biological environment.

One potential method for producing pH sensitive QD is synthesis of QDs using a basic mercaptopropyl-acid to add a pH sensitivity (Tomasulo *et al.*, 2006), these QDs are, however, not commercially available or easily reproducible in a biology laboratory.

We thus investigated the option of using FRET with commercial available components. FRET can be used with conjugated proteins, such as maltose binding protein, and other organic dyes that are lipid soluble and will associate within the lipid coating of QDs making them useful to measure enzyme kinetics or structural changes. Following up on these observations, we developed a FRET based sensor to monitor environmental pH.

In this study, we have taken advantage of the capability of QDs to FRET with a conjugated indicator dye in order to develop a more reliable construct for a pH sensor

with a strong persistent signal in order to be able to measure pH changes. We used the pH sensitive indicator dye, SNARF-1, which undergoes a difference in fluorescence, which we proposed would lead to an efficiency of FRET-based on changes of pH (Medintz & Mattoussi, 2009). We first determined the native pH sensitivity of different batches of commercial QDs from the same lot, then conjugated the pH sensitive dye SNARF-1 to the coating of these QDs, and finally measured their ability to FRET with the conjugated SNARF-1. The resultant QDs conjugated to SNARF-1 provided a nanoscale sensor capable of undergoing a robust change in fluorescence intensity that is capable of detecting pH changes between pH 5 to 8, which is the range found in single synaptic vesicles during vesicle recycling (Ahdut-Hacohen *et al.*, 2004), thus allowing pH to be a measure of vesicular release (Zhang & Johnson, 2007; Zhang *et al.*, 2009).

Methods:

SNARF-1 carboxylic acid, acetate, succinimidyl ester (Invitrogen) and Adirondack Green-T2-MP-Amine functionalized CdSe/ZnS, PEG encapsulated QDs (Lot #51019W2, Evident Technologies 2 batches) were conjugated with a carboxyl ester reaction. It should be noted that the QD in this paper are from Evident, however, we and others have found a intrinsic pH sensitivity in batches of QD from Invitrogen (Lot #55934A). Reactions were carried out according to instructions given by Evident for amine to succinimidyl ester binding. Briefly, different ratios (1:10, 1:50, 1:150) of QDs and SNARF-1 were mixed in a tube containing 50 μ l of 50 mM phosphate buffer and 1 μ l of DMSO. The mixture was allowed to react for an hour at room temperature before

being washed at least 5 times using Microcon Ultracel YM-30 regenerated cellulose filters (Millipore) before collecting the conjugated QD/SNARF-1.

Photoluminescence measurements were made using a Horiba Jobin Yvon Fluorolog-3 spectrofluorometer. Photoluminescence lifetime measurements were made on the same spectrofluorometer in a different configuration, which allowed for time-correlated single photon counting. Using a different pulsed diode laser sources at the labeled wavelength, the resolution of lifetime measurements was ~ 100 ps. An integrating sphere accessory on the spectrofluorometer was used to measure quantum efficiency of the sample. Fluorescence lifetime measurements of dots and fluorescein were taken on a Model TM-3/2005 Lifetime Spectrofluorometer from Photon Technologies International (PTI). The out put (pulsewidth; ≈ 800 ps, repetition rate; 10 Hz) from a GL-3300 Nitrogen pumped Dye laser (Model GL-302) was used to excite the probes at various wavelengths between 420 nm and 510 nm. Data collection and analysis was performed using the FeliX32™ Advanced Fluorescence Analysis Software Package (PTI). In a typical experiment, a 40 μ L cuvette was placed in the spectrofluorometer's temperature-controlled sample holder. Lifetime measurements were performed at room temperature.

Results:

It was first necessary to account for the intrinsic pH sensitivity of the QDs. To do this, we used equal concentrations of QDs in a cacodylate buffer at pH 5 and pH 7.5 and measured the emission resulting from a 450 nm excitation. We found that the QDs themselves had an intrinsic 3 fold change of emission intensity to this change of 2.5 pH units. Additionally, the measured quantum yield was found to be lower than the reported 50% for these QDs (Table C-1, <http://www.evidenttech.com/products/evidots/evidot520nm.html>). Finally, the QDs showed a range of variability of intrinsic pH quenching, which was apparent even between batches of the same lot (Table C-1). This was true of all QDs tested including Evident, Invitrogen, and self-prepared QDs (data not shown). We were not able to check whether the pH change was reversible due to our experimental protocol.

We predicted that the multiple binding sites of the QDs would allow us to take advantage of the overlapping integrals of SNARF-1 and the QDs to create a FRET based pH sensor (Figure C.5). We evaluated the effectiveness of SNARF-1 binding to QDs after a conjugation at 150 : 1 SNARF-1 : QDs by comparing the individual spectra for QDs and for SNARF-1 to the absorption spectra of the conjugated SNARF-1 QDs. Using a known concentration of SNARF-1 we calculated that there were approximately 10 SNARF-1 molecules per single QD (Figure C.6). In order to improve the conjugational yield, we changed our method of conjugation and began with the SNARF-1 QDs in an organic solution (DMSO) and then gradually increased the concentration of water. This method produced significantly higher yields in subsequent conjugations.

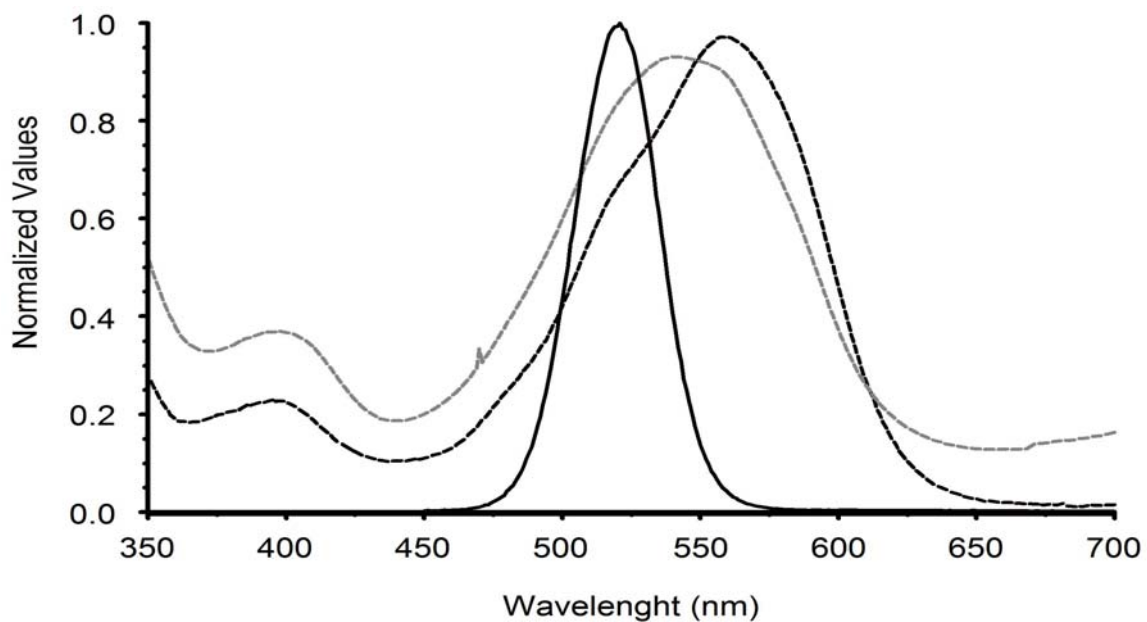


Figure C.5 Overlap of emission spectra of SNARF and QD.

Change in overlap between the QD and SNARF-1. QD emission spectra normalized to 1 (black). SNARF-1 Absorption Spectra normalized to each other pH 5 (gray dashed) pH 7.5 (black dashed).

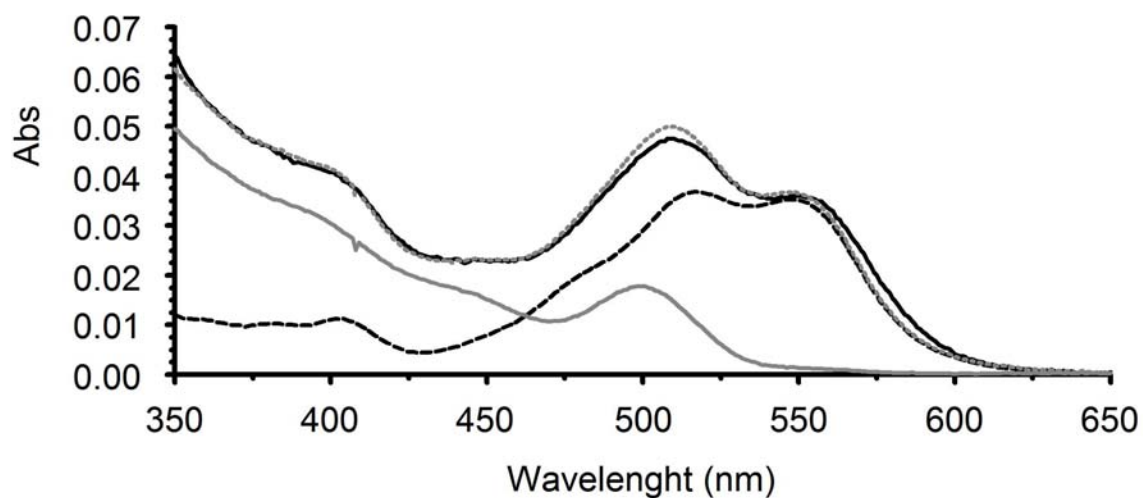


Figure C.6 Absorption spectra of QD and SNARF-1, conjugation.

Typical Absorption spectra after conjugation 1:10 initial ration of SNARF-1 with QD (solid black). The absorption signal for the SNARF-1 alone (black dashed) was scaled to match the intensity of the signal for the conjugated sample at 556 nm. The signal for the QD alone (solid gray) was scaled to the remaining peak at 500 nm, both signals were scaled less than 90% of the original spectra. The gray-dashed is the summation of the individual SNARF and QD sample's absorption.

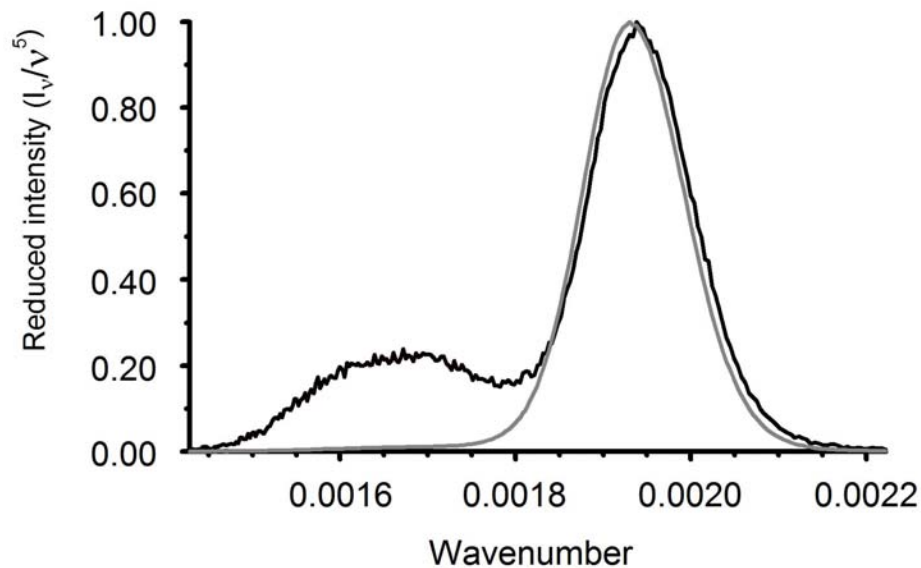


Figure C.7 FRET-based quenching of quantum dot/SNARF dye conjugates. Reduced Emission Spectra from 350 nm excitation of conjugated particles (black) compared to non-conjugated components (gray) Note that despite being extensively quenched, the QD retains the same shape of emission peak after conjugation.

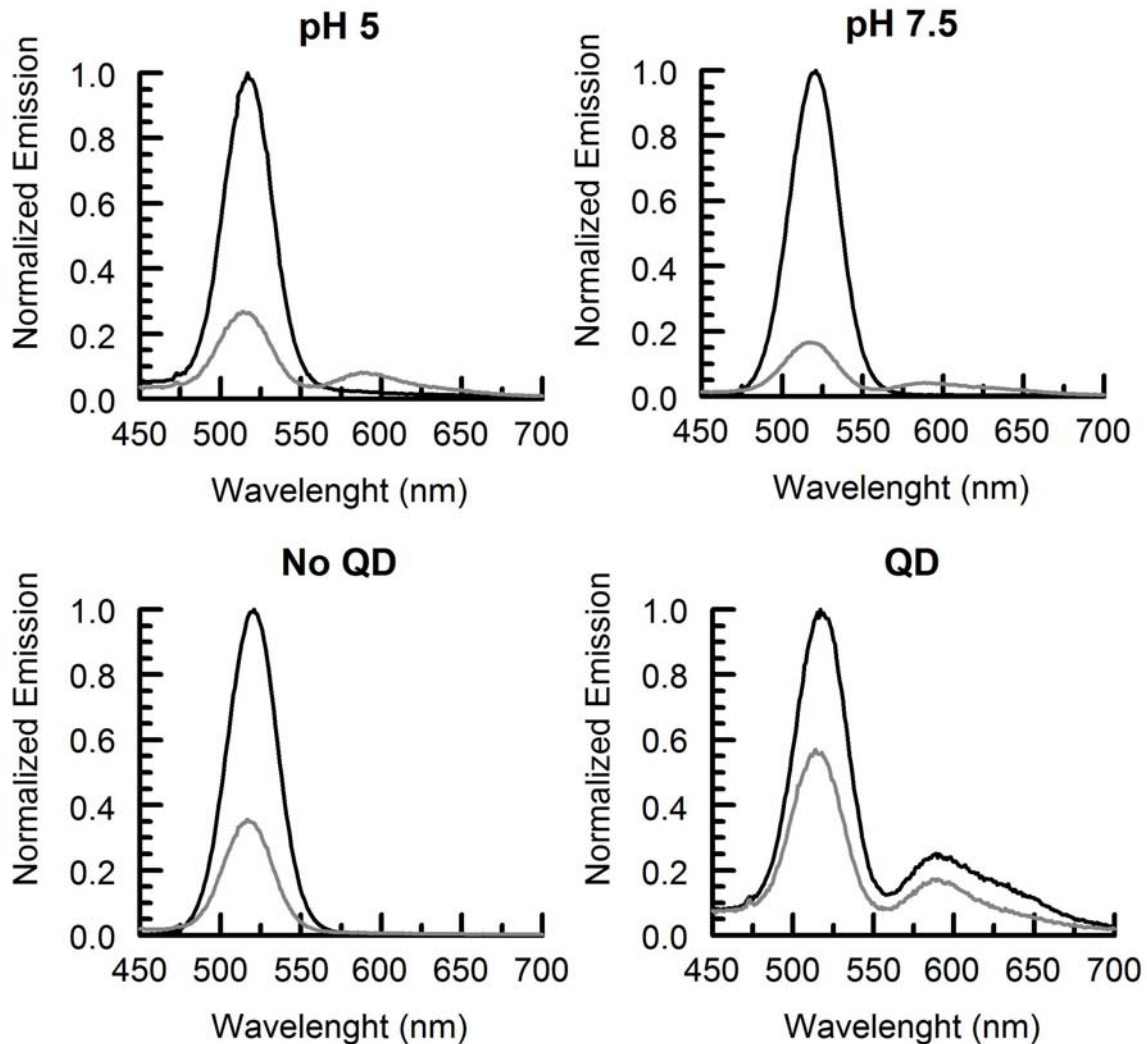


Figure C.8 SNARF-QD pH dependence.

Top: SNARF-QD emission (gray) is pH-dependent in a 0.2 M cacodylate buffer at pH 5.0 (left) and 7.5 (right), normalized to the intensity of the non-conjugated quantum dot (black). Bottom: the pH dependence intrinsic to QDs (left) and that resulting from the SNARF quenching (right) are in the opposite relative quenching pH 5.0 (gray), pH 7.5 (black). Conjugates were made using a SNARF-1:QD ratio of 5:1.

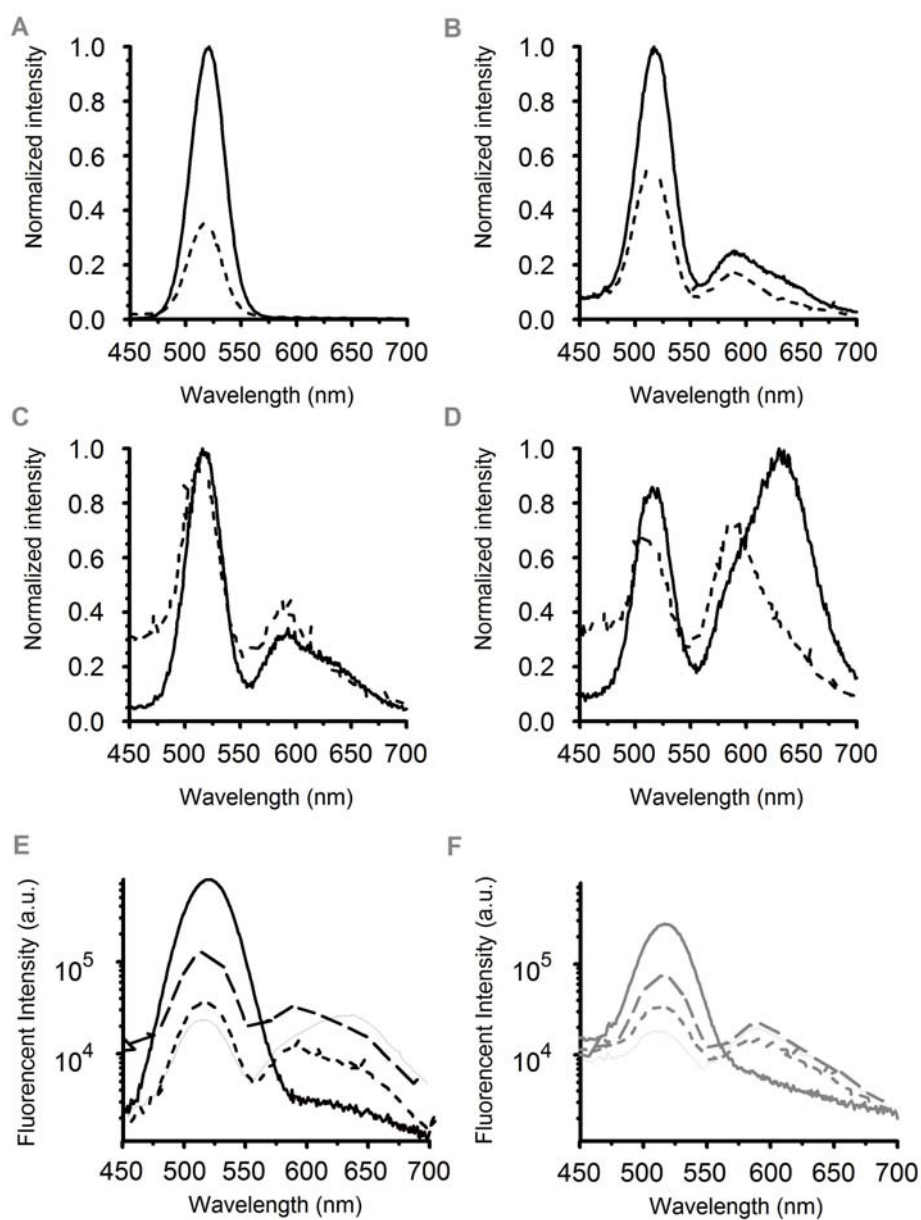


Figure C.9 Concentration-dependent quenching by SNARF-1.

Varying ratios of SNARF-1 to QD provide different amounts of quenching and excitation of the SNARF-1 at pH 5.0 (dashed) and pH 7.5 (black) in a cacodylate buffer. Original ratios used in the conjugation reaction of SNARF-1 to Evident Adirondack green QDs was as follows **A.** QD₀-0:1; **B.** QD₁-5:1; **C.** QD₂-20:1; **D.** QD₃-75:1. Similar results were seen in pH of 7.5 based on ratio of SNARF-1 binding. **E.** Concentration dependence of fluorescence at pH 7.5 (ratio SNARF:QD; solid line 0:1; long dashed line 5:1; short dashed line 20:1; thin solid line 75:1). **F.** Concentration dependence of fluorescence at pH 5.

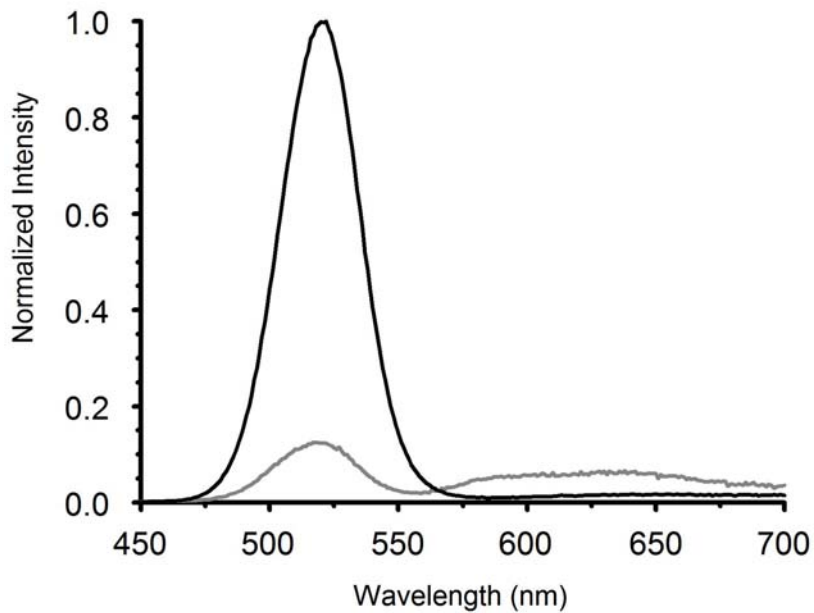


Figure C.10 SNARF quenching of quantum dot emission is stable after storage. Evaluation of the stability of the SNARF-1 to QD binding using sample QD3 (gray) from Figure 5, evaluating the quenching two months after conjugation after washing the sample again to remove any SNARF-1 that might have become unbound. Similarly treated QD sample (black). Similar amount of quenching were seen at both time points ~96%.

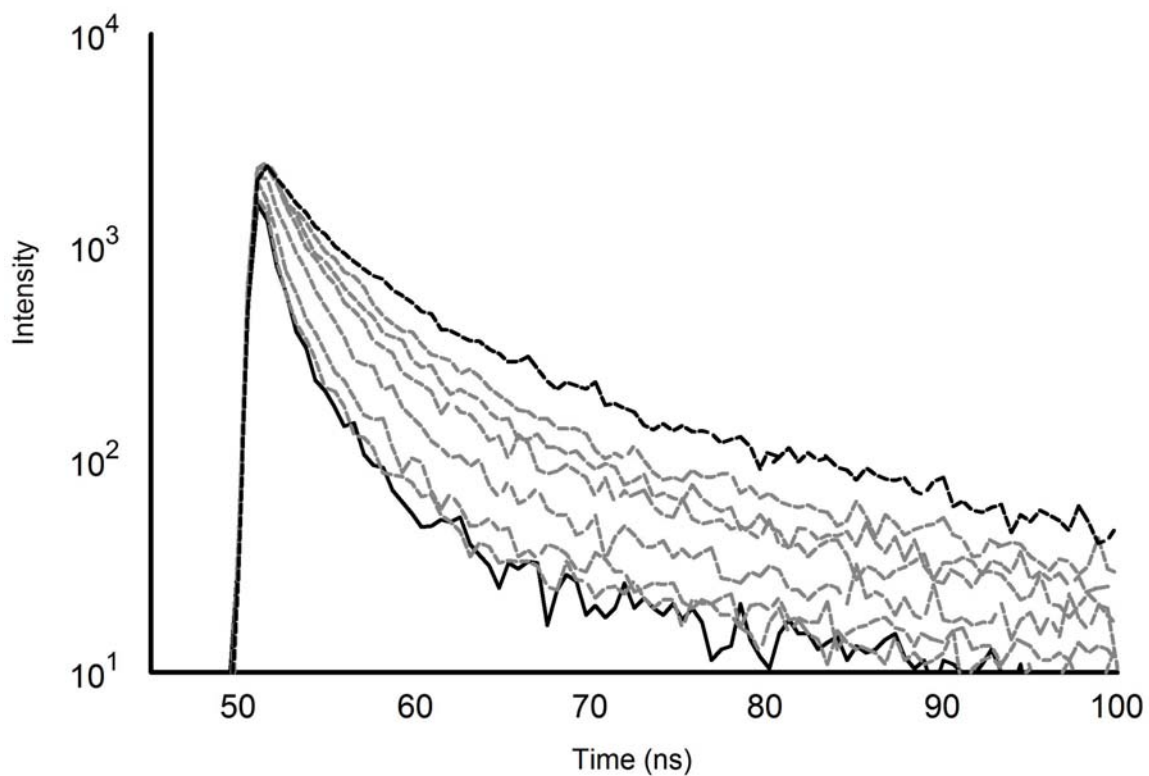


Figure C.11 Fluorescent lifetime measurements.

Fluorescent decay was measured after stepped bleaching experiments. The lifetime of the conjugate increased with bleaching (time point 1(black)), each bleaching time point shown reflects 20 min steps (light gray-dashed). Compared to the non-conjugated quantum dot (black-dashed)

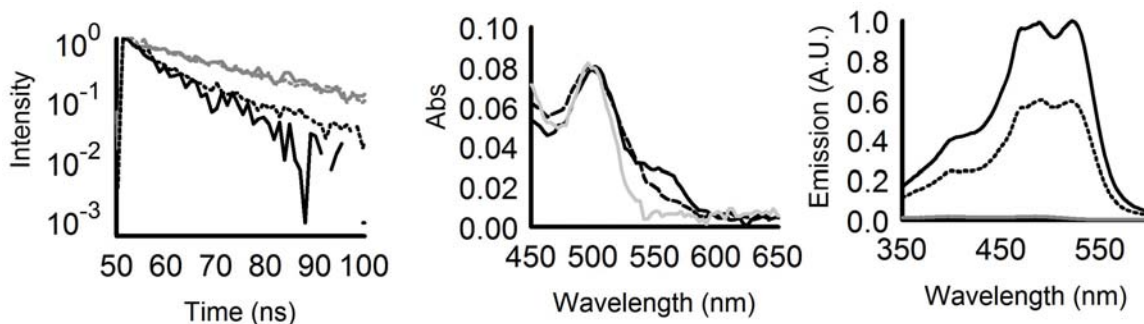


Figure C.12 Lifetime recovery after photobleaching.

A. Lifetime measurements before and after photo bleaching for non-conjugated Evident 514 QD (grey) and SNARF-1 conjugated QD (black solid) before and after bleaching (solid versus dashed). Comparing the normalized integral of the decay between 50 and 150ns reveals a 32% recovery of the decay curve. **B.** Absorption spectrum of the conjugated QD before and after bleaching, the peak at 560 (SNARF) is reduced after photo bleaching 40.48% as measured by comparing the integration of the spectra from 500 to 600 nm. **C.** Excitation Spectrum, rerecorded at 620 nm peak SNARF emission reduced by 39.98% also measured by comparing integration of the spectra from 350 to 610 nm.

We measured the emission properties of the QDs, SNARF-1, and the conjugated QD/SNARF-1 at excitation wavelengths of 350, 480 and 515 nm. As demonstrated by the shape of the emission curve of the non-conjugated and the conjugated QDs were similar in the reduced normalized spectra at 350 nm (Figure C.7) and at a 450 nm excitation. Furthermore, there was an increase in the SNARF-1 activation emission apparent in the emission of the QDs. Importantly as expected for FRET between the QDs and the SNARF-1, there was 96% quenching due to conjugation of the QDs at pH 7.5 in a Tris buffer (Figure C.8). By evaluating the difference in quenching of the QDs that resulted from the conjugation of SNARF-1 to the QDs, we found that the conjugated QDs underwent a quenching sensitivity that was accurately predicted by using overlap integral analysis of a reduction of the Förster distance of $R_0=44$ to $R_0=42$.

We next determined that the amount of quenching was dependent upon increasing ratios of SNARF-1 to QDs (Figure C.9, Table C-2). We measured the stability of the binding of SNARF-1 to the QDs, by evaluating the quenching after 2 months and found that the SNARF-1 binding was stable, and that the quenching of the QDs was persistent over this time period (Figure C.10).

To measure the stability of the interaction between the QDs and SNARF-1, we measured the lifetimes and determined that the lifetime of the conjugated QDs was significantly reduced after conjugation to the SNARF-1. Both the quenching and the reduction in time constant were recovered after photobleaching, although the original lifetime was not recovered during these experiments (Figure C.11). Finally, as shown in Figure C.12, the emission, absorption, and lifetime measurements exhibited a correlated recovery during photobleaching.

Discussion:

While the intrinsic pH sensing properties of these QDs have been exploited, (Zhang *et al.*, 2007; Duong & Rhee, 2008) its basis is not clearly understood nor is it specifically controlled among different batches of QDs. This intrinsic pH sensitivity appears to result from some event that occurs during shipping and storage and results in QDs with a lower quantum yield and a pH sensitivity that is highly variable within lots. This pH sensitivity is possibly due to destabilization or deterioration of the outer coating that helps to maintain the QD integrity. Without an intact coating, the QDs change their ability to release photons thereby reducing their quantum yield. Although these QDs have been useful for a variety of applications that do not require pH sensing (Lidke *et al.*, 2007), their use for biological measurements could be affected by the underlying basis of this pH sensitivity. For instance, these QDs may be subject to heavy metal leaching and become toxic due to exposure of their core (Hardman, 2006; Clift *et al.*, 2008).

Our object was to maintain an environmentally insensitive outer coat of the QDs while providing a pH sensing feature to produce QDs that can be safely used for biological applications. The inherent pH sensitivity, which occurs in some QDs between construction and use is too variable for dependable use and introduces too much potential for biological toxicity. On the other hand, when QDs are stabilized and made insensitive to the environment, it becomes necessary to attach a reversible indicator to their coating to make them sensitive to environmental pH. We demonstrate here a FRET-based mechanism that can be used to increase the pH sensitivity of QDs that are otherwise environmentally insensitive to pH.

We have shown that the quenching of the QDs is affected both by the environmental pH and by conjugation. We have shown that this quenching is dependent on the amount of SNARF-1 bound to the QDs. This quenching reversed when the SNARF-1 was bleached, and the amount of recovery was dependent on the amount of SNARF-1 bleached as shown by the emission, absorption, and lifetime measurements. While the FRET quenching was not more efficient than the intrinsic sensitivity of the QDs, it represents a controlled property that does not indicate an underlying degradation of the nanoparticle.

We have also shown that this method is sufficiently sensitive so that it can be used to detect a pH change between pH 5 and pH 7.5, which spans the biologically relevant range necessary to monitor the pH changes in a synaptic vesicle or endocytic compartment. We have shown that neurons can take up QDs (Fan *et al.*, 2005). The next step will be to test these QDs in a neuronal tissue preparation to ascertain whether vesicles can take them up and if they can measure the pH changes that occur when vesicles fuse with the cell membrane and their interior is exposed to the extracellular environment. Every batch of QDs tested had a variable intrinsic pH sensitivity, which would both degrade their usefulness for other measurements and indicate a potential source of toxicity. In the future it will be necessary that the coating of the QDs be improved to make them safe for biological use before adding extrinsic pH sensitivity to their coating.

Table C-1 Quantum Yield of commercial quantum dots.

The quantum yield of different wavelength quantum dots, versus excitation wavelength, compared to the control fluorescein.

	Quantum Yield			Quenching
	430 nm	488 nm	540 nm	pH5 to pH7.5
Fluorescein		86.90%		
QD514	24.70%	18.30%		25.24%
QD514	28.10%			64.45%
QD513	20.70%	13.10%		35.97%
QD599		14.90%	9.80%	45.58%

Table C-2 Quenching of quantum dots dependant on pH.

The quenching of different conjugations quantum dots, versus pH, compared to the non-conjugated quantum dots. QD₁-5:1; QD₂-20:1; QD₃-75:1.

	Quenching		R ₀	
	ph 7.5	ph 5	ph 7.5	ph 5
QD ₁	0.16766	0.268833	44.31576	42.6818
QD ₂	0.046732	0.125171	44.62505	42.68718
QD ₃	0.034698	0.071346	44.5141	42.95015

References:

- ABDULREDA, M. H., BHALLA, A., CHAPMAN, E. R. & MOY, V. T. (2008). Atomic force microscope spectroscopy reveals a hemifusion intermediate during soluble N-ethylmaleimide-sensitive factor-attachment protein receptors-mediated membrane fusion. *Biophys J* **94**, 648-655.
- AHDUT-HACOHEN, R., DURIDANOVA, D., MEIRI, H. & RAHAMIMOFF, R. (2004). Hydrogen ions control synaptic vesicle ion channel activity in Torpedo electromotor neurones. *J Physiol* **556**, 347-352.
- AMARAL, D. & LAVENEX, P. (2007). The Hippocampus Book. In *The Hippocampus Book*. ed. ANDERSON, P., MORRIS, R., AMARAL, D., BLISS, T. & O'KEEFE, J., pp. 37-45. Oxford University Press US.
- ANDERSEN, P., BLISS, T. V., LOMO, T., OLSEN, L. I. & SKREDE, K. K. (1969). Lamellar organization of hippocampal excitatory pathways. *Acta Physiol Scand* **76**, 4A-5A.
- ANDERSON, J. R. (1976). *Language, Memory and Thought*. Erlbaum, Mahwah, NJ.
- ANDERSON, J. R., BOTHELL, D., BYRNE, M. D., DOUGLASS, S., LEBIERE, C. & QIN, Y. (2004). An integrated theory of the mind. *Psychol Rev* **111**, 1036-1060.
- ANDERSON, J. R., FINCHAM, J. M., QIN, Y. & STOCCO, A. (2008). A central circuit of the mind. *Trends Cogn Sci* **12**, 136-143.
- ANDERSON, P. (2002). Assessment and development of executive function (EF) during childhood. *Child Neuropsychol* **8**, 71-82.
- APONTE, Y., BISCHOFBERGER, J. & JONAS, P. (2008). Efficient Ca²⁺ buffering in fast-spiking basket cells of rat hippocampus. *J Physiol* **586**, 2061-2075.
- ATLURI, P. P. & REGEHR, W. G. (1996). Determinants of the time course of facilitation at the granule cell to Purkinje cell synapse. *J Neurosci* **16**, 5661-5671.
- AUGUSTINE, G. J. & NEHER, E. (1992). Neuronal Ca²⁺ signalling takes the local route. *Curr Opin Neurobiol* **2**, 302-307.
- BAILEY, C. H., KANDEL, P. & CHEN, M. (1981). Active zone at Aplysia synapses: organization of presynaptic dense projections. *J Neurophysiol* **46**, 356-368.
- BAKER, H. L., ERRINGTON, R. J., DAVIES, S. C. & CAMPBELL, A. K. (2002). A mathematical model predicts that calreticulin interacts with the endoplasmic reticulum Ca(2+)-ATPase. *Biophys J* **82**, 582-590.

- BARK, C. (2009). SNAP-25 and gene-targeted mouse mutants. *Ann N Y Acad Sci* **1152**, 145-153.
- BARK, C., BELLINGER, F. P., KAUSHAL, A., MATHEWS, J. R., PARTRIDGE, L. D. & WILSON, M. C. (2004). Developmentally regulated switch in alternatively spliced SNAP-25 isoforms alters facilitation of synaptic transmission. *J Neurosci* **24**, 8796-8805.
- BARK, I. C. (1993). Structure of the chicken gene for SNAP-25 reveals duplicated exon encoding distinct isoforms of the protein. *J Mol Biol* **233**, 67-76.
- BARK, I. C., HAHN, K. M., RYABININ, A. E. & WILSON, M. C. (1995). Differential expression of SNAP-25 protein isoforms during divergent vesicle fusion events of neural development. *Proc Natl Acad Sci U S A* **92**, 1510-1514.
- BARK, I. C. & WILSON, M. C. (1994). Human cDNA clones encoding two different isoforms of the nerve terminal protein SNAP-25. *Gene* **139**, 291-292.
- BEN-ARI, Y. (2002). Excitatory actions of gaba during development: the nature of the nurture. *Nat Rev Neurosci* **3**, 728-739.
- BERROUT, J. & ISOKAWA, M. (2009). Homeostatic and stimulus-induced coupling of the L-type Ca²⁺ channel to the ryanodine receptor in the hippocampal neuron in slices. *Cell Calcium* **46**, 30-38.
- BETZ, W. J. (1970). Depression of transmitter release at the neuromuscular junction of the frog. *J Physiol* **206**, 629-644.
- BEZPROZVANNY, I., SCHELLER, R. H. & TSIEN, R. W. (1995). Functional impact of syntaxin on gating of N-type and Q-type calcium channels. *Nature* **378**, 623-626.
- BLATOW, M., CAPUTI, A., BURNASHEV, N., MONYER, H. & ROZOV, A. (2003). Ca²⁺ buffer saturation underlies paired pulse facilitation in calbindin-D28k-containing terminals. *Neuron* **38**, 79-88.
- BLISS, T. V. & LOMO, T. (1973). Long-lasting potentiation of synaptic transmission in the dentate area of the anaesthetized rabbit following stimulation of the perforant path. *J Physiol* **232**, 331-356.
- BOSCHERT, U., O'SHAUGHNESSY, C., DICKINSON, R., TESSARI, M., BENDOTTI, C., CATSICAS, S. & PICH, E. M. (1996). Developmental and plasticity-related differential expression of two SNAP-25 isoforms in the rat brain. *J Comp Neurol* **367**, 177-193.
- BOYD, I. A. & MARTIN, A. R. (1956). The end-plate potential in mammalian muscle. *J Physiol* **132**, 74-91.

- BRONK, P., DEAK, F., WILSON, M. C., LIU, X., SUDHOF, T. C. & KAVALALI, E. T. (2007). Differential effects of SNAP-25 deletion on Ca²⁺-dependent and Ca²⁺-independent neurotransmission. *J Neurophysiol* **98**, 794-806.
- BURGESS, N., BARRY, C. & O'KEEFE, J. (2007). An oscillatory interference model of grid cell firing. *Hippocampus* **17**, 801-812.
- BURNASHEV, N. & ROZOV, A. (2005). Presynaptic Ca²⁺ dynamics, Ca²⁺ buffers and synaptic efficacy. *Cell Calcium* **37**, 489-495.
- CABEZAS, C. & BUNO, W. (2006). Distinct transmitter release properties determine differences in short-term plasticity at functional and silent synapses. *J Neurophysiol* **95**, 3024-3034.
- CAREY, B. (2008). H.M., an Unforgettable Amnesiac, Dies at 82. *New York Times*.
- CARTER, A. G., VOGT, K. E., FOSTER, K. A. & REGEHR, W. G. (2002). Assessing the role of calcium-induced calcium release in short-term presynaptic plasticity at excitatory central synapses. *J Neurosci* **22**, 21-28.
- CATSICAS, S., LARHAMMAR, D., BLOMQUIST, A., SANNA, P. P., MILNER, R. J. & WILSON, M. C. (1991). Expression of a conserved cell-type-specific protein in nerve terminals coincides with synaptogenesis. *Proc Natl Acad Sci U S A* **88**, 785-789.
- CATTERALL, W. A. (1999). Interactions of presynaptic Ca²⁺ channels and snare proteins in neurotransmitter release. *Ann N Y Acad Sci* **868**, 144-159.
- CATTERALL, W. A. & FEW, A. P. (2008). Calcium channel regulation and presynaptic plasticity. *Neuron* **59**, 882-901.
- CLIFT, M. J., ROTHEN-RUTISHAUSER, B., BROWN, D. M., DUFFIN, R., DONALDSON, K., PROUDFOOT, L., GUY, K. & STONE, V. (2008). The impact of different nanoparticle surface chemistry and size on uptake and toxicity in a murine macrophage cell line. *Toxicol Appl Pharmacol*.
- COGHILL, D. & BANASCHEWSKI, T. (2009). The genetics of attention-deficit/hyperactivity disorder. *Expert Rev Neurother* **9**, 1547-1565.
- COLLIN, T., MARTY, A. & LLANO, I. (2005). Presynaptic calcium stores and synaptic transmission. *Curr Opin Neurobiol* **15**, 275-281.
- CONTI, A. C., MAAS, J. W., JR., MUGLIA, L. M., DAVE, B. A., VOGT, S. K., TRAN, T. T., RAYHEL, E. J. & MUGLIA, L. J. (2007). Distinct regional and subcellular localization of adenylyl cyclases type 1 and 8 in mouse brain. *Neuroscience* **146**, 713-729.

- COON, A. L., WALLACE, D. R., MACTUTUS, C. F. & BOOZE, R. M. (1999). L-type calcium channels in the hippocampus and cerebellum of Alzheimer's disease brain tissue. *Neurobiol Aging* **20**, 597-603.
- CORKIN, S. (2002). What's new with the amnesic patient H.M.? *Nat Rev Neurosci* **3**, 153-160.
- CORRADINI, I., VERDERIO, C., SALA, M., WILSON, M. C. & MATTEOLI, M. (2009). SNAP-25 in neuropsychiatric disorders. *Ann N Y Acad Sci* **1152**, 93-99.
- DANGLLOT, L., TRILLER, A. & MARTY, S. (2006). The development of hippocampal interneurons in rodents. *Hippocampus* **16**, 1032-1060.
- DE ALMEIDA, L., IDIART, M. & LISMAN, J. E. (2009). The input-output transformation of the hippocampal granule cells: from grid cells to place fields. *J Neurosci* **29**, 7504-7512.
- DE YOUNG, G. W. & KEIZER, J. (1992). A single-pool inositol 1,4,5-trisphosphate-receptor-based model for agonist-stimulated oscillations in Ca^{2+} concentration. *Proc Natl Acad Sci U S A* **89**, 9895-9899.
- DEKAY, J. G., CHANG, T. C., MILLS, N., SPEED, H. E. & DOBRUNZ, L. E. (2006). Responses of excitatory hippocampal synapses to natural stimulus patterns reveal a decrease in short-term facilitation and increase in short-term depression during postnatal development. *Hippocampus* **16**, 66-79.
- DEL CASTILLO, J. & KATZ, B. (1954a). Quantal components of the end-plate potential. *J Physiol* **124**, 560-573.
- DEL CASTILLO, J. & KATZ, B. (1954b). Statistical factors involved in neuromuscular facilitation and depression. *J Physiol* **124**, 574-585.
- DELGADO-MARTINEZ, I., NEHRING, R. B. & SORENSEN, J. B. (2007). Differential abilities of SNAP-25 homologs to support neuronal function. *J Neurosci* **27**, 9380-9391.
- DITTMAN, J. S., KREITZER, A. C. & REGEHR, W. G. (2000). Interplay between facilitation, depression, and residual calcium at three presynaptic terminals. *J Neurosci* **20**, 1374-1385.
- DOBRUNZ, L. E. (2002). Release probability is regulated by the size of the readily releasable vesicle pool at excitatory synapses in hippocampus. *Int J Dev Neurosci* **20**, 225-236.
- DOBRUNZ, L. E. & STEVENS, C. F. (1997). Heterogeneity of release probability, facilitation, and depletion at central synapses. *Neuron* **18**, 995-1008.

- DODE, L., VILSEN, B., VAN BAELEN, K., WUYTACK, F., CLAUSEN, J. D. & ANDERSEN, J. P. (2002). Dissection of the functional differences between sarco(endo)plasmic reticulum Ca²⁺-ATPase (SERCA) 1 and 3 isoforms by steady-state and transient kinetic analyses. *J Biol Chem* **277**, 45579-45591.
- DUMAN, J. G., CHEN, L. & HILLE, B. (2008). Calcium transport mechanisms of PC12 cells. *J Gen Physiol* **131**, 307-323.
- DUMAS, T. C. (2005). Late postnatal maturation of excitatory synaptic transmission permits adult-like expression of hippocampal-dependent behaviors. *Hippocampus* **15**, 562-578.
- DUONG, H. D. & RHEE, J. I. (2008). Use of CdSe/ZnS luminescent quantum dots incorporated within sol-gel matrix for urea detection. *Anal Chim Acta* **626**, 53-61.
- ELMQVIST, D. & QUASTEL, D. M. (1965). Presynaptic Action of Hemicholinium at the Neuromuscular Junction. *J Physiol* **177**, 463-482.
- EMPTAGE, N. J., REID, C. A. & FINE, A. (2001). Calcium stores in hippocampal synaptic boutons mediate short-term plasticity, store-operated Ca²⁺ entry, and spontaneous transmitter release. *Neuron* **29**, 197-208.
- FAN, H., LEVE, E. W., SCULLIN, C., GABALDON, J., TALLANT, D., BUNGE, S., BOYLE, T., WILSON, M. C. & BRINKER, C. J. (2005). Surfactant-assisted synthesis of water-soluble and biocompatible semiconductor quantum dot micelles. *Nano Lett* **5**, 645-648.
- FENG, R., RAMPON, C., TANG, Y. P., SHROM, D., JIN, J., KYIN, M., SOPHER, B., MILLER, M. W., WARE, C. B., MARTIN, G. M., KIM, S. H., LANGDON, R. B., SISODIA, S. S. & TSIEN, J. Z. (2001). Deficient neurogenesis in forebrain-specific presenilin-1 knockout mice is associated with reduced clearance of hippocampal memory traces. *Neuron* **32**, 911-926.
- FUKUDA, R., MCNEW, J. A., WEBER, T., PARLATI, F., ENGEL, T., NICKEL, W., ROTHMAN, J. E. & SOLLNER, T. H. (2000). Functional architecture of an intracellular membrane t-SNARE. *Nature* **407**, 198-202.
- FYHN, M., HAFTING, T., WITTER, M. P., MOSER, E. I. & MOSER, M. B. (2008). Grid cells in mice. *Hippocampus* **18**, 1230-1238.
- GAO, B. X. & ZISKIND-CONHAIM, L. (1998). Development of ionic currents underlying changes in action potential waveforms in rat spinal motoneurons. *J Neurophysiol* **80**, 3047-3061.

- GAO, X. P., SU, L. Y., ZHAO, A. L., LUO, X. R. & XIA, K. (2009). [Association of 14 polymorphisms in the five candidate genes and attention deficit hyperactivity disorder]. *Zhongguo Dang Dai Er Ke Za Zhi* **11**, 617-622.
- GASPARINI, S., SAVIANE, C., VORONIN, L. L. & CHERUBINI, E. (2000). Silent synapses in the developing hippocampus: lack of functional AMPA receptors or low probability of glutamate release? *Proc Natl Acad Sci U S A* **97**, 9741-9746.
- GEDDES, J. W., HESS, E. J., HART, R. A., KESSLAK, J. P., COTMAN, C. W. & WILSON, M. C. (1990). Lesions of hippocampal circuitry define synaptosomal-associated protein-25 (SNAP-25) as a novel presynaptic marker. *Neuroscience* **38**, 515-525.
- GONELLE-GISPERT, C., HALBAN, P. A., NIEMANN, H., PALMER, M., CATSICAS, S. & SADOUL, K. (1999). SNAP-25a and -25b isoforms are both expressed in insulin-secreting cells and can function in insulin secretion. *Biochem J* **339** (Pt 1), 159-165.
- GOSSO, M. F., DE GEUS, E. J., VAN BELZEN, M. J., POLDERMAN, T. J., HEUTINK, P., BOOMSMA, D. I. & POSTHUMA, D. (2006). The SNAP-25 gene is associated with cognitive ability: evidence from a family-based study in two independent Dutch cohorts. *Mol Psychiatry* **11**, 878-886.
- GRAHAM, M. E., WASHBOURNE, P., WILSON, M. C. & BURGOYNE, R. D. (2002). Molecular analysis of SNAP-25 function in exocytosis. *Ann N Y Acad Sci* **971**, 210-221.
- GRANT, N. J., HEPP, R., KRAUSE, W., AUNIS, D., OEHME, P. & LANGLEY, K. (1999). Differential expression of SNAP-25 isoforms and SNAP-23 in the adrenal gland. *J Neurochem* **72**, 363-372.
- GREENGARD, P., VALTORTA, F., CZERNIK, A. J. & BENFENATI, F. (1993). Synaptic vesicle phosphoproteins and regulation of synaptic function. *Science* **259**, 780-785.
- GROVER, L. M., KIM, E., COOKE, J. D. & HOLMES, W. R. (2009). LTP in hippocampal area CA1 is induced by burst stimulation over a broad frequency range centered around delta. *Learn Mem* **16**, 69-81.
- GRUMELLI, C., BERGHUIS, P., POZZI, D., CALEO, M., ANTONUCCI, F., BONANNO, G., CARMIGNOTO, G., DOBSZAY, M. B., HARKANY, T., MATTEOLI, M. & VERDERIO, C. (2008). Calpain activity contributes to the control of SNAP-25 levels in neurons. *Mol Cell Neurosci* **39**, 314-323.
- HAFTING, T., FYHN, M., MOLDEN, S., MOSER, M. B. & MOSER, E. I. (2005). Microstructure of a spatial map in the entorhinal cortex. *Nature* **436**, 801-806.

- HAMMOND, S. M., CAUDY, A. A. & HANNON, G. J. (2001). Post-transcriptional gene silencing by double-stranded RNA. *Nat Rev Genet* **2**, 110-119.
- HANSE, E., TAIRA, T., LAURI, S. & GROG, L. (2009). Glutamate synapse in developing brain: an integrative perspective beyond the silent state. *Trends Neurosci* **32**, 532-537.
- HARDMAN, R. (2006). A toxicologic review of quantum dots: toxicity depends on physicochemical and environmental factors. *Environ Health Perspect* **114**, 165-172.
- HEBB, D. O. (1949). *The Organization of Behavior*. John Wiley & Sons, New York.
- HENZE, D. A., WITTNER, L. & BUZSAKI, G. (2002). Single granule cells reliably discharge targets in the hippocampal CA3 network in vivo. *Nat Neurosci* **5**, 790-795.
- HEUSER, J. E. & REESE, T. S. (1973). Evidence for recycling of synaptic vesicle membrane during transmitter release at the frog neuromuscular junction. *J Cell Biol* **57**, 315-344.
- HIGGINS, E. R., CANNELL, M. B. & SNEYD, J. (2006). A buffering SERCA pump in models of calcium dynamics. *Biophys J* **91**, 151-163.
- HIROKAWA, N. (1989). The arrangement of actin filaments in the postsynaptic cytoplasm of the cerebellar cortex revealed by quick-freeze deep-etch electron microscopy. *Neurosci Res* **6**, 269-275.
- HOFFMAN, A. F., LAARIS, N., KAWAMURA, M., MASINO, S. A. & LUPICA, C. R. (2010). Control of cannabinoid CB1 receptor function on glutamate axon terminals by endogenous adenosine acting at A1 receptors. *J Neurosci* **30**, 545-555.
- HOSHINO, A., MANABE, N., FUJIOKA, K., SUZUKI, K., YASUHARA, M. & YAMAMOTO, K. (2007). Use of fluorescent quantum dot bioconjugates for cellular imaging of immune cells, cell organelle labeling, and nanomedicine: surface modification regulates biological function, including cytotoxicity. *J Artif Organs* **10**, 149-157.
- HU, K. & DAVLETOV, B. (2003). SNAREs and control of synaptic release probabilities. *Faseb J* **17**, 130-135.
- HUHN, Z., ORBAN, G., ERDI, P. & LENGYEL, M. (2005). Theta oscillation-coupled dendritic spiking integrates inputs on a long time scale. *Hippocampus* **15**, 950-962.
- ISOKAWA, M. & ALGER, B. E. (2006). Ryanodine receptor regulates endogenous cannabinoid mobilization in the hippocampus. *J Neurophysiol* **95**, 3001-3011.

- JACOBSSON, G., BARK, C. & MEISTER, B. (1999). Differential expression of SNAP-25a and SNAP-25b RNA transcripts in cranial nerve nuclei. *J Comp Neurol* **411**, 591-600.
- JAFRI, M. S. & KEIZER, J. (1995). On the roles of Ca²⁺ diffusion, Ca²⁺ buffers, and the endoplasmic reticulum in IP₃-induced Ca²⁺ waves. *Biophys J* **69**, 2139-2153.
- JIANG, X. Y. & ABRAMS, T. W. (1998). Use-dependent decline of paired-pulse facilitation at Aplysia sensory neuron synapses suggests a distinct vesicle pool or release mechanism. *J Neurosci* **18**, 10310-10319.
- JOHANSSON, J. U., ERICSSON, J., JANSON, J., BERAKI, S., STANIC, D., MANDIC, S. A., WIKSTROM, M. A., HOKFELT, T., OGREN, S. O., ROZELL, B., BERGGREN, P. O. & BARK, C. (2008). An ancient duplication of exon 5 in the Snap25 gene is required for complex neuronal development/function. *PLoS Genet* **4**, e1000278.
- JOHNSON, D. & WU, S. M.-S. (1995). *Foundations of Cellular Neurophysiology*. Massachusetts Institute of Technology, Cambridge, Massachusetts.
- JONES, M. W. & WILSON, M. A. (2005a). Phase precession of medial prefrontal cortical activity relative to the hippocampal theta rhythm. *Hippocampus* **15**, 867-873.
- JONES, M. W. & WILSON, M. A. (2005b). Theta rhythms coordinate hippocampal-prefrontal interactions in a spatial memory task. *PLoS Biol* **3**, e402.
- KAMIYA, H. & OZAWA, S. (1999). Dual mechanism for presynaptic modulation by axonal metabotropic glutamate receptor at the mouse mossy fibre-CA3 synapse. *J Physiol* **518 (Pt 2)**, 497-506.
- KATAOKA, M., KUWAHARA, R., MATSUO, R., SEKIGUCHI, M., INOKUCHI, K. & TAKAHASHI, M. (2006). Development- and activity-dependent regulation of SNAP-25 phosphorylation in rat brain. *Neurosci Lett* **407**, 258-262.
- KATZ, B. & MILEDI, R. (1967). The timing of calcium action during neuromuscular transmission. *J Physiol* **189**, 535-544.
- KATZ, B. & MILEDI, R. (1968). The role of calcium in neuromuscular facilitation. *J Physiol* **195**, 481-492.
- KIM, D. K. & CATTERALL, W. A. (1997). Ca²⁺-dependent and -independent interactions of the isoforms of the alpha1A subunit of brain Ca²⁺ channels with presynaptic SNARE proteins. *Proc Natl Acad Sci U S A* **94**, 14782-14786.
- KIM, S., YUN, H. M., BAIK, J. H., CHUNG, K. C., NAH, S. Y. & RHIM, H. (2007). Functional interaction of neuronal Cav1.3 L-type calcium channel with ryanodine receptor type 2 in the rat hippocampus. *J Biol Chem* **282**, 32877-32889.

- KOESTER, H. J. & SAKMANN, B. (2000). Calcium dynamics associated with action potentials in single nerve terminals of pyramidal cells in layer 2/3 of the young rat neocortex. *J Physiol* **529 Pt 3**, 625-646.
- LANDAU, E. (2009). Brain of world's best-known amnesiac. In *CNN*, vol. 2009. CNN.
- LANDFIELD, P. W. (1996). Aging-related increase in hippocampal calcium channels. *Life Sci* **59**, 399-404.
- LANDIS, D. M., HALL, A. K., WEINSTEIN, L. A. & REESE, T. S. (1988). The organization of cytoplasm at the presynaptic active zone of a central nervous system synapse. *Neuron* **1**, 201-209.
- LAU, C. G., TAKAYASU, Y., RODENAS-RUANO, A., PATERNAIN, A. V., LERMA, J., BENNETT, M. V. & ZUKIN, R. S. (2010). SNAP-25 is a target of protein kinase C phosphorylation critical to NMDA receptor trafficking. *J Neurosci* **30**, 242-254.
- LAURI, S. E., VESIKANSA, A., SEGERSTRALE, M., COLLINGRIDGE, G. L., ISAAC, J. T. & TAIRA, T. (2006). Functional maturation of CA1 synapses involves activity-dependent loss of tonic kainate receptor-mediated inhibition of glutamate release. *Neuron* **50**, 415-429.
- LI, C., LI, X., CHEN, W., YU, S., CHEN, J., WANG, H. & RUAN, D. (2007). The different roles of cyclinD1-CDK4 in STP and mGluR-LTD during the postnatal development in mice hippocampus area CA1. *BMC Dev Biol* **7**, 57.
- LI, Y., WU, Y. & ZHOU, Y. (2006). Modulation of inactivation properties of CaV2.2 channels by 14-3-3 proteins. *Neuron* **51**, 755-771.
- LIDKE, D. S., NAGY, P., JOVIN, T. M. & ARNDT-JOVIN, D. J. (2007). Biotin-ligand complexes with streptavidin quantum dots for in vivo cell labeling of membrane receptors. *Methods Mol Biol* **374**, 69-79.
- LILEY, A. W. & NORTH, K. A. (1953). An electrical investigation of effects of repetitive stimulation on mammalian neuromuscular junction. *J Neurophysiol* **16**, 509-527.
- LISMAN, J. E., RAGHAVACHARI, S. & TSIEN, R. W. (2007). The sequence of events that underlie quantal transmission at central glutamatergic synapses. *Nat Rev Neurosci* **8**, 597-609.
- LIU, P., JENKINS, N. A. & COPELAND, N. G. (2003). A highly efficient recombineering-based method for generating conditional knockout mutations. *Genome Res* **13**, 476-484.

- LLINAS, R., GRUNER, J. A., SUGIMORI, M., MCGUINNESS, T. L. & GREENGARD, P. (1991). Regulation by synapsin I and Ca(2+)-calmodulin-dependent protein kinase II of the transmitter release in squid giant synapse. *J Physiol* **436**, 257-282.
- LOCKERY, S. R. & SPITZER, N. C. (1992). Reconstruction of action potential development from whole-cell currents of differentiating spinal neurons. *J Neurosci* **12**, 2268-2287.
- LUBENOV, E. V. & SIAPAS, A. G. (2009). Hippocampal theta oscillations are travelling waves. *Nature* **459**, 534-539.
- MAIWALD, T. & TIMMER, J. (2008). Dynamical modeling and multi-experiment fitting with PottersWheel. *Bioinformatics* **24**, 2037-2043.
- MARTIN, E. D. & BUNO, W. (2003). Caffeine-Mediated Presynaptic Long-Term Potentiation in Hippocampal CA1 Pyramidal Neurons
10.1152/jn.00601.2002. *J Neurophysiol* **89**, 3029-3038.
- MATSUDA, S., KOBAYASHI, Y. & ISHIZUKA, N. (2004). A quantitative analysis of the laminar distribution of synaptic boutons in field CA3 of the rat hippocampus. *Neurosci Res* **49**, 241-252.
- MATTEOLI, M., POZZI, D., GRUMELLI, C., CONDLIFFE, S. B., FRASSONI, C., HARKANY, T. & VERDERIO, C. (2009). The synaptic split of SNAP-25: different roles in glutamatergic and GABAergic neurons? *Neuroscience* **158**, 223-230.
- MCGUINNESS, L., BARDO, S. J. & EMPTAGE, N. J. (2007). The lysosome or lysosome-related organelle may serve as a Ca²⁺ store in the boutons of hippocampal pyramidal cells. *Neuropharmacology* **52**, 126-135.
- MEDINTZ, I. L. & MATTOUSSI, H. (2009). Quantum dot-based resonance energy transfer and its growing application in biology. *Phys Chem Chem Phys* **11**, 17-45.
- MEGIAS, M., EMRI, Z., FREUND, T. F. & GULYAS, A. I. (2001). Total number and distribution of inhibitory and excitatory synapses on hippocampal CA1 pyramidal cells. *Neuroscience* **102**, 527-540.
- MEINRENKEN, C. J., BORST, J. G. & SAKMANN, B. (2002). Calcium secretion coupling at calyx of held governed by nonuniform channel-vesicle topography. *J Neurosci* **22**, 1648-1667.
- METZ, A. E., JARSKY, T., MARTINA, M. & SPRUSTON, N. (2005). R-type calcium channels contribute to afterdepolarization and bursting in hippocampal CA1 pyramidal neurons. *J Neurosci* **25**, 5763-5773.

- MOCHIDA, S., FEW, A. P., SCHEUER, T. & CATTERALL, W. A. (2008). Regulation of presynaptic Ca(V)2.1 channels by Ca²⁺ sensor proteins mediates short-term synaptic plasticity. *Neuron* **57**, 210-216.
- MORI, F., FUKAYA, M., ABE, H., WAKABAYASHI, K. & WATANABE, M. (2000). Developmental changes in expression of the three ryanodine receptor mRNAs in the mouse brain. *Neurosci Lett* **285**, 57-60.
- MOZHAYEVA, M. G., SARA, Y., LIU, X. & KAVALALI, E. T. (2002). Development of vesicle pools during maturation of hippocampal synapses. *J Neurosci* **22**, 654-665.
- MUKHAMEDYAROV, M. A., KOCHUNOVA, J. O., YUSUPOVA, E. R., HAIDAROV, B. A., ZEFIROV, A. L. & PALOTAS, A. (2010). The contribution of calcium/calmodulin-dependent protein-kinase II (CaMKII) to short-term plasticity at the neuromuscular junction. *Brain Res Bull* **81**, 613-616.
- NAGY, G., MILOSEVIC, I., FASSHAUER, D., MULLER, E. M., DE GROOT, B. L., LANG, T., WILSON, M. C. & SORENSEN, J. B. (2005). Alternative splicing of SNAP-25 regulates secretion through nonconservative substitutions in the SNARE domain. *Mol Biol Cell* **16**, 5675-5685.
- NAGY, G., REIM, K., MATTI, U., BROSE, N., BINZ, T., RETTIG, J., NEHER, E. & SORENSEN, J. B. (2004). Regulation of releasable vesicle pool sizes by protein kinase A-dependent phosphorylation of SNAP-25. *Neuron* **41**, 417-429.
- NEHER, E. & AUGUSTINE, G. J. (1992). Calcium gradients and buffers in bovine chromaffin cells. *J Physiol* **450**, 273-301.
- OHBAYASHI, K., FUKURA, H., INOUE, H. K., KOMIYA, Y. & IGARASHI, M. (1998). Stimulation of L-type Ca²⁺ channel in growth cones activates two independent signaling pathways. *J Neurosci Res* **51**, 682-696.
- O'KEEFE, J. & DOSTROVSKY, J. (1971). The hippocampus as a spatial map. Preliminary evidence from unit activity in the freely-moving rat. *Brain Res* **34**, 171-175.
- OSSEN-SAND, A., CATSICAS, M., STAPLE, J. K., JONES, K. A., AYALA, G., KNOWLES, J., GRENNINGLOH, G. & CATSICAS, S. (1993). Inhibition of axonal growth by SNAP-25 antisense oligonucleotides in vitro and in vivo. *Nature* **364**, 445-448.
- OYLER, G. A., HIGGINS, G. A., HART, R. A., BATTENBERG, E., BILLINGSLEY, M., BLOOM, F. E. & WILSON, M. C. (1989). The identification of a novel synaptosomal-associated protein, SNAP-25, differentially expressed by neuronal subpopulations. *J Cell Biol* **109**, 3039-3052.

- OYLER, G. A., POLLI, J. W., WILSON, M. C. & BILLINGSLEY, M. L. (1991). Developmental expression of the 25-kDa synaptosomal-associated protein (SNAP-25) in rat brain. *Proc Natl Acad Sci U S A* **88**, 5247-5251.
- PALOP, J. J. & MUCKE, L. (2009). Epilepsy and cognitive impairments in Alzheimer disease. *Arch Neurol* **66**, 435-440.
- PARTRIDGE, L. D. & VALENZUELA, C. F. (2002). Neurosteroids enhance bandpass filter characteristics of the rat Schaffer collateral-to-CA1 synapse. *Neurosci Lett* **326**, 1-4.
- PENFIELD, W. (1952). Memory mechanisms. *AMA Arch Neurol Psychiatry* **67**, 178-198.
- POZZI, D., CONDLIFFE, S., BOZZI, Y., CHIKHLADZE, M., GRUMELLI, C., PROUX-GILLARDEAUX, V., TAKAHASHI, M., FRANCESCHETTI, S., VERDERIO, C. & MATTEOLI, M. (2008). Activity-dependent phosphorylation of Ser187 is required for SNAP-25-negative modulation of neuronal voltage-gated calcium channels. *Proc Natl Acad Sci U S A* **105**, 323-328.
- RAMÓN Y CAJAL, S. (1911). *Histologie du Systeme Nerveux de l'Homme et des Vertebretes*, vol. II. Maloine, Paris.
- REGEHR, W. G. & ATLURI, P. P. (1995). Calcium transients in cerebellar granule cell presynaptic terminals. *Biophys J* **68**, 2156-2170.
- REGEHR, W. G. & TANK, D. W. (1991). Selective fura-2 loading of presynaptic terminals and nerve cell processes by local perfusion in mammalian brain slice. *J Neurosci Methods* **37**, 111-119.
- RETTIG, J., SHENG, Z. H., KIM, D. K., HODSON, C. D., SNUTCH, T. P. & CATTERALL, W. A. (1996). Isoform-specific interaction of the alpha1A subunits of brain Ca²⁺ channels with the presynaptic proteins syntaxin and SNAP-25. *Proc Natl Acad Sci U S A* **93**, 7363-7368.
- RICHARDSON, T. L., TURNER, R. W. & MILLER, J. J. (1987). Action-potential discharge in hippocampal CA1 pyramidal neurons: current source-density analysis. *J Neurophysiol* **58**, 981-996.
- ROZOV, A., BURNASHEV, N., SAKMANN, B. & NEHER, E. (2001). Transmitter release modulation by intracellular Ca²⁺ buffers in facilitating and depressing nerve terminals of pyramidal cells in layer 2/3 of the rat neocortex indicates a target cell-specific difference in presynaptic calcium dynamics. *J Physiol* **531**, 807-826.
- RUBENSTEIN, J. L., GREENGARD, P. & CZERNIK, A. J. (1993). Calcium-dependent serine phosphorylation of synaptophysin. *Synapse* **13**, 161-172.

- SALLERT, M., RANTAMAKI, T., VESIKANSA, A., ANTHONI, H., HARJU, K., YLI-KAUHALUOMA, J., TAIRA, T., CASTREN, E. & LAURI, S. E. (2009). Brain-derived neurotrophic factor controls activity-dependent maturation of CA1 synapses by downregulating tonic activation of presynaptic kainate receptors. *J Neurosci* **29**, 11294-11303.
- SCHIESS, A. R., SCULLIN, C. & PARTRIDGE, L. D. (2010). Maturation of Schaffer collateral synapses generates a phenotype of unreliable basal evoked release and very reliable facilitated release. *Eur J Neuroscience* epub.
- SCHIESS, A. R., SCULLIN, C., WILSON, M. & PARTRIDGE, L. D. (2005). In *Society for Neuroscience*, Washington D.C.
- SCHIESS, A. R., SCULLIN, C. S. & PARTRIDGE, L. D. (2006). Neurosteroid-induced enhancement of short-term facilitation involves a component downstream from presynaptic calcium in hippocampal slices. *J Physiol* **576**, 833-847.
- SCHNEGGENBURGER, R. & NEHER, E. (2000). Intracellular calcium dependence of transmitter release rates at a fast central synapse. *Nature* **406**, 889-893.
- SCULLIN, C., WILSON, M. & PARTRIDGE, L. D. (2010). Developmental changes in presynaptic Ca²⁺ clearance kinetics and synaptic plasticity in mouse Schaffer collateral terminals. *Eur J Neuroscience* **31**, 817-826.
- SCULLIN, C. S. & PARTRIDGE, L. D. (2010). Contributions of SERCA pump and ryanodine-sensitive stores to presynaptic residual Ca(2+). *Cell Calcium* **47**, 326-338.
- SELAK, S., PATERNAIN, A. V., ALLER, M. I., PICO, E., RIVERA, R. & LERMA, J. (2009). A role for SNAP25 in internalization of kainate receptors and synaptic plasticity. *Neuron* **63**, 357-371.
- SHAHREZAEI, V. & DELANEY, K. R. (2005). Brevity of the Ca²⁺ microdomain and active zone geometry prevent Ca²⁺-sensor saturation for neurotransmitter release. *J Neurophysiol* **94**, 1912-1919.
- SHIMAZAKI, Y., NISHIKI, T., OMORI, A., SEKIGUCHI, M., KAMATA, Y., KOZAKI, S. & TAKAHASHI, M. (1996). Phosphorylation of 25-kDa synaptosome-associated protein. Possible involvement in protein kinase C-mediated regulation of neurotransmitter release. *J Biol Chem* **271**, 14548-14553.
- SINHA, S. R., WU, L. G. & SAGGAU, P. (1997). Presynaptic calcium dynamics and transmitter release evoked by single action potentials at mammalian central synapses. *Biophys J* **72**, 637-651.

- SIPPY, T., CRUZ-MARTIN, A., JEROMIN, A. & SCHWEIZER, F. E. (2003). Acute changes in short-term plasticity at synapses with elevated levels of neuronal calcium sensor-1. *Nat Neurosci* **6**, 1031-1038.
- SOLLNER, T., WHITEHEART, S. W., BRUNNER, M., ERDJUMENT-BROMAGE, H., GEROMANOS, S., TEMPST, P. & ROTHMAN, J. E. (1993). SNAP receptors implicated in vesicle targeting and fusion. *Nature* **362**, 318-324.
- SOLOVYOVA, N. & VERKHRATSKY, A. (2002). Monitoring of free calcium in the neuronal endoplasmic reticulum: an overview of modern approaches. *J Neurosci Methods* **122**, 1-12.
- SORENSEN, J. B. (2005). SNARE complexes prepare for membrane fusion. *Trends Neurosci* **28**, 453-455.
- SORENSEN, J. B., MATTI, U., WEI, S. H., NEHRING, R. B., VOETS, T., ASHERY, U., BINZ, T., NEHER, E. & RETTIG, J. (2002). The SNARE protein SNAP-25 is linked to fast calcium triggering of exocytosis. *Proc Natl Acad Sci U S A* **99**, 1627-1632.
- SORENSEN, J. B., NAGY, G., VAROQUEAUX, F., NEHRING, R. B., BROSE, N., WILSON, M. C. & NEHER, E. (2003). Differential control of the releasable vesicle pools by SNAP-25 splice variants and SNAP-23. *Cell* **114**, 75-86.
- SORENSEN, J. B., WIEDERHOLD, K., MULLER, E. M., MILOSEVIC, I., NAGY, G., DE GROOT, B. L., GRUBMULLER, H. & FASSHAUER, D. (2006). Sequential N- to C-terminal SNARE complex assembly drives priming and fusion of secretory vesicles. *Embo J* **25**, 955-966.
- SPEED, H. E. & DOBRUNZ, L. E. (2007). Developmental decrease in short-term facilitation at Schaffer collateral synapses in hippocampus is mGluR1-sensitive. *J Neurophysiol.*
- SPEED, H. E. & DOBRUNZ, L. E. (2009). Developmental changes in short-term facilitation are opposite at temporoammonic synapses compared to Schaffer collateral synapses onto CA1 pyramidal cells. *Hippocampus* **19**, 187-204.
- STEFFENSEN, S. C., JONES, M. D., HALES, K. & ALLISON, D. W. (2006). Dehydroepiandrosterone sulfate and estrone sulfate reduce GABA-recurrent inhibition in the hippocampus via muscarinic acetylcholine receptors. *Hippocampus* **16**, 1080-1090.
- SUDHOF, T. C. (2004). The synaptic vesicle cycle. *Annu Rev Neurosci* **27**, 509-547.
- SUH, Y. H., TERASHIMA, A., PETRALIA, R. S., WENTHOLD, R. J., ISAAC, J. T., ROCHE, K. W. & ROCHE, P. A. (2010). A neuronal role for SNAP-23 in postsynaptic glutamate receptor trafficking. *Nat Neurosci.*

- SULLIVAN, J. M. (2007). A simple depletion model of the readily releasable pool of synaptic vesicles cannot account for paired-pulse depression. *J Neurophysiol* **97**, 948-950.
- SUTTON, R. B., FASSHAUER, D., JAHN, R. & BRUNGER, A. T. (1998). Crystal structure of a SNARE complex involved in synaptic exocytosis at 2.4 Å resolution. *Nature* **395**, 347-353.
- TAFOYA, L. C., MAMELI, M., MIYASHITA, T., GUZOWSKI, J. F., VALENZUELA, C. F. & WILSON, M. C. (2006). Expression and function of SNAP-25 as a universal SNARE component in GABAergic neurons. *J Neurosci* **26**, 7826-7838.
- TAFOYA, L. C., SHUTTLEWORTH, C. W., YANAGAWA, Y., OBATA, K. & WILSON, M. C. (2008). The role of the t-SNARE SNAP-25 in action potential-dependent calcium signaling and expression in GABAergic and glutamatergic neurons. *BMC Neurosci* **9**, 105.
- TAKEUCHI, A. (1958). The long-lasting depression in neuromuscular transmission of frog. *Jpn J Physiol* **8**, 102-113.
- THIES, R. E. (1965). Neuromuscular Depression and the Apparent Depletion of Transmitter in Mammalian Muscle. *J Neurophysiol* **28**, 428-442.
- THOMPSON, P. M., EGBUFOAMA, S. & VAWTER, M. P. (2003). SNAP-25 reduction in the hippocampus of patients with schizophrenia. *Prog Neuropsychopharmacol Biol Psychiatry* **27**, 411-417.
- THOMPSON, P. M., SOWER, A. C. & PERRONE-BIZZOZERO, N. I. (1998). Altered levels of the synaptosomal associated protein SNAP-25 in schizophrenia. *Biol Psychiatry* **43**, 239-243.
- TOJIMA, T., AKIYAMA, H., ITOFUSA, R., LI, Y., KATAYAMA, H., MIYAWAKI, A. & KAMIGUCHI, H. (2007). Attractive axon guidance involves asymmetric membrane transport and exocytosis in the growth cone. *Nat Neurosci* **10**, 58-66.
- TOMASULO, M., YILDIZ, I., KAA NUMALLE, S. L. & RAYMO, F. M. (2006). pH-sensitive ligand for luminescent quantum dots. *Langmuir* **22**, 10284-10290.
- TSUJIMOTO, T., JEROMIN, A., SAITOH, N., RODER, J. C. & TAKAHASHI, T. (2002). Neuronal calcium sensor 1 and activity-dependent facilitation of P/Q-type calcium currents at presynaptic nerve terminals. *Science* **295**, 2276-2279.
- TURNER, K. M., BURGOYNE, R. D. & MORGAN, A. (1999). Protein phosphorylation and the regulation of synaptic membrane traffic. *Trends Neurosci* **22**, 459-464.

- VENTRIGLIA, F. & MAIO, V. D. (2005). Neural Code and Irregular Spike Trains. In *Brain, Vision, and Artificial Intelligence*, vol. 1. ed. DE GREGORIO, M., MAIO, V. D., FRUCCI, M. & MUSIO, C., pp. 89-98. Springer-Verlag Berlin Heidelberg, Naples, Italy.
- VERDERIO, C., POZZI, D., PRAVETTONI, E., INVERARDI, F., SCHENK, U., COCO, S., PROUX-GILLARDEAUX, V., GALLI, T., ROSSETTO, O., FRASSONI, C. & MATTEOLI, M. (2004). SNAP-25 modulation of calcium dynamics underlies differences in GABAergic and glutamatergic responsiveness to depolarization. *Neuron* **41**, 599-610.
- VERKHRATSKY, A. (2005). Physiology and pathophysiology of the calcium store in the endoplasmic reticulum of neurons. *Physiol Rev* **85**, 201-279.
- VERTES, R. P. (2005). Hippocampal theta rhythm: a tag for short-term memory. *Hippocampus* **15**, 923-935.
- VILLARREAL, D. M., GROSS, A. L. & DERRICK, B. E. (2007). Modulation of CA3 afferent inputs by novelty and theta rhythm. *J Neurosci* **27**, 13457-13467.
- WASHBOURNE, P., THOMPSON, P. M., CARTA, M., COSTA, E. T., MATHEWS, J. R., LOPEZ-BENDITO, G., MOLNAR, Z., BECHER, M. W., VALENZUELA, C. F., PARTRIDGE, L. D. & WILSON, M. C. (2002). Genetic ablation of the t-SNARE SNAP-25 distinguishes mechanisms of neuroexocytosis. *Nat Neurosci* **5**, 19-26.
- WASLING, P., HANSE, E. & GUSTAFSSON, B. (2004). Developmental changes in release properties of the CA3-CA1 glutamate synapse in rat hippocampus. *J Neurophysiol* **92**, 2714-2724.
- WHEELER, D. B., RANDALL, A. & TSIEN, R. W. (1994). Roles of N-type and Q-type Ca²⁺ channels in supporting hippocampal synaptic transmission. *Science* **264**, 107-111.
- WISER, O., BENNETT, M. K. & ATLAS, D. (1996). Functional interaction of syntaxin and SNAP-25 with voltage-sensitive L- and N-type Ca²⁺ channels. *Embo J* **15**, 4100-4110.
- WISER, O., TOBI, D., TRUS, M. & ATLAS, D. (1997). Synaptotagmin restores kinetic properties of a syntaxin-associated N-type voltage sensitive calcium channel. *FEBS Lett* **404**, 203-207.
- WITTER, M. P. & MOSER, E. I. (2006). Spatial representation and the architecture of the entorhinal cortex. *Trends Neurosci* **29**, 671-678.
- WOOD, E. R., DUDCHENKO, P. A. & EICHENBAUM, H. (1999). The global record of memory in hippocampal neuronal activity. *Nature* **397**, 613-616.

- WU, L. G. & SAGGAU, P. (1994). Presynaptic calcium is increased during normal synaptic transmission and paired-pulse facilitation, but not in long-term potentiation in area CA1 of hippocampus. *J Neurosci* **14**, 645-654.
- WU, Y., CAMPOS, S. K., LOPEZ, G. P., OZBUN, M. A., SKLAR, L. A. & BURANDA, T. (2007a). The development of quantum dot calibration beads and quantitative multicolor bioassays in flow cytometry and microscopy. *Anal Biochem* **364**, 180-192.
- WU, Y., LOPEZ, G. P., SKLAR, L. A. & BURANDA, T. (2007b). Spectroscopic characterization of streptavidin functionalized quantum dots. *Anal Biochem* **364**, 193-203.
- XING, Y., XIA, Z. & RAO, J. (2009). Semiconductor quantum dots for biosensing and in vivo imaging. *IEEE Trans Nanobioscience* **8**, 4-12.
- XU-FRIEDMAN, M. A. & REGEHR, W. G. (2004). Structural contributions to short-term synaptic plasticity. *Physiol Rev* **84**, 69-85.
- YAO, J., QI, J. & CHEN, G. (2006). Actin-Dependent Activation of Presynaptic Silent Synapses Contributes to Long-Term Synaptic Plasticity in Developing Hippocampal Neurons. *J. Neurosci.* **26**, 8137-8147.
- YOKOYAMA, C. T., MYERS, S. J., FU, J., MOCKUS, S. M., SCHEUER, T. & CATTERALL, W. A. (2005). Mechanism of SNARE protein binding and regulation of Cav2 channels by phosphorylation of the synaptic protein interaction site. *Mol Cell Neurosci* **28**, 1-17.
- YOKOYAMA, C. T., SHENG, Z. H. & CATTERALL, W. A. (1997). Phosphorylation of the synaptic protein interaction site on N-type calcium channels inhibits interactions with SNARE proteins. *J Neurosci* **17**, 6929-6938.
- ZHANG, C. Y. & JOHNSON, L. W. (2007). Quantifying RNA-peptide interaction by single-quantum dot-based nanosensor: an approach for drug screening. *Anal Chem* **79**, 7775-7781.
- ZHANG, H. Y., ZHU, Y. B., CHANG, H. & CHEN, J. C. (2008). [Association between SNAP-25 gene polymorphism and attention deficit hyperactivity disorder]. *Zhonghua Er Ke Za Zhi* **46**, 564-569.
- ZHANG, Q., CAO, Y. Q. & TSIEN, R. W. (2007). Quantum dots provide an optical signal specific to full collapse fusion of synaptic vesicles. *Proc Natl Acad Sci U S A* **104**, 17843-17848.
- ZHANG, Q., LI, Y. & TSIEN, R. W. (2009). The dynamic control of kiss-and-run and vesicular reuse probed with single nanoparticles. *Science* **323**, 1448-1453.

- ZHONG, H., YOKOYAMA, C. T., SCHEUER, T. & CATTERALL, W. A. (1999). Reciprocal regulation of P/Q-type Ca²⁺ channels by SNAP-25, syntaxin and synaptotagmin. *Nat Neurosci* **2**, 939-941.
- ZHONG, P., CHEN, Y. A., TAM, D., CHUNG, D., SCHELLER, R. H. & MILJANICH, G. P. (1997). An alpha-helical minimal binding domain within the H3 domain of syntaxin is required for SNAP-25 binding. *Biochemistry* **36**, 4317-4326.
- ZOLA-MORGAN, S., SQUIRE, L. R. & AMARAL, D. G. (1986). Human amnesia and the medial temporal region: enduring memory impairment following a bilateral lesion limited to field CA1 of the hippocampus. *J Neurosci* **6**, 2950-2967.
- ZUCKER, R. S. (1999). Calcium- and activity-dependent synaptic plasticity. *Curr Opin Neurobiol* **9**, 305-313.
- ZUCKER, R. S. & REGEHR, W. G. (2002). Short-term synaptic plasticity. *Annu Rev Physiol* **64**, 355-405.